Micro Flow Control Using Thermally Responsive Polymer Solutions

by

Vahid Bazargan

B.Sc., Mechanical Engineering, Sharif University of Technology, Iran, 2006

B.Sc., Chemical and Petroleum Engineering, Sharif University of Technology, Iran, 2006

A THESIS SUBMITTED IN PARTIAL FULFILLMENT OF THE REQUIREMENTS FOR THE DEGREE OF

MASTER OF APPLIED SCIENCE

in

THE FACULTY OF GRADUATE STUDIES

(Mechanical Engineering)

The University of British Columbia

(Vancouver)

October 2008

Abstract

Microfluidics refers to devices and methods for controlling and manipulating fluid flows at length scales less than a millimeter. Miniaturization of a laboratory to a small device, usually termed as lab-on-a-chip, is an advanced technology that integrates a microfluidic system including channels, mixers, reservoirs, pumps and valves on a micro scale chip and can manipulate very small sample volumes of fluids.

While several flow control concepts for microfluidic devices have been developed to date, here flow control concepts based on thermally responsive polymer solutions are presented. In particular, flow control concepts base on the thermally triggered reversible phase change of aqueous solutions of the polymer Pluronic will be discussed. Selective heating of small regions of microfluidic channels, which leads to localized gel formation in these channels and reversible channel blockage, will be used to control a membrane valve that controls flow in a separate channel. This new technology will allow generating inexpensive portable bioanalysis tools where microvalve actuation occurs simply through heaters at a constant pressure source without a need for large external pressure control systems as is currently the case. Furthermore, a concept for controlled cross-channel transport of particles and potentially cells is presented that relies on the continuous regeneration of a gel wall at the diffusive interface of two co-streaming fluids in a microfluidic channel.

Contents

Abstract ..... **ii**

Contents ..... **iii**

List of Tables ..... **vi**

List of Figures ..... **vii**

Acknowledgment ..... **xv**

Dedication ..... **xvi**

CHAPTER 1 ..... **1**

Introduction **1**

1.1 Preliminary Remarks 1

1.2 Flow in Microfluidic Channels 2

1.3 Microflow Control Concepts 5

1.4 Research Objectives 7

1.5 Organization of the Thesis 8

CHAPTER 2 ..... **9**

Properties of Thermally Responsive Fluids **9**

2.1 Introduction 9

2.2 Thermally Responsive Fluids 11

2.3 Properties of Pluronic Solutions 12

CHAPTER 3 ..... **22**

Fabrication Techniques and Experimental Setup 22

3.1 Introduction 22

3.2 Fabrication of Microchannels using Soft Lithography 24

3.2.1 Photolithography 24

3.2.2 Soft Lithography 31

3.3 Fabrication of a Multilayer Microfluidic Platform 35

3.4 Parylene Coating of the Channels 42

3.5 Experimental Setup 46

3.6 Micro Particle Image Velocimetry (PIV) 47

CHAPTER 4 52

Moving Temporary Wall in Microfluidic Devices 52

4.1 Introduction 52

4.2 Experimental Results 54

4.2.1 Wall Formation inside the Channel 55

4.2.2 Flow Field in the Microchannel 57

4.2.3 Variation of Wall Thickness 60

4.2.4 Diffusion across the Microchannel 65

4.2.5 Mechanics of Wall Formation 70

4.3 Analytical Discussion 74

4.4 Conclusion 77

CHAPTER 5 78

A Multi-layer Microfluidic Platform Using Thermally Actuated Polymer Solutions

78

5.1 Introduction 78

5.2 Flow Control Mechanisms 80

5.2.1 Principle of an Active Thermal Hydrogel Valve 80

5.2.2 Principle of a Low-Actuation Pressure Microfluidic PDMS Valve 83

5.2.3 Principle of a Thermally Actuated Microfluidic Relay Valve 86

5.3 Experimental Results 89

5.3.1 Membrane Deflection through Pressure 89

5.3.2 Flow Control with Heaters 92

5.3.3 Demonstration of the Thermally Actuated Microfluidic Relay Valve 96

5.4 Conclusion 101

CHAPTER 6 102

6.1 Summary 102

6.2 Future Work 103

Bibliography 105

Appendices 123

A. Spin Coating 123

B. Protocol for the Fabrication of SPR220-7.0 Mold 127

C. Oxygen Plasma Bonding Protocol 130

D. Spinning of PDMS Protocol 132

E. Fabrication of the Heaters by Lift-Off Process 133

List of Tables

Table 3.2-1 Physico-chemical properties of PDMS [150]…… 32

List of Figures

Figure 2.3.1 Viscosity as a function of temperature for different concentrations of Pluronic F127 in water from cone and plate viscometry at controlled shear stress (0.6 Pa·s) [9, 55]. This phase change is reversible and it is not associated with a volumetric change of the material..... 15

Figure 2.3.2 Shear thinning behaviour of 15wt% Pluronic solution [9, 55]. Viscosity is measured for different shear rates when the temperature increases from 25 to 35... 16

Figure 2.3.3 Viscosity as a function of temperature for different concentrations of sodium phosphate in a 15 wt% Pluronic F127 solution in water from cone and plate viscometry at controlled shear stress (0.6 Pa·s) [134]. 18

Figure 2.3.4 Viscosity as a function of temperature for high concentrations of sodium phosphate in a 15 wt% Pluronic F127 solution in water from cone and plate viscometry at controlled shear stress (0.6 Pa·s) [134]. 19

Figure 2.3.5 Phase diagram for a 15 wt% Pluronic F127 solution in water and sodium phosphate [134]..... 20

Figure 3.2.1 Yellow-room for Photolithography, Cleanroom class1000, Ampel, Nanofabrication Facility, UBC. 25

Figure 3.2.2 Exposed positive photoresist areas are dissolved by the developer solution and the mask pattern is transferred to the substrate through the photoresist. 27

Figure 3.2.3 Spin Coater 29

Figure 3.2.4 A pattern is printed on a transparency mask (a) and then attached to a heavy glass plate (b) for optical aligning enhancement purposes. It is put with a well-defined distance over the photoresist layer covered on a substrate. 30
Figure 3.2.5 Spectral content of the exposure lamp [149] 31
Figure 3.2.6 Soft lithography processes (a) mixed PDMS is poured over the substrate enclosed in a container (b) PDMS is cut and peeled off from the substrate (c) PDMS is trimmed (d) small holes are punched for the inlets and outlets (d) the PDMS chip is then bonded to a cleaned glass micro slide via the oxygen plasma method. 34
Figure 3.3.1 Reflowing of patterned photoresist of fluidic channel; (a) regular rectangular cross-section shape after photolithography process (Appendix B), (b) rounded shape of cross-section after reflowing (the edges of the channel are too steep for the Wyko NT1100 Optical Profiler to measure), (c) deflection of the membrane upon pressurizing, fluidic channel cannot be completely sealed, (d) complete sealing after reflowing. 37
Figure 3.3.2 Fabrication process of a multilayer thermally actuated micro relay Valve; (a) Fluidic layer and control layer are fabricated separately, (b) aligned and bonded together and peeled-off from the substrate. Heater elements pattern is fabricated on the glass substrate, (c) the whole chip is aligned and bonded using air (oxygen) plasma. 41
Figure 3.4.1 Conventional Parylene types structure; N, C and D [163]. 43
Figure 3.4.2 Parylene coating deposition (a) process steps [163] (b) Parylene coater used in this work. The probe on the right belongs to the liquid cold trap, while the coating chamber is kept at room temperature. 45

Figure 3.4.3 Parylene coating inside a microchannel (a) walls of the channel (part of its cross section is shown) are coated with a 4 μm thick layer [by courtesy of Jonas Flueckiger] (b) for long channel intermediate holes are being punched to give better access to the entire channel for sufficient Parylene coating. 46
Figure 3.5.1 Experimental Setup 47
Figure 3.6.1 Micro Particle Image Velocimetry (micro PIV) measurement technique for calculating the velocity field inside a microchannel [168]; (a) two laser pulses are exposured with a time difference through a filter (b) in a cross-correlation method, the captured images are compared in two different frames with Δt between them (c) Cross-correlation function R of image transmissivity (d) vector field inside micro chip at exposured area is achieved. 50
Figure 4.2.1 (a) Outline of the Y-shaped microfluidic device used for experimentation; the device consist of a structured PDMS piece that is bonded to a glass substrate; fluids are coming from inlet 1 and 2 and exiting the channel from the outlet, (b) Pluronic and Na_3PO_4 solutions are flowing side by side in the device where diffusion along the channel produces a mixed zone where the concentration of saline in the Pluronic stream increases along the channel. 55
Figure 4.2.2 Wall formation inside a 500μm wide and 10μm high microfluidic channel 56
Figure 4.2.3 Flow field of the Pluronic solution in the channel at a flow rate of $\boldsymbol{Qp = 3\mu l/h}$ in the presence of a 1 mol/L saline solution at a flow rate of $\boldsymbol{Qs = 30\mu l/h}$, and at a temperature T = 24°C. In (b) a finer resolution for the vector field measurement is chosen so that the velocity profile of the Pluronic solution is better illustrated..... 58

Figure 4.2.4 Flow velocity profiles from PIV at x = 1.5 mm, normalized separately for the Pluronic solution and the sodium phosphate solution with the flow rates of $\boldsymbol{Qp = 3\mu l/h}$ and $\boldsymbol{Qs = 30\mu l/h}$ respectively. 59

Figure 4.2.5 Thickness of the gel wall formed by a 15 wt% Pluronic F127 solution and sodium phosphate solution (a) at a concentration of 0.65 mol/L for different pressures (b) at a pressure $\boldsymbol{p = 5\ psi}$ driving the flow for different concentrations. The temperature of the device in both experiments is 24°C. 61

Figure 4.2.6 Change of the gel wall thickness per length along the channel as a function of (a) the pressure $\boldsymbol{p}$ driving the fluids and (b) the sodium phosphate concentration. The solid lines show curve fits to (a) $\boldsymbol{a1p - 1}$ (b) $\boldsymbol{a2cs + a3}$ 63

Figure 4.2.7 Epifluorescence images of the Pluronic solution (top bright stream) beside saline (bottom dark stream) flowing side by side at an ambient temperature T = 24°C; the Pluronic stream is seeded with fluorescent particles for flow visualization; (a) 15 wt% Pluronic solution and Na_3PO_4 solution with c_s= 1 mol/L at 5 psi (wall present), (b) 15 wt% Pluronic solution and Na_3PO_4 solution with c_s = 0.2 mol/L at 5 psi (no gel wall). 64

Figure 4.2.8 Section of the main channel of the device. Rhodamine B as a fluorescent dye is introduced into saline solution with the concentration of 0.3g/L. Brightness signal intensity of fluorescent under UV light can be calibrated with its bulk concentration to show the amount of dye diffusing into Pluronic stream across the channel. 66

Figure 4.2.9 Intensity of fluorescent dye across the channel at x = 3 mm downstream from the channel junction. Sodium Phosphate solution with the concentration of

0.2 mol/L is moving along Pluronic solution 15wt%; no gel formation is observed at the interface. 67

Figure 4.2.10 Fluorescence intensity of Rhodamine B diffusing from the saline solution across the gel wall into the 15 wt% Pluronic F127 solution, C_S = 1 mol/L, at x = 3 mm far from the entrance. 68

Figure 4.2.11 Fluorescence intensity of Rhodamine B in different regions; Pluronic solution, Sodium Phosphate solution (Saline) and Gel. Experiments show higher brightness intensity of dye inside Pluronic solution than Saline and Gel region. 69

Figure 4.2.12 Saline concentration across the channel; a 15wt% Pluronic Solution seeded with fluorescent particles moving along the sodium phosphate solution with the concentration of 1 mol/L at T=24ºC. 71

Figure 4.2.13 Movement of the wall; (a) Average of 50 streak images shows the direction of motion of the gel wall along the channel at a constant pressure p = 5 psi; (b) the velocity field from PIV of the moving wall shows a velocity toward the saline solution. The much higher velocities of the two streams compared to wall movement are not shown in this picture. 73

Figure 5.2.1 A schematic illustration of the principle of an active valve using a thermally responsive fluid in a microfluidic network. (a) Fluid from one channel is diverted into two channels at a channel bifurcation; (b) activating an integrated heater leads to localized gel formation in the corresponding microchannel, which subsequently blocks this channel to flow [9]. 81

Figure 5.2.2 The flow field at the channel bifurcation shown in Figure 5.2.1. The velocities were evaluated from images of the seed particles PIV; (a) before valve

actuation, (b) 33 ms later; blue: below 40 µm/s, green: 40-80 µm/s, yellow: 80-120 µm/s, orange: 120-160 µm/s [9]. 82

Figure 5.2.3 Multilayer PDMS valve schematic layout, (a) top-view: one fluidic channel above one control channel, the channels are separated at their intersection by a membrane. (b) side-view: the control channel is not pressurized and the valve is open (c) side-view: pressurizing the control channel deflects the membrane upward and it closes the working channel at the intersection. 84

Figure 5.2.4 Top-view and cross-sectional view of the multilayer PDMS microfluidic valve, (a) before pressurizing the control channel, and (b) after pressurizing the control channel , the membrane is deflected effecting a tight seal of the fluidic channel [160]. 85

Figure 5.2.5 Concept of the microfluidic relay valve; a) schematic top-view of the device layout with one fluidic channel above one control channel including heater; b) Side-view: When the heater is turned off, the thermally responsive fluid is driven through the control channel by a constant pressure source P_c, high enough to deflect the membrane; c) Side-view: When the heater is turned on, gel blocks the control channel and allows the membrane returning back and opening the fluid channel to flow at P_f. 87

Figure 5.2.6 A thermally actuated microfluidic relay valve 88

Figure 5.3.1 Schematic of the control and working channels; the membrane at the intersection has the dimension of 100 µm × 100 µm and it is 10 µm thick. 90

Figure 5.3.2 Membrane deflection at different pressure of the control channel shown in Figure 5.3.1; while there is no deflection at the pressure P_c = 3 psi (equal to P_f), the

membrane is fully deflected at the pressure P_c = 20 psi and closes the fluidic layer. Higher pressures of the control channel as shown in (e) results to control channel expansion. 91

Figure 5.3.3 Closing the working channel (P_f = 3 psi) through pressurizing the control channel; at P_c = 20 psi the working channel is effectively closed. 92

Figure 5.3.4 Pluronic solution 15wt% seeded with fluorescent particles is flowing inside the control channel near the heater element when the heater is off. When the heater is turned on the Pluronic solution receives enough heat in this area to form a gel and block the channel depending on the pressure driving the fluid. 94

Figure 5.3.5 Performance of the heater shown in Figure 5.3.4 at P_c = 20 psi; (a) average velocity for a section of the control channel is calculated using PIV before and after heater activation; (b) the 15 mW power versus time, the device can be kept closed for several minutes without a major change to the re-liquefying time. 95

Figure 5.3.6 Valve operation; Normalized velocity profile of each fluid is shown versus time upon an applied voltage pulse between t =10 s and t = 35 s; the heat pulse results in local gel formation inside control channel near the heaters. The process is reversible and the control fluid is cooled below its gel temperature and is opened to flow with $\Delta t_{c2} \cong 3.6\ \Delta t_{c1.}$ 98

Figure 5.3.7 Control and fluidic channels seeded with Fluorescent particles with a concentration of 0.02 wt % when the heater is switched on the control channel is blocked and the fluidic channel starts to flow (the control channel is out of focus). The valve is closed at (a); it starts to open at (b) and it is near fully-opened at (c).. 99

Figure 5.3.8 Velocity vector fields for control and working fluids before and after heater activation; (a) at t = 6 s the heater is off and the working fluid channel is closed while control fluid is driven with the average velocity V_c; (b) at t = 27.1 s the heater is on and the valve for the working fluid is opened to flow with the average velocity of V_f while the control fluid is stopped. 100

Figure A.1 A schematic view of a spin coater 123

Figure D.1 PDMS Spinning Curve 132

Acknowledgment

I would like to thank Dr. Boris Stoeber for his inspiration, friendship, encouragement, patience and unconditional support over the last two years. He taught me line by line and step by step and I was very fortunate to have this opportunity to work with him.

I would like to thank Dr. Mu Chiao and Dr. Karen Cheung for sharing their lab equipment, for being generous with their time and knowledge, and for providing intellectual support.

I am grateful to my dear friends: Mohammad Sepasi, Amin Karami, Daria Amin-Shahidi and Arash Jamalian for being supportive during these two years. We had a wonderful time together here. I would like to also thank Nazly and Jonas for their valuable input, Lars, Ramin, Micheal, Reynald and MEMS group members.

Finally, I wish to express my genuine gratitude to my father for his impressive daily 10 minute talks and my mother who is the source of all goodness.

Dedication

To my brothers Hamid and Mohammad

CHAPTER 1

Introduction

1.1 Preliminary Remarks

Microfluidics describes any kind of experimental and theoretical research of liquid streams generated in micro scale devices comprising microsized channels, including fabrication, handling and practical use of these chips [1]. This includes methods for handling, controlling and manipulating fluid flows in microchips such as for example streams of gases or fluidized solid particles. There are now several examples of systems and processes taking advantage of microfluidic devices such as inkjet printers, blood-cell-separation equipment, biochemical assays, chemical synthesis, genetic analysis, drug screening, electrochromatography, surface micromachining, laser ablation, mechanical micromilling. Particular applications include DNA analysis [2-5], capillary electrophoresis [6], PCR amplification [7-10], flow cytometry [11], chemical gradient formation [12, 13], immunoassays [14], cell manipulation [15], cell separation [16] and cell patterning [17, 18]. In addition to performing a complete process on a single microchip, microfluidic devices have also been used for single-structured measurement tasks including molecular diffusion

coefficients [19, 20], fluid viscosity [21], pH [22, 23], chemical binding coefficients [19] and enzyme reaction kinetics [24-26].

Microfluidic devices also provide the opportunity to study micro flow phenomena and understand the interplay between forces happening at small length scales. It will be discussed in section 1.2 that as an effect of miniaturization some of the forces that were not pronounced in macro scales become important. On the other hand, the forces of actuators, traditionally used for macro scale driving sources do not usually scale favorably for integration into microfluidic devices. In particular, using traditional concepts for an external actuator for micro valves or micro pumps limits the size of these devices and their scalability [27, 28]. Electrokinetic pumping and electroosmotic flow [29-32], electrowetting and surface tension-driven flows [33-36], electromagnetic forces [37, 38], and acoustic streaming [39-41] are examples of effects that can offer significantly high forces in microfluidic devices while permitting scalability and integratability. These effects are usually negligible at macroscopic length scales.

Thus, maintaining scalability of the devices by using favorable actuation forces, they can manipulate very small sample volumes of fluids to perform several operations in parallel on a single small size device, often termed as lab-on-a-chip (LOC).

1.2 Flow in Microfluidic Channels

Typical dimensions L of the height and width of microfluidic channels range from several microns to several 100s of microns. Aqueous liquids that are most

commonly transported in microfluidic systems have a density $\rho = 1000$ kg/m^3 and a shear viscosity $\mu = 10^{-3}$ Pa • s. With a typical flow velocity U = 1 mm/s, flow in microchannels is characterized by a very low Reynolds number $Re = \rho L U / \mu \approx 10^{-2} << 1$. The Reynolds number compares inertial forces and viscous forces of a fluid, so that a low Reynolds number corresponds to high viscous forces compared to inertia forces in a flow. Consequently, microfluidic flow is dominated by viscous forces, and inertia can in most cases be neglected [42, 43]. The flow regime in microfluidic channels can therefore be considered laminar in most cases [44]; while turbulence is not impossible in microfluidic devices, it is rather uncommon [43, 45].

The relative magnitude of the forces acting on a fluid can be well characterized using scaling laws. A scaling law describes the change of different forces with respect to a characteristic length scale, L while other conditions are constant, i.e. pressure, time and temperature. Surface forces and volume forces are proportional to L^2 and L^3, respectively. So the ratio of surface to volume forces is proportional to L^{-1} and increases dramatically at the micro scale ($L \sim 10^{-6}$ m) compared to conventional macro scale devices with dimension on the order of a few meters.

Thus, scaling laws are a tool to describe the effect of size on the relative importance of different forces. For example, consider gravity and capillary forces. The gravitational force is proportional to the mass, or volume, of a body, and therefore is proportional to L^3. The capillary force or the wetting force is what retains the fluid meniscus in a restriction. It occurs when the adhesive intermolecular forces between the liquid and a substance are stronger than the cohesive intermolecular forces inside the liquid. The amount of wetting depends on the energies (or surface

tensions) of the interfaces involved such that the total energy is minimized and it can be shown that it is proportional to L [44]. So the ratio of capillary force to gravity scales as L^{-2}. And so one can assume the predominance of capillary forces compared to gravity at small length scales while at the macro scale the capillary effect is neglected compared to gravity. Hence, the relative importance of various effects with characteristic size variation is of our particular interest for the study of governing microfluidic phenomena. This is conventionally described and characterized by using dimensionless parameters. The Reynolds number that was mentioned above is one of these dimensionless parameters and it shows the relative importance of inertial forces and viscous forces of a fluid.

The Péclet number, $Pe = L\,U / D$, is another dimensionless number describing the ratio of convection of a flow to diffusion, and it can be defined either for molecular diffusion Pe_m or for thermal diffusion Pe_T, using the molecular diffusion constant D or the thermal diffusivity α, respectively. The Péclet number can also be interpreted as the ratio of a characteristic diffusion time scale to a characteristic convection time scale. The molecular diffusion coefficient is low especially for liquids, such as $D = 6 \cdot 10^{-10}\ m^2/s$ for molecular diffusion of sodium phosphate in water [42]. The associated Péclet number $Pe \approx 100$ indicates high convective effects compared to molecular diffusion. However, in general there is no characteristic order of magnitude for the Péclet number in microfluidic devices [46]. In absence of turbulence in microfluidic systems as mentioned above, molecular diffusion is important for mixing, which can become rather difficult for long diffusion time scales [47]. Depending on the particular application purely diffusive mixing might be either

desired, especially where controlled mixing or separation of the species is needed, or not sufficient, when rapid mixing is required. For the latter case, several mixing strategies have been proposed for microfluidic devices that are effective despite the diffusion process being relatively slow [48-50].

For the thermal Péclet number heat transfer is analogous to mass transfer. With a much larger thermal diffusivity than molecular diffusivity, heat diffusion is often more significant than convection so that heat diffusion can be considered very effective over the typical short length scales of microfluidic devices [48, 51-54]. With a thermal diffusivity of water $\alpha = 1.41 \cdot 10^{-7}\ m^2 / s$, a typical time scale $t \sim L^2 / \alpha = 0.7$ ms for heat diffusion can be achieved across a 10 μm deep channel.

1.3 Microflow Control Concepts

As described in Section 1.2, fluids are expected to behave quite differently in microfluidic systems as compared to large scale systems because the different forces governing flow scale differently. This led to the development of new flow control strategies for small-scale systems as most conventional flow control concepts cannot be simply miniaturized. At the same time, microfluidics allows taking advantage of forces and effects that are negligible in large scale systems, thus opening new opportunities for innovation. The category of microvalves that are closest to their large scale counterparts simply obstruct a fluid conduit by moving a solid into the flow path; some of the actuation methods including electrostatic, piezoelectric, pneumatic, thermopneumatic, and electromagnetic actuation are more effective at the micro scale than in large-scale systems [19-24]. Among these concepts, passive micro

check valves have been developed [23] that use drag forces rather than inertia forces as well as microflow control strategies based on surface tension [8]. A common disadvantage of many of these designs is the requirement for complicated fabrication schemes, as well as unacceptable leakage rates, the need for complex external actuation, or the risk of irreversible blockage of the valve seat.

A different approach to valve actuation has been achieved using environmentally responsive polymers that undergo a volumetric or phase change in response to changes in temperature or concentrations. These concepts take advantage of the relatively fast propagation of temperature or concentration changes on the micro scale as discussed in Section 1.2, leading to fast actuator response. In one of the first examples of this approach, Fréchet and co-workers [2, 5] grafted a temperature-sensitive polymer (poly N-iso propylacrylamide) to the pore surfaces of a porous polymer monolith in a microchannel. As the device temperature transitioned through the lower critical solution temperature, the grafted polymer chain would undergo reversible swelling and collapse, leading to closing or opening of the pores of the polymer monolith, thus opening or closing the channel to flow. Mastrangelo and co-workers [3, 4] included paraffin in a sealed reservoir; upon heating the high volumetric expansion of the paraffin was used to actuate a membrane that then obstructed a flow channel, acting as a valve. This method separated the actuator from the fluid to be controlled, allowing a wide range of applications. A different category of environmentally responsive flow control methods uses hydrogels, which are either anchored inside microfluidic channels, or are transported with the flow. Such

hydrogels and hydrogel-based flow control will be studied more in the following chapter.

1.4 Research Objectives

The aim of this study is to develop new methods for flow control in microfluidic devices by using thermally responsive polymer (Pluronic) solutions with applications in the growing field of biotechnology. In particular, it focuses on the applications of Pluronic solutions as biocompatible thermally responsive working fluids for flow control in microfluidic systems which allow generating inexpensive portable bioanalysis tools. In order to use the Pluronic solution in the devices effectively, its material properties will be studied first.

The potential of cross-channel transport of cells in a microfluidic system using Pluronic solutions is being investigated. This method relies on the continuous regeneration of a gel wall at the diffusive interface of two co-streaming fluids in a microfluidic channel.

Furthermore, a new microflow control concept based on these thermally responsive polymer solutions is being developed in a multilayer PDMS device toward the fabrication of integrated microfluidic systems with valves, mixers and peristaltic pumps. Compared to the current technology that requires large external pneumatic control systems, this new technology is expected to allow generating inexpensive portable bioanalysis tools where microvalve actuation occurs simply through heaters and a constant pressure source.

1.5 Organization of the Thesis

This thesis is organized in the following order. Chapter 1: The flow properties in small size devices are introduced and different techniques for flow control in such devices are being presented.

Chapter 2: The material properties of the Pluronic solutions are investigated and their gel formation ability is determined at different temperature using rheometry. Furthermore, the effect of salt on the gelation of the Pluronic solutions is investigated for sodium phosphate.

Chapter 3: The fabrication process for the devices used in the project is discussed. Also the experimental setup is presented and particle image velocimetry for measuring the flow velocity in microfluidic channels is explained.

Chapter 4: The cross-channel transport of particles or cells in a microfluidic system using Pluronic solutions is being investigated. In particular, the formation of temporary gel walls inside a microfluidic device will be shown and the mechanics of this separation wall formation will be investigated.

Chapter 5: A thermally actuated microfluidic relay valve is presented and the valve performance is demonstrated.

Chapter 6: The conclusions drawn from the investigation are presented, and the prospects for applications and further developments are discussed.

CHAPTER 2

Properties of Thermally Responsive Fluids

2.1 Introduction

A wide variety of environmentally responsive fluids has been employed so far for flow control purposes in microfluidic devices. The actuation of these fluids occurs in form of a change in the temperature [55-64], viscosity [65, 66], phase [24, 67-71], volume [3, 72, 73], pH or ionic strength [72-84]. Most of these hydrogel microvalve principles take advantage of the favorable scaling of their underlying physical principles of operation at small length scales.

So-called environmentally responsive fluids or smart hydrogels were first reported to exhibit a significant expansion as a function of the pH value of the surrounding fluid by Kuhn *et al.* in 1948 [82]. This work was followed by work demonstrating the reversible volume change of these materials as a function of salt concentration in large scale systems in 1950 [81]. The hydrogels investigated in these studies were able to change their volume in a reversible and reproducible manner by more than one order of magnitude, which corresponds to the largest volume change

known for solid state materials. These studies, as well as the following work by T. Tanaka [73] at the beginning of the 1980s, inspired the development of other hydrogels with sensitivity to particular environmental parameters and the application of these materials in medicine, for pharmaceuticals, in sensors and for tissue engineering. Meanwhile, the potential of these hydrogels to control or regulate the transport of fluids was investigated and demonstrated through the first macrovalve for flow control that would reliably operate over a wide range of flow rates [83]. However, the major disadvantage of hydrogel-based valve principles was their slow response [73].

The first technologically relevant application of smart hydrogels to flow control was achieved with the pH-sensitive microvalve presented by Beebe *et al.* in 2000 [72] which relied on the swelling of a hydrogel in response to a change in pH, and used *in situ* photo patterning of the hydrogel in a microfluidic channel. The authors achieved a relatively fast valve response (less than 10 seconds), and demonstrated the use of hydrogel valves for autonomous microflow control. Since the swelling of hydrogel is diffusion controlled, the response time of these valves is mainly determined by the characteristic size of the actuator [77] and scales favorably at small length scales as discussed in Chapter 1. Specifically functionalized hydrogels have been developed for applications as microvalves in response to different parameters [56, 85-87] and micro sensors [77, 77, 84, 88]. Current applications for biocompatible smart gels include artificial muscles [89-93], and drug delivery [89, 90, 92, 92-98].

In a fundamentally different approach, thermally responsive polymer solutions have also been used as the working fluid in microfluidic devices. These polymer solutions solidify reversibly upon heating, so that selective heating of specific areas of a microfluidic system then causes localized gel formation to temporarily block a channel. Shirasaki and co-workers [8] used external infrared lasers for heating and localized gel formation and channel blockage for cell sorting; however, this approach depends significantly on transparency and absorbance of the materials involved. In a slightly different approach, electric heaters were integrated into a microflow system [85] to achieve rapid and controlled heating of the fluid and subsequent valving, taking advantage of the fast time scales for thermal diffusion in microdevices.

2.2 Thermally Responsive Fluids

Temperature responsive fluids (TRF) or temperature responsive hydrogels are among the most commonly studied and used materials for environmentally responsive microsystems [55-64]. Temperature responsive hydrogels react to the local temperature through phase transition or swelling and this thermo sensitivity can be used as an actuation method. Based on their reversible actuation mechanisms, smart hydrogels have been widely used in microvalves and microsensors as mentioned earlier [56, 88], where materials that are responsive to temperature changes offer the simplest way to control and modulate their actuation. Recently, these materials have gained increasing attention because of their potential application to biomedical systems and devices for tissues engineering [57, 58, 98], cell handling [97, 98] and drug delivery [97-110].

Thermally responsive fluids that undergo a phase change have a critical solution temperature (CST) at which the phase transition occurs, which can take place in form of a sol-gel transition upon heating or cooling. This transition occurs through interaction of polymer and water molecules in the case of TRFs exhibiting a critical phase separation temperature; otherwise, phase transition at a critical gelation temperature can be caused by intermolecular forces between polymer groups in the presence of water in form of hydrogen bonding and hydrophobic interactions due to the presence of hydrophobic groups such as methyl, ethyl and propyl [58]. Among the first group, poly(N-iso-propylacrylamide) (PNIPAAm) and also poly(N,N-diethylacrylamide) (PDEAAm) are the most extensively used materials [111]. The fundamental behavior of NIPAAm has been extensively studied and the possibility to form copolymers of NIPAAm by using other monomers has been demonstrated [112]. Gelation based on sol-gel transition of polymer solutions through hydrophobic/hydrophilic interaction on the other hand can be achieved with certain types of block copolymers made of poly-ethylene-oxide (PEO) and poly-propylene-oxide (PPO). Pluronics (or Poloxamers) and Tetronics consisting of PEO-PPO block copolymers belong to this group and are commercially available and commonly used to form TRFs [58, 61, 100, 113-116].

2.3 Properties of Pluronic Solutions

Pluronics are biocompatible symmetric triblock copolymers of poly(ethylene oxide)x -poly(propylene oxide)y -poly(ethylene oxide)x; P(EO)x–P(PO)y–P(EO)x. These amphiphilic copolymer have hydrophilic EO(x) and hydrophobic PO(y) units

where x and y can take on specific values depending on the particular kind of Pluronic [117]. Aqueous Pluronic solutions undergo reversible gel formation at a specific critical solution temperature that depends on the polymer concentration, its molecular weight and the polymer architecture [58, 61, 100, 113-116]. The sol-gel transition of Pluronic solutions occurs through three dimensional packing of polymer micelles, to achieve a hydrophilic/hydrophobic balance to form a lattice [63].

Above the critical micelle concentration (CMC) the polymers aggregate into multi molecular structures with a hydrophobic central core (PO) and a hydrophilic shell (EO) facing the external medium [118, 119]. At higher concentrations, above the critical gel concentration (CGC) the micelles can take on a cubic lattice structure [63]. Elevated temperatures lead to dehydration of the hydrophobic core and also increase the hydrophobicity of the hydrophilic blocks, which eventually leads to gel formation [120, 121]. The aggregation and phase behaviour of Pluronics have been extensively studied using several techniques including light scattering, NMR, SANS, SAXS, DSC, microscopy, and rheology [9, 63, 121-127].

Pluronic F127, or Poloxamer 407, has previously been used for several applications in drug delivery. Its chemical formula is $(PEO)_{106}(PPO)_{70}(PEO)_{106}$, it is a nonionic surfactant, and in aqueous solution it can thermo-reversibly change from its liquid phase into a gel structure at a gelation temperature T_G, which depends on its concentration. Aqueous solutions of Pluronic F127 are non-Newtonian fluids with thermo-thickening and shear thinning properties [9, 55]. The rheological properties of Pluronic F127 solutions including the effect of salts on gelation as well as their biocompatibility will be further discussed. In all these rheometry experiments

Pluronic F127 from BASF was used as received without further purification. Aqueous solutions of Pluronic F127 were achieved by mixing the polymer with distilled water under gentle agitation.

Thermo-thickening

Pluronic F127 solutions are thermo thickening materials. This means that upon heating their viscosity increases gradually over a wide range of temperatures until to their gel point, where the viscosity appears to increase dramatically. At higher concentration of Pluronic, gel forms at lower temperature. Stoeber *et al.* have shown this behaviour using rheometry for different concentration of Pluronic F127 [9, 55]. Continuous cone and plate vioscometry characterizes this phase transition under conditions that are relevant for the application to fluids streaming in microfluidic channels. This change in viscosity or phase change is completely reversible and after one thermal cycle, the shear viscosity returns to its original value. The phase transition between liquid and gel occurs over a narrow temperature range (0.5°C) as shown in Figure 2.3.1.

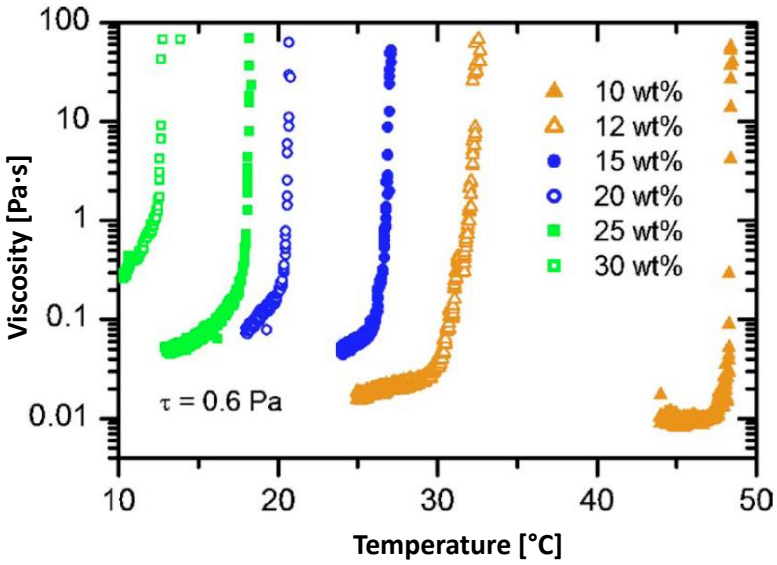

Figure 2.3.1 Viscosity as a function of temperature for different concentrations of Pluronic F127 in water from cone and plate viscometry at controlled shear stress (0.6 Pa·s) [9, 55]**. This phase change is reversible and it is not associated with a volumetric change of the material.**

Shear-thinning

Pluronic F127 solutions also show pseudo plastic flow behaviour (i.e. shear thinning). The viscosity of the solution occurs to decrease for increasing shear stress at a constant temperature as previously shown using rheometry [9, 55]. This behaviour is documented in Figure 2.3.2 and it shows that the viscosity decreases at higher shear rates. If at a set shear rate the corresponding shear stress exceeds the yield stress of the gel, the gel is reported to be constantly fractured [9, 55, 127]. However at low temperatures where the solution exists as an isotropic, micellar liquid, the shear viscosity is independent of shear rate and the solution of Pluronic F127 can be considered Newtonian. The shear thinning behaviour of

Pluronic solutions is believed to be related to the changes in its elasticity as a result of hard sphere interaction between packed micelles and hydrophobic interactions between the PPO core and water upon applied forces [128].

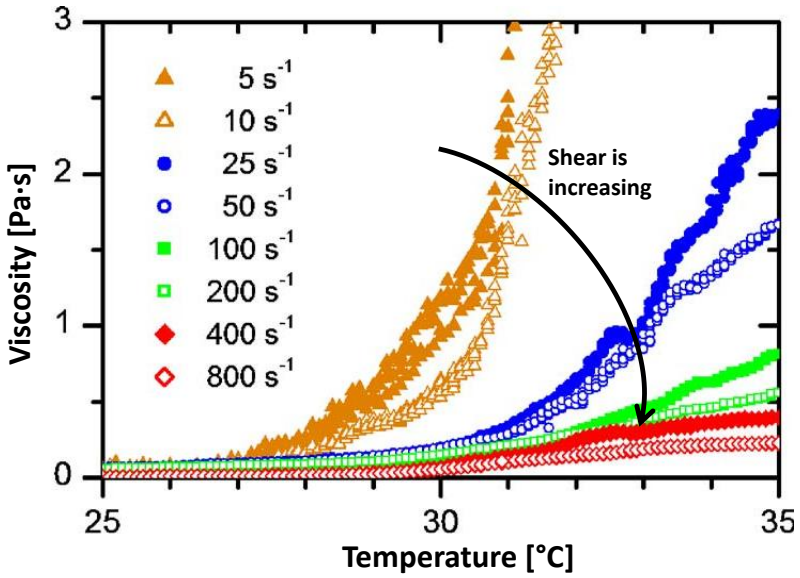

Figure 2.3.2 Shear thinning behaviour of 15wt% Pluronic solution [9, 55]**. Viscosity is measured for different shear rates when the temperature increases from 25 to 35.**

Effect of Ions on the Gelation Temperature of Pluronic Solutions

The effect of salt on micellization and also on the gelation temperature of Pluronic F127 has previously been shown [129-131][132]. In general, a lowering of the micellization and gelation temperature is observed upon addition of salt except for salts with large polarizable anions such as SCN^- and I^- where an initial increase is often encountered. The effect is often discussed in terms of "salting in" and "salting out", of "structure-making" and "structure-breaking", additives. The addition of salt is expected to further dehydrate PPO blocks and induce some dehydration of the PEO

blocks [132]. Almgren *et al.* have used a simple but effective approach to qualitatively predict the effects of additives: type one, those that increase the polarity difference between the solvent and the polymer will favor phase separation and decrease the micellization temperature. Salts such as NaCl, $MgSO_4$ and KF are depleted in the immediate vicinity of the polymer with its low polarizability, and increase the polarity of water. Phase separation is facilitated and so micellization occurs at a lower temperature. For salts of type 2, such as NaI or NaSCN on the other hand, the large, polarizable anion seems to partition slightly in favor of the polymer, increasing its polarity and thereby reducing the polarity difference. The polymer becomes more compatible with the solvent, and the micellization temperature is increased. It has been observed that the effect of salt on changing the gelation temperature is also consistent with the "salting-in" and the "salting-out" effect and the behavior of different types of salts on the micellization temperature is identical to the effect on the gelation temperature of Pluronic solutions [132, 133].

It has been also reported by Pandit *et al.* that the gel formation ability of Pluronic F127 can be lost at elevated concentrations of some salts [133]. The authors showed this effect for several salts by measuring the gel formation temperature and gel melting temperature for a solution of Pluronic F127. Here, the effect of sodium phosphate (Na_3PO_4, art. no. SX0710-1, EMD Chemicals, Inc.) on the gel formation of a 15 wt% Pluronic F127 solution was investigated, using cone and plate viscometry [134]. The viscosity of Pluronic solutions with sodium phosphate concentrations ranging from 0 to 0.253 mol/L of solution was measured at constant shear stress (τ =

0.6 Pa) while slowly increasing the temperature of the sample at a rate of 2°C / minute. Figure 2.3.3 shows the measured viscosity as a function of temperature.

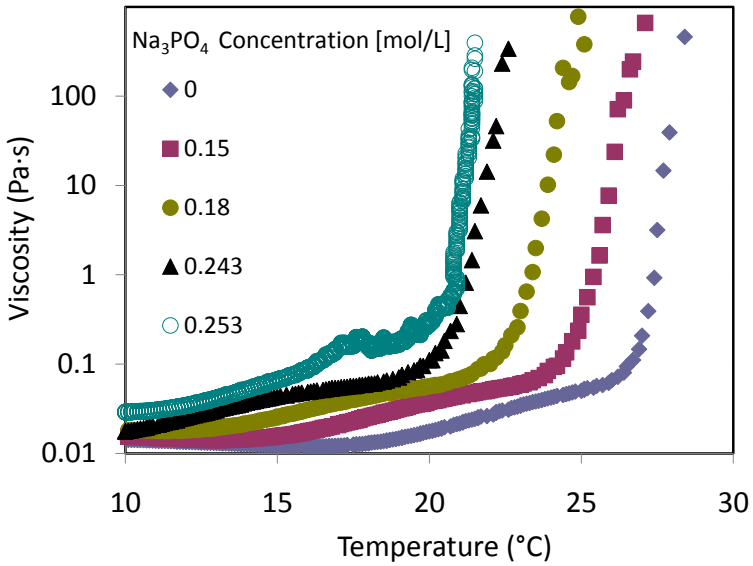

Figure 2.3.3 Viscosity as a function of temperature for different concentrations of sodium phosphate in a 15 wt% Pluronic F127 solution in water from cone and plate viscometry at controlled shear stress (0.6 Pa·s) [134]**.**

For each sample the viscosity increased first slowly until to a certain temperature from which on the viscosity occurred to increase by several orders of magnitude over only a few degrees Celsius in the same way as in the absence of salt. According to the measurements shown in Figure 2.3.3 the gel formation temperature of 26.5°C for a 15 wt% solution of Pluronic F127 decreases to 19.8°C for a sodium phosphate concentration of 0.253 mol/L.

At sodium phosphate concentrations above $C_{sp} = 0.253$ mol/L, no gel formation was observed using cone and plate viscometry at $\tau = 0.6$ Pa s, which is consistent with the work by N. K. Pandit and J. Kisaka [133]. However, Figure 2.3.4

reveals a slight increase in viscosity between T = 18°C and T = 27°C at C_{sp} = 0.275 mol/L of solution to no significant change in viscosity at C_{sp} = 0.300 mol/L of solution. The apparent slight increase in viscosity between these two sodium phosphate concentrations including the high noise level of the measurement might indicate the formation of a very soft gel over a narrow temperature range. Above the certain concentration C_{sp} = 0.253 mol/L of salt in a 15 wt% Pluronic F127 solution, the gel formation ability of the solution is lost. The effect of sodium phosphate on the gel formation temperature of a 15 wt% Pluronic F127 solution has been summarized in the phase diagram in Figure 2.3.5.

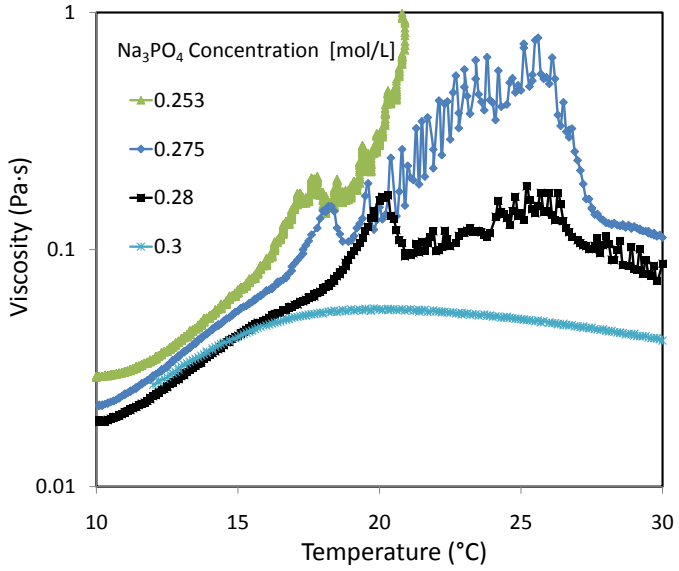

Figure 2.3.4 Viscosity as a function of temperature for high concentrations of sodium phosphate in a 15 wt% Pluronic F127 solution in water from cone and plate viscometry at controlled shear stress (0.6 Pa·s) [134]**.**

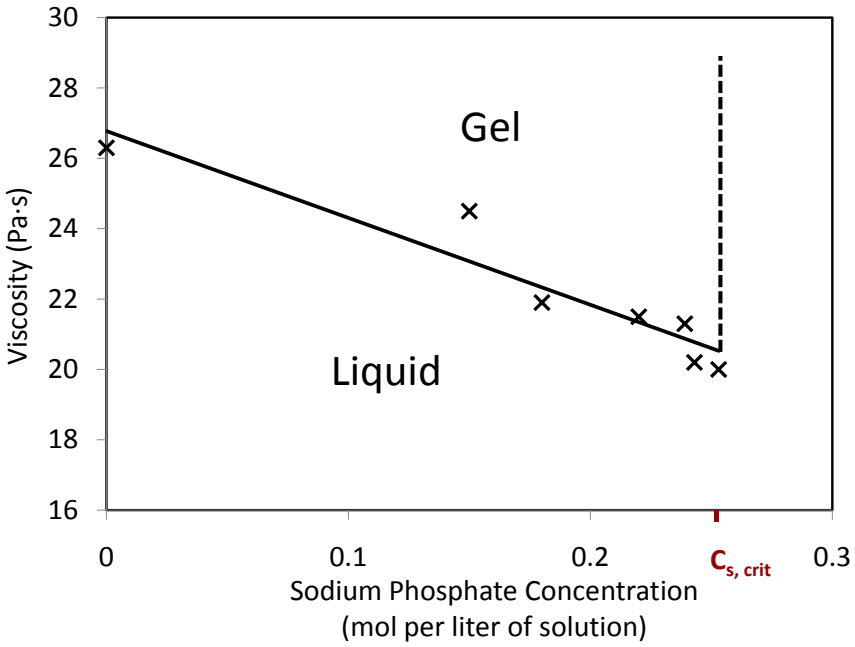

Figure 2.3.5 Phase diagram for a 15 wt% Pluronic F127 solution in water and sodium phosphate [134]**.**

Biocompatibility

Pluronic F127 solutions have been extensively studied as a potential drug delivery system due to their excellent biocompatibility [135] and ease of injection [136]. These block copolymers are among the very few synthetic polymeric materials approved by the U.S. Food and Drug Administration for use as food additives and pharmaceutical ingredients [137]. The micelles produced from Pluronic block copolymers have been found to increase the bioavailability of drugs. In recent years, these systems have been evaluated as potential candidates in gene therapies and vaccination strategies [137]. However, Khattak *et al.* showed that Pluronic F127 solutions at high concentrations, 15 to 20 wt%, can be problematic [138]. The authors measured the effect of F127 on viability and proliferation of human liver carcinoma cells at different concentrations, i.e. for

both liquid and gel formulations over 5 days. Even though at low concentrations (up to 5 wt%) cells proliferated and maintained high viability, at concentrations of 10 wt% and above the authors observed a significant decrease in cell viability, and no cell proliferation was evident after 5 days, while high concentrations (15 to 20 wt%), and in the gel phase, Pluronic F127 was reported to lead to complete cell death within 5 days [138]; however, addition of hydrocortisone let to a significant improvement in cell viability. In a different study, Wasan *et al.* showed that high concentration of Pluronic F127 led to notable toxicity after intraperitoneal injection in rats [135]. Therefore, while low concentration of Pluronic solutions below 10 wt% are biocompatible, higher concentrations up to 20 wt% are only recommended for delivery applications less than a day.

CHAPTER 3

Fabrication Techniques and Experimental Setup

3.1 Introduction

Small scale devices for microfluidic applications need careful and special methods of construction called microfabrication techniques. The domain of microfabrication involves length scales from as small as a fraction of a micrometer up to several centimeters. Cleanroom facilities, where the air is filtered to achieve a required level of cleanliness from impurities, and the temperature is controlled, are often necessary for manufacturing these small scale devices. Some subcategories of these techniques can be defined as “silicon technologies” and “soft fabrication technologies”. In soft fabrication technology, or soft lithography, polymers form the structured elements. Even though silicon microfabrication technology for MEMS and microfluidic devices is well established, often soft lithography is preferred. It has recently gained increased attention as it is less expensive and it allows easy and rapid prototyping [72]. Nevertheless, there are a few limitations to this technique, such as difficulties in designing active or moving parts due to common subtractive fabrication steps. Multilayer soft lithography (MSL) has

recently been developed as a fabrication technology based on soft fabrication techniques that bonds several device layers together [139]. This method will be further discussed in Section 3.3 and a thermally responsive fast micro relay valve fabricated using this method will be shown in Chapter 5.

In Section 3.2 the standard fabrication steps for forming a microfluidic channel using soft lithography are explained, where the elastomer PDMS (polydimethyl siloxane) provides the microfluidic structure. This device is later used for flow studies in Chapter 4. In Section 3.4 a method is presented for reducing the permeability of PDMS.

In Section 3.5 the general experimental set up and equipment used for flow visualization and investigation is presented. In Section 3.6, Particle Image Velocimetry (PIV), a technique for measuring the velocity field within a channel at a specified section, is introduced.

Further information regarding the fabrication of MEMS devices and especially microfluidic devices, using both silicon and soft technologies, can be found in several citations, such as [24, 71]. This chapter is not intended to be exhaustive and will only discuss fabrication of microfluidic channels by soft lithography methods (Section 3.2) including MSL (Section 3.3) for the fabrication of the device described in Chapter 5.

3.2 Fabrication of Microchannels using Soft Lithography

Typically microchannels are fabricated in various designs with rectangular or semicircular cross sections with cross-sectional dimensions from a few micrometers to several 100s micrometers and lengths of several millimeters depending on the application of the microfluidic device. Various such applications where discussed in Chapter 1.

In order to make channels with the desirable dimensions, first the layout of the structure is transferred to a substrate. This step is done by a method called photolithography in which photo sensitive materials called photoresist are structured in the dimensions of the future flow channel. Then the soft elastomer, PDMS which is liquid at ambient temperature, is poured over the molds. PDMS can then be cured at elevated temperatures. The cured PDMS sample is then peeled off the substrate and bonded to a glass micro slide, forming a close microfluidic device (these steps are described in detail below). Soft lithography is now a major technique for fabricating micro structures, and it has been extensively discussed in the literature [139-148].

3.2.1 Photolithography

The advent of photography was heralded by Niépce, a French researcher (1765-1833) who successfully created the first photograph. Photomasking followed later, much later indeed, by chemical processing and led to photolithography which now plays a central role in fabrication of ICs as well as MEMS and microfluidic

devices [24, 71]. In photolithography a thin layer of a photo-sensitive material i.e. photoresist, is selectively exposed by a light through an optical photomask. This mask protects certain parts of a photoresist layer from the illumination which will define the desirable patterns on the substrate after development. Here we have used optical lithography as the most conventional method for fabrication of microchannels using light with a spectral band between 250~450 nm. This procedure is done in a cleanroom environment in a yellow room which has light at the wavelengths that do not expose the photoresist (Figure 3.2.1).

Figure 3.2.1 Yellow-room for Photolithography, Cleanroom class1000, Ampel, Nanofabrication Facility, UBC.

Photoresists are photosensitive polymers whose chemical properties are changing upon exposure to light. They are able to undergo one of many possible reactions upon exposure, such as chain scission, cross-linking or other chemical

modifications in their polymer structure, polarity or solubility. Photoresists are divided into two primary classes, positive and negative photoresists. Positive resists are photoresists that become more soluble in the developer (aqueous based solvents) upon exposure. These resists typically undergo chain scission or have inhibitors that are rendered inactive when exposed. The use of such resists results in a wafer image that is identical to that of the mask (see Figure 3.2.2). AZ and SPR series and PMMA (Poly Methyl Metha Crylate) are examples of positive resists which usually offer higher resolution for pattern transfer. These resists are soluble in highly basic solutions such as KOH, TMAH, ketones and acetates. Negative photoresists are those that become less soluble in the developer upon exposure because of changed end-groups or a cross-linked network. The “negative” term implies the opposite image of the printout pattern transferred to the wafer. KTFR and SU8 are examples of types of negative photoresists. SU8 can be used both as a mold and also to form structures with a high aspect ratio.

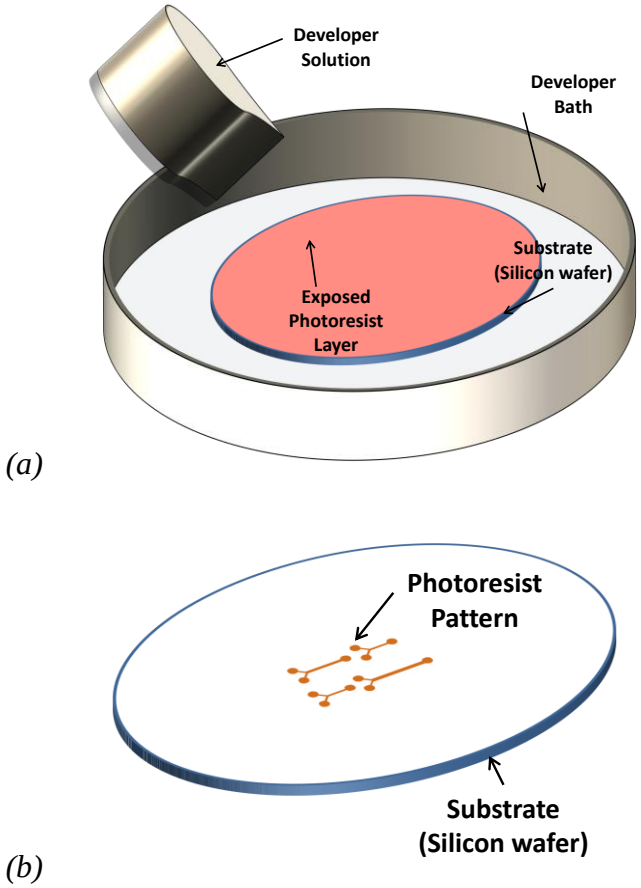

Figure 3.2.2 Exposed positive photoresist areas are dissolved by the developer solution and the mask pattern is transferred to the substrate through the photoresist.

The thickness of the photoresist layer will depend on the viscosity of the photoresist in solution and on the spin speed of the spin coating process (see Appendix A). The thickness of the layer achieved by spin coating is fairly uniform (to about several tens of nanometers [46]) across a substrate (silicon 4 inch wafers in mechanical grade from UniversiyWafer, South Boston, MA, USA). For a thickness h_0 of the initial layer poured with a pipette over the substrate, the thickness

$$h = \frac{h_0}{\sqrt{1 + \frac{4\rho\omega^2}{3\mu} {h_0}^2 t}}$$

(3-1)

of the coated layer depends on the density ρ of the fluid, rotation speed ω, on the time t of the spin process and on the viscosity μ of the photoresist. However this equation assumes that the entire surface is coated with a uniform thickness h_0 before spin coating which is not practically achievable. This equation was derived for Newtonian fluids where the film will thin out progressively over time with no equilibrium thickness. However, the flow behavior of Photoresists is non-Newtonian. Some other empirical relations exist which are based on more practical parameters such as the amount of fluid poured on the surface. Besides an experimental calibration curve is often provided by the photoresist manufacturing company.

After spin coating, the coated layer of photoresist is soft baked to remove the solvent and form a stable film for the exposure step. Then as it was shown in Figure 3.2.2, the coated wafer is put in the developer bath and the exposed area are solved and washed away (for positive photoresists). The positive photoresist SPR220-7.0 by Shipley was used in the photolithography process to fabricate channel molds with the height around 10 μm and it was developed by the MF-24A developer by Microchem. These patters on a glass substrate are then used as the mold to form microchannels for the experiments that will be shown in Chapter 4 and in Chapter 5.

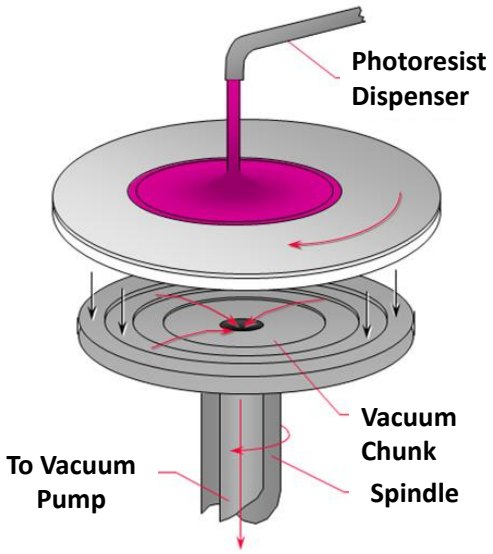

Figure 3.2.3 Spin Coater

Photomasks are generally thick plates (a few millimeter in thickness) made of quartz which carry the photolithographic pattern for example in a chrome layer. When moderate resolution is sufficient at the order of 50µm, high-quality printout on a transparency paper attached to a thick glass plate can be used. Many of the masks used for the work were produced by CAS (CAD/Art Services, Inc., Bandon, OR, U.S.A) in form of photoplot film with a resolution of 5 µm. The printed mask as shown in Figure 3.2.4 is attached to a thick glass plate to keep it flat and the light is exposed through it onto a thin layer of photoresist on a wafer, while having a well defined distance between mask and wafer.

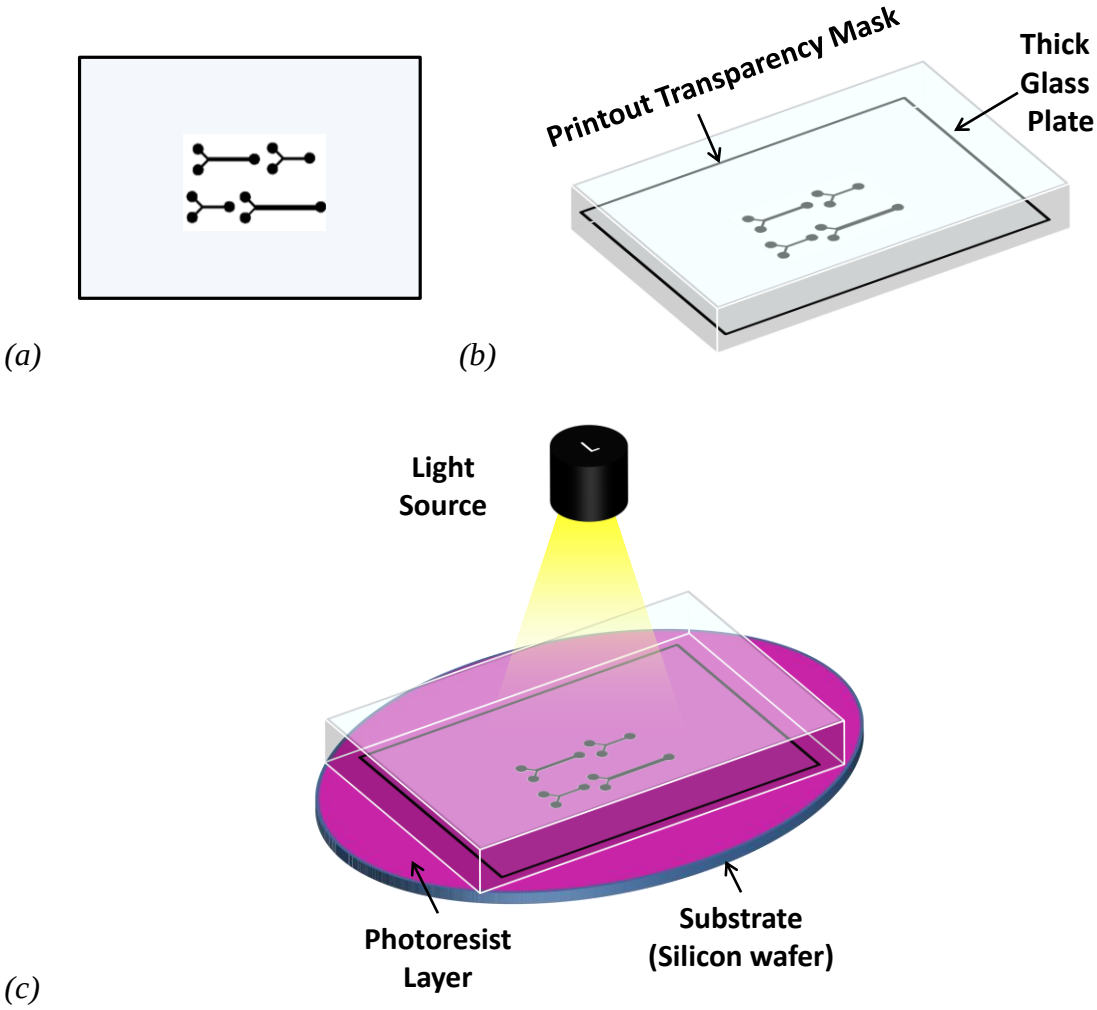

Figure 3.2.4 A pattern is printed on a transparency mask (a) and then attached to a heavy glass plate (b) for optical aligning enhancement purposes. It is put with a well-defined distance over the photoresist layer covered on a substrate.

The exposure process of the samples in our experiments is done by a Canon Mask Aligner PLA-501F (100mm) in the Ampel cleanroom, UBC. This mask aligner has three contact modes; contact hard, contact soft and proximity (the mask can be set to be between 10-90 μm above the resist). The latter case is usually more favorable since the contact mode carries the risk of resist sticking to the mask or scratching of

the mask. It uses a super high pressure mercury lamp USHIO (250W) with the light spectrum shown below. Based on the energy given to square inches of the substrate per second, the required time for exposing the whole layer of a certain photoresist with a specified thickness can be determined.

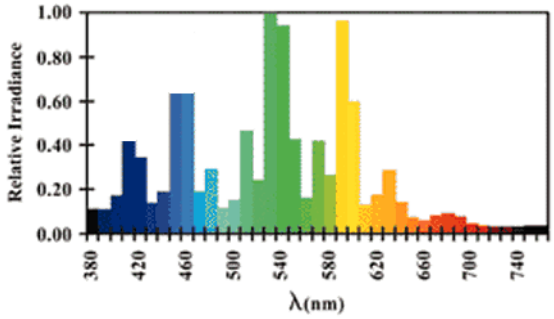

Figure 3.2.5 Spectral content of the exposure lamp [149]

3.2.2 Soft Lithography

This is a molding process and a photolithographed pattern of photoresist on the substrate serves as the molds for forming the microchannels and has the dimensions of these channels. As previously mentioned, in the soft lithography process, this pattern is used to fabricate the final device using an elastomer which becomes cured at elevated temperatures. We have used PDMS as an elastomer to make microfluidic channels [140, 141]. PDMS belongs to a family of polymers that notably contain silicon oils and some of its physico-chemical properties are mentioned in Table 3.2-1. The PDMS we used is a two-component system containing RTV615A and RTV615B purchased from GE Silicone. They consist of a vinyl terminate prepolymer with high molecular weight and a crosslinker containing several hydride groups on shorter polydimethylsiloxane chains. RTV615A and RTV615 B are usually mixed with a mixer at a ratio of 1:10. The mixer, ARE250, from THINKY

corporation, provides excellent mixing as well as de-aerating enabling it to mix these components uniformly without leaving any large bubbles of air inside the mixture.

Table 3.2-1 Physico-chemical properties of PDMS [150]

Density	Around 0.97 kg/m^3
Optical	Transparent, between 300nm and 2200nm, Index of refraction of 1.4
Electrical	Insulating, breaking field 20 kV/cm, Conductivity 4×10^{13} Ω·m
Mechanical	Elastomeric, Young's modulus 360-870 kPa, Poisson ratio 0.5
Thermal	Thermal conductivity~0.15 W/mK,
Hydrophobicity	Highly hydrophobic, contact angle 90-120°
Toxicity	Nontoxic, Nonirritating to skin, no adverse effects on rabbits and mice, only mild inflammatory reaction when implanted

Afterwards, this mixture is poured on the photoresist and the substrate and it is cured at 80°C for 2 hours for complete curing (Figure 3.2.6). 3 or 4 hours more of curing has been recommended for biological analysis devices for improved biocompatibility and cell viability. Then, the PDMS layer is cut with the knife and is peeled off from the substrate. If the mixing was correctly completed, no sticking of the PDMS to the substrate should occur during the peeling off process. To avoid sticking of PDMS to the surface when a thin PDMS layer over the substrate is used, molds are exposured to tri-methyl-chloro-silane (TMCS) vapor for a few minutes

arranged in a close container sealed with parafilm [142, 151, 152]. The peeled-off PDMS device, which now carries the pattern of the photoresist is carefully cut and trimmed. Small holes are punched in the areas designed for inlets and outlets (see Figure 3.2.6). The last step is to bond this device to a glass microscope slide for boundary creation to form the remaining 4^{th} wall of the device. Bonding is assisted by a method in which both surfaces are exposed to an air plasma [152-154]. It is believed that air (oxygen) plasma introduces silanol groups (Si-OH) to the PDMS surface at the expense of methyl groups ($Si\text{-}CH_3$). Bringing the surfaces into contact yields Si-O-Si bonds under loss of a water molecule. These covalent bonds form a tight, irreversible seal which will be torn if the bonds are attempted to be broken [150, 152-155]. Another bonding method, without the use of air (oxygen) plasma, is based on diffusion and discussed in the next chapter. Then, for the ultimate sealing and bonding of glass to PDMS, the entire chip is heated at 80°C for one more hour.

We have also investigated using an adhesion promoter to improve adhesion of PDMS to glass but also to other substrates as well as aluminum and silicon without the use of air plasma [156].

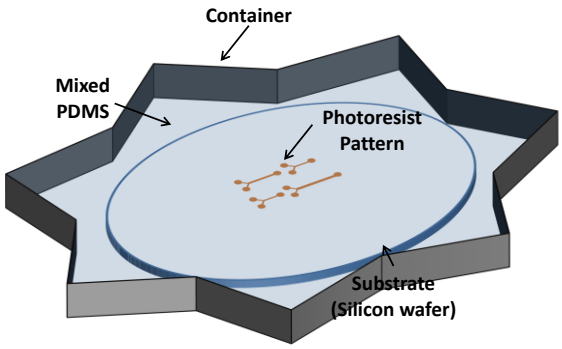

(a)

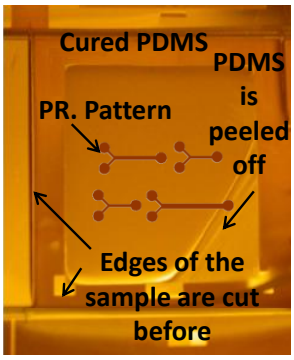

(b)

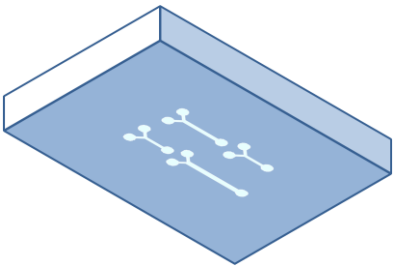

(c)

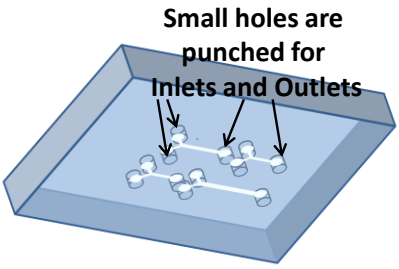

(d)

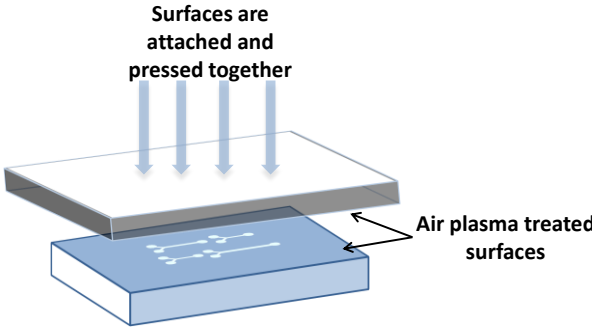

(e)

Figure 3.2.6 Soft lithography processes (a) mixed PDMS is poured over the substrate enclosed in a container (b) PDMS is cut and peeled off from the substrate (c) PDMS is trimmed (d) small holes are punched for the inlets and outlets (d) the PDMS chip is then bonded to a cleaned glass micro slide via the oxygen plasma method.

The Y-channel used in Chapter 4 was fabricated following the above photolithography process and soft-lithography steps. SPR220-7.0 from Microchem Corporation is used as the photoresist to form the mold in all devices. The protocols for SPR220-7.0 and oxygen plasma bonding can be found in Appendixes B and C respectively.

3.3 Fabrication of a Multilayer Microfluidic Platform

This section explains the method and steps that were used to fabricate the device that was used in Chapter 5 to show the proof of the concept of a thermally actuated microfluidic relay valve. The multilayer softlithography (MSL) technique was first developed by S. Quake *et al.* for fabrication of valves and pumps in PDMS [43, 142, 151, 157-159]. This technique is fully described in [135] and it is based on diffusion (of cross linker) between PDMS (GE RTV 615 A and B from General Electrics) layers mixed and cured with different base and hardener ratios, in our experiment RTV615A and RTV615B respectively. Here, bonding of PDMS to PDMS layers is used to demonstrate a new valving concept for a 2D microfluidic platform [135]with applications to biological assays as well as microfluidics.

The valve concept uses flow channels in two different layers, the fluidic layer and the control layer. The control layer is the layer that will be used to control the flow inside the fluidic layer. These layers are placed on top of each other in a way that at the intersection of channels in different layers a thin PDMS membrane separates these channels. This membrane will deflect into the fluidic channel and close this channel if the pressure in the control channel is high enough. Depending on

the order in which they are placed on each other, i.e. either fluidic channel top-control channel below or the opposite, the corresponding valve operation is characterized as push-up or push-down mechanism [158].

The fabrication of the control layers and the fluidic layers is consistent with the fabrication methods mentioned in the previous section. The molds for the fluidic channel and for the control channel are fabricated separately on different substrates. Then, fluidic channel molds are baked for 1 hour at 140°C so that the channels cross-section is rounded. This helps for better sealing of the fluidic channel by the deflected membrane [135]. While incomplete sealing with a rectangular cross-section appears as an "island" of contact in the flow channel, complete sealing accompanied with reflowed rounded shape is shown in Figure 3.3.1 where there is a continuous contact edge joining left and right edges of the flow channel. Therefore a lower pressure inside control channels are required to entirely close reflowed fluidic channels with a rounded cross-sectional area compared to the ones with rectangular cross-section.

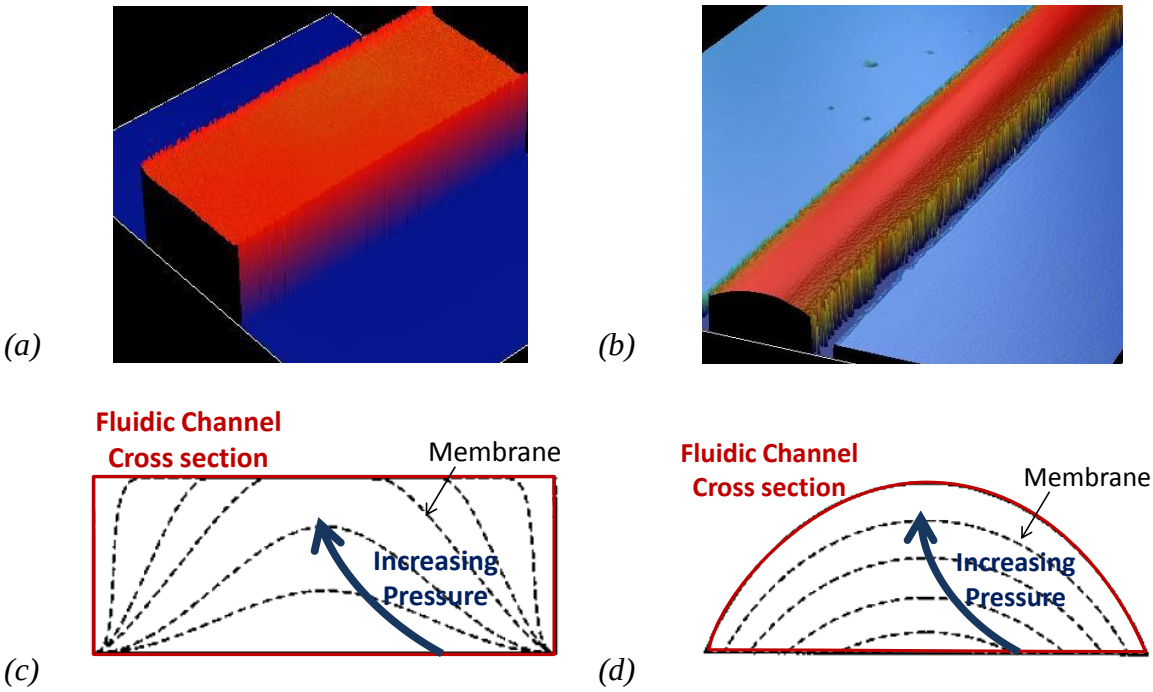

Figure 3.3.1 Reflowing of patterned photoresist of fluidic channel; (a) regular rectangular cross-section shape after photolithography process (Appendix B), (b) rounded shape of cross-section after reflowing (the edges of the channel are too steep for the Wyko NT1100 Optical Profiler to measure), (c) deflection of the membrane upon pressurizing, fluidic channel cannot be completely sealed, (d) complete sealing after reflowing.

Then two different batches of PDMS are mixed with different ratios of resin to hardener 1:5 and 1:20 for the fluidic and control channel molds respectively. As mentioned before, in the push-up mechanism the control channels are fabricated below the fluidic layer and the membrane is deflected upwards to close the fluidic channel (as shown in Figure 3.3.1). This mechanism needs a lower pressure for actuation than push-down mechanism [160]. The fluidic layer containing the fluid

channels is fabricated in a thick layer of PDMS while the control layer containing the control channels is thin. PDMS with the ratio of 1:20 (RTV615A to RTV615B) is spun over the control channel substrate. The thickness of the PDMS over the sample is defined by the spinning speed where acceleration and viscosity of mixture is kept constant with following the same procedure for spinning and mixing (i.e. linear acceleration and fixed mixing and de-aerating time). Since PDMS is non-Newtonian and viscoelastic, spinning conditions should be set carefully to achieve the aimed thickness (Appendix D). Following the mixing and de-aerating procedures in Appendix D, it can be shown that PDMS can be uniformly coated on a 4-inch wafer and its thickness

$$\text{Thickness}(\mu\text{m}) \cong \frac{\text{K(constant)}}{\text{speed of spinning(rpm)}} \qquad \textbf{(3-2)}$$

can be estimated approximately with $k = 70175\ \mu\text{m} \cdot \text{rpm}$. After spin coating of PDMS over the control channel mold, it is put into the oven at 80°C for 1.5 hour to be cured.

The fabrication of the fluidic layer follows exactly the same microchannel fabrication procedure of the last section but with the PDMS ratio of 1:5; PDMS is peeled off after curing at 80°C for 1.5 hour. Curing of control and fluidic molds are done at the same time in the oven. Afterwards, the fluidic layer is carefully peeled-off from its surface and small holes for the inlets and outlets are being punched. The device is cleaned with ethanol and distilled water and dried. Then it is put on top of the PDMS layer with the control channels and the devices are optically aligned. No additional pressure is needed when the surfaces are being pressed together, however

visible bubbles between the surfaces have to be avoided during this process. The assembled PDMS layers are then put into the oven at 80°C for three hours. Since the concentration of the cross-linker is different in both layers, diffusion happens between the layers at the interface, making them bond together irreversibly during these 3 hours. Afterwards, the whole chip is peeled off from the control channel substrate, it is cut, trimmed and small holes for the inlets and outlets are being punched using a sharp needle (16 Gau-. ge = 1.65 mm diameter). In the current devices, some holes in the control channels are designed for Parylene coating (see Section 3.4) in a following process step and they will be closed in the final steps of fabrication. These holes are being punched in this step, too, very carefully not to damage the control channels. The whole chip is then carefully cleaned with ethanol and distilled water and it is dried. The process is illustrated in Figure 3.3.2.

In the process presented by S. Quake *et al.* [135] it was suggested to bond assembled set of PDMS layers to a cleaned glass slide to complete the fabrication of the device by pressing them together and heating them for 3 hours in an oven at 80°C. However, this bonding of PDMS to a bare micro slide is reversible and the PDMS can be peeled off afterwards. If a stronger bonding is needed, another layer of PDMS with different ratio of curing agent to resin, such as 1:10 can be spun onto the substrate and cured, and the entire fluidic and control layer can be bonded to this PDMS layer following the same procedure mentioned above. We have instead used the oxygen plasma and descum process described in Appendix C. This method of bonding followed by a pressing of the chip to glass under 10 lb weight for one day, seems necessary for our device as the whole PDMS chip is put on the glass substrate, which

carries heater elements with a maximum height of ~350 nm. Even though PDMS is stiff, under pressure for sufficient time after air plasma treatment, the surface of PDMS chip bends and sticks to the glass layer near the heater elements preventing leakage and providing a good seal.

The heaters on the substrate are fabricated by a lift-off process, which is explained in detail in Appendix E. We have used SPR220-7.0 to make the pattern on the glass substrate. Then evaporation of chromium (~20 nm) as an adhesive layer and gold, 99.99% from Technic Inc., Canada, (~300 nm) as the main electrical conductor material are deposited on the surface by e-beam evaporation 2000 (DeeWong). Afterwards photoresist is removed with acetone and the heaters remain patterned on the glass substrate. Finally, as mentioned above, the PDMS chip is bonded to the glass with the heaters and the fabrication of the device is complete.

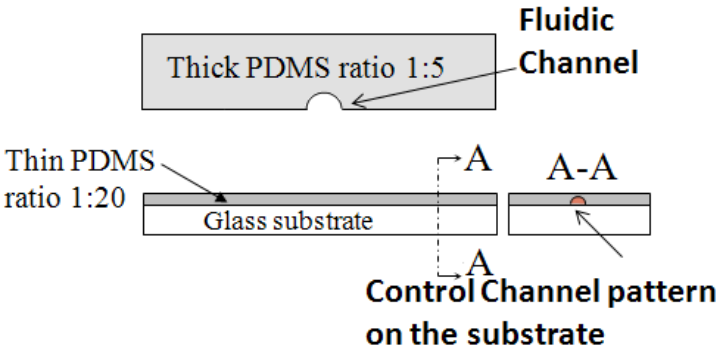

(a)

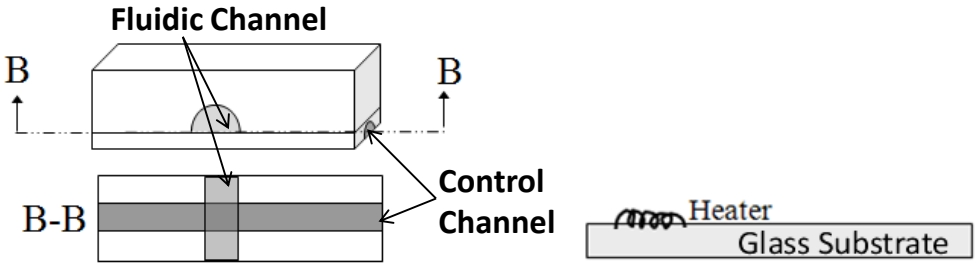

(b)

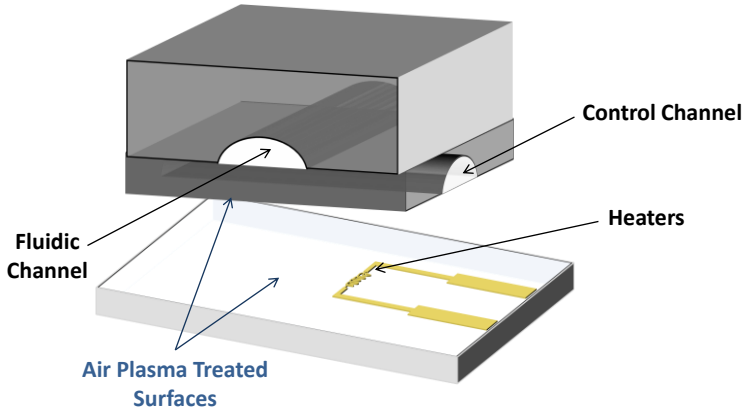

(c)

Figure 3.3.2 Fabrication process of a multilayer thermally actuated micro relay Valve; (a) Fluidic layer and control layer are fabricated separately, (b) aligned and bonded together and peeled-off from the substrate. Heater elements pattern is fabricated on the glass substrate, (c) the whole chip is aligned and bonded using air (oxygen) plasma.

3.4 Parylene Coating of the Channels

Parylene is the tradename for a variety of polyxylene polymers that can be polymerized from the vapour phase onto a surface, resulting in very uniform conformal coatings. Parylene is a biocompatible material with FDA approval, and it is highly corrosion resistant with low mechanical stress and low permeability to gases; it provides a thin and transparent coating. Parylene is inert and insoluble in most solvent systems within its useful range of temperature. Additionally, Parylene coatings offer thermal and UV stability, and dry-film lubricity. It can be used as a structural material for microvalves and micropumps and also to improve the biocompatibility of microfluidic device [161]. Parylene is being frequently used in the microelectronics industry as a surface passivation layer but has also been used in a wide variety of additional applications, including fabrication of microvalves in silicon microfluidic devices [162].

The three most common Parylene types are N, C, and D, as shown in Figure 3.4.1. Parylene N has a high dielectric strength with low dissipation factor and a frequency-independent dielectric const. Parylene C provides a useful combination of electrical and physical properties with low permeability to moisture and other corrosive gases; Parylene D has the same properties as Parylene C and additionally it withstands higher temperatures.

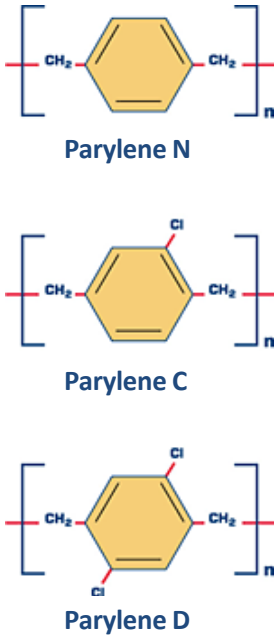

Figure 3.4.1 Conventional Parylene types structure; N, C and D [163]**.**

In this work, Parylene C was used for coating the inside of PDMS microchannels with a Parylene coater PDS2010 from Specialty Coating Systems. After fabrication microchannels are placed inside the coating chamber while inlet and outlet holes of the channels are open and so that Parylene in the vapour phase can reach the inside of these channels and coat the channel walls. The starting material for this deposition process is Parylene dimer in powder form. The Parylene deposition process consists of three steps that are being done at three different chambers with different temperatures: vaporization, pyrolysis and deposition. First the dimer is vaporized by heating. The conditions for vaporization are 150°C and 1 Torr, at which Parylene is in its dimer form (di-para-xylene). Then the dimer vapor is transported to a reaction zone where it is cracked at an elevated temperature to form the Parylene monomer (para-xylene). This pyrolysis step is maintained at 690°C and 0.5 Torr. Polymer (poly-para-xylene) is finally coated on the target at the deposition step the

conditions for which are 35°C and 0.1 Torr [164, 165]. The thickness of the coating layer on an open surface is estimated from the quantity of Parylene granule used for the process at 1.5 $\mu m \cdot g^{-1}$. However, Parylene has a very low diffusion length to reach inside microfluidic channels; this length is highly dependent on the cross sectional dimension of a channel. For example a 1 micrometer thick coating of a channel with rectangular cross section of 100 μm by 10 μm is achieved until 4 mm inside the channel. The Parylene deposition process is shown schematically in Figure 3.4.2.a. The result is a transparent and flexible coating that is strongly bonded to the PDMS.

The main reason for coating the inside of the microchannels with Parylene is to make the channel impermeable to the diffusion of water and thus prevent evaporation. Experiments have shown that about 1 μm is sufficient to prevent water diffusion and thus evaporation. Though, as mentioned earlier the Parylene diffusion length inside a micro channel with small dimensions is fairly short so that additional access holes ("intermediate holes") have to be punched along a long flow channel to achieve the required layer thickness along the entire channel (see Figure 3.4.3). After Parylene deposition, these holes are blocked by epoxy or dead-end tubing.

(a)

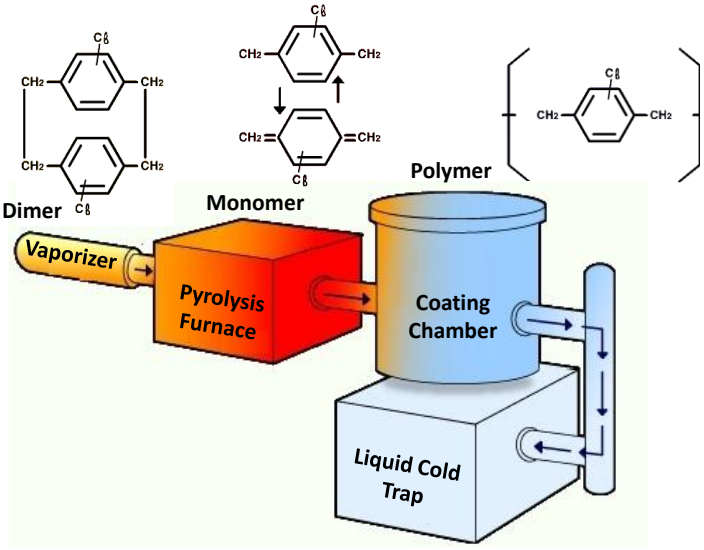

(b)

Figure 3.4.2 Parylene coating deposition (a) process steps [163] **(b) Parylene coater used in this work. The probe on the right belongs to the liquid cold trap, while the coating chamber is kept at room temperature.**

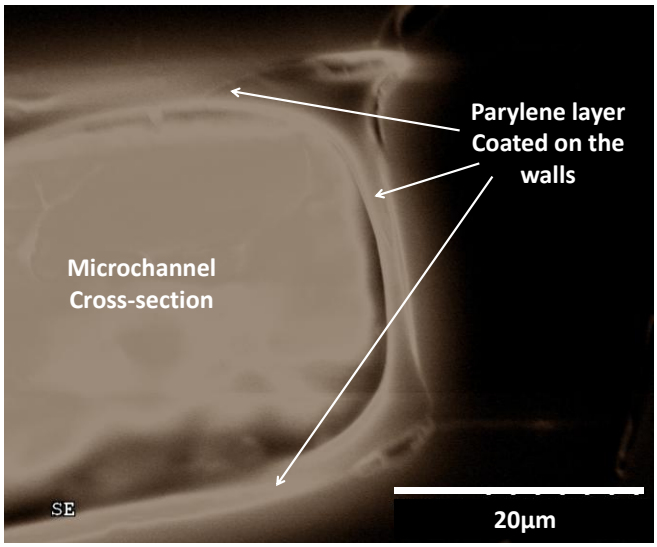

(a)

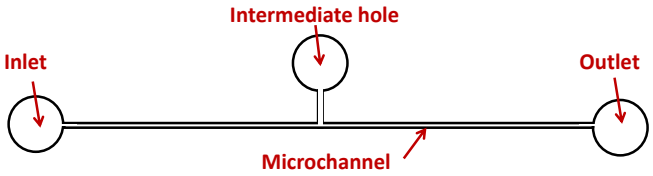

(b)

Figure 3.4.3 Parylene coating inside a microchannel (a) walls of the channel (part of its cross section is shown) are coated with a 4 µm thick layer [by courtesy of Jonas Flueckiger] (b) for long channel intermediate holes are being punched to give better access to the entire channel for sufficient Parylene coating.

3.5 Experimental Setup

The whole device is visualized by an inverted stage microscope and the external pressure control system and the flow control instrumentation are connected to flexible Tygon tubing inserted in the small holes of the microfluidic device. The 8-channel pressure source MFCS-8C 1000 by FLUIGENT provides pressures up to 1 bar with a 14 bit resolution to introduce the fluids into the microfluidic device. The

pressures can be set independently through a PC. The flow is imaged using the inverted stage microscope TE2000U by Nikon, which has been integrated into a microPIV (particle image velocimetry) system by LaVision. This microPIV system (details of this technique will be given in the next section) includes a dual Nd:YAG laser illumination (New Wave Research Solo I, 2 x 15 mJ/pulse) at 532 nm, as well as a continuous light source (metal halide lamp x-cite). Microscopic images were captured with an Imager Pro X 2M PIV camera. The basic setup is shown below.

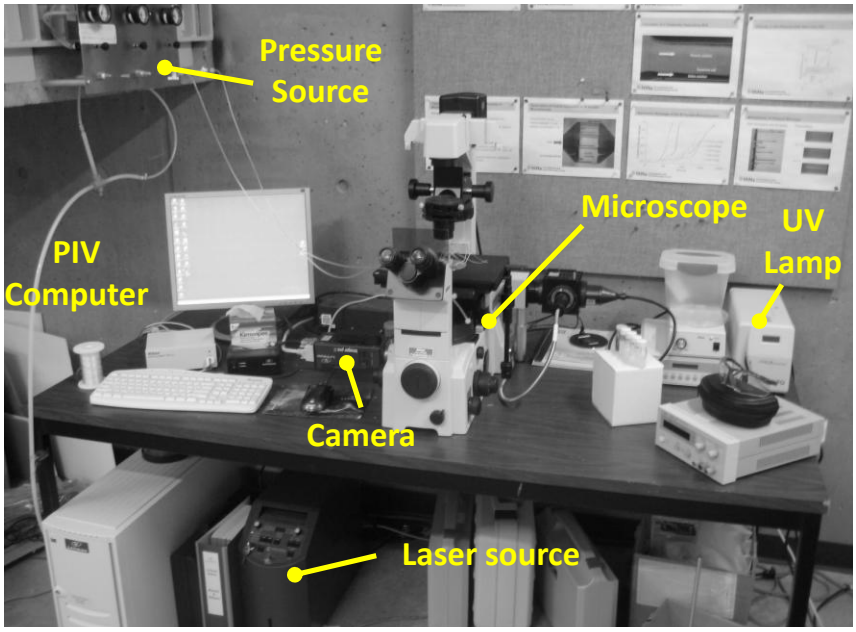

Figure 3.5.1 Experimental Setup

3.6 Micro Particle Image Velocimetry (PIV)

Particle Image Velocimetry (PIV) is a well-established measurement technique for macroscopic flows, and is extensively described in the literature. Micro-PIV is a modification of PIV in order to access and address the small scales of micro-fluidic devices. The first successful micro-PIV experiment was conducted by

Santiago *et al.* in 1999 [165], where the velocity field in a Hele-Shaw flow around a 30 micron elliptical cylinder was recorded. The system utilized a CCD camera, an epi-fluorescence microscope equipped with color filters, seeding particles tagged with a fluorescent dye, and a Hg-arc lamp to illuminate the flow continuously. A year later, Meinhart *et al.* [166] demonstrated a micro-PIV system consisting of the same general components with the exception that the continuous light source was replaced by two pulsed Nd:YAG lasers. The technique was applied to flow in a microchannel, and results with high spatial resolution and accuracy were reported.

The micro PIV technique for calculating the velocity field of flow in a microfluidic environment is based on the seeding the fluid under investigation with small particles for visualization. Fluorescent polystyrene beads with specific gravity of approximately 1.05 g/cm^3 available from a number of manufacturers are conventional seeding particles for this purpose. Particles with diameters ranging from tens of nanometers up to several microns, and fluorescent properties covering a vast range of excitation and emission wavelengths, have been widely used [167]. The requirement that particles faithfully follow the flow (small particle diameter) and have a density closely matching that of the suspending fluid is not difficult to satisfy for liquid flows. In addition, the particles should be large enough to dampen the effects of particle-fluid interactions (Brownian motion), and to provide a sufficiently strong fluorescent signal. When seed particles become sufficiently small, Brownian motion gives rise to random particle movement, preventing the particles to follow the flow faithfully [167].

The micro-PIV setup consists of a CCD-camera, dichromatic mirror, microscope objective lens and a concave (negative focal length) lens. The microflow is seeded with fluorescent particles. Their excitation and emission spectra are chosen such that they closely match the wavelength of the illuminating laser light and pass-wavelength of the dichroic filter. At time t, a pulse of laser light is directed through the concave lens, reflected via the dichroic, and sent through the objective lens in order to illuminate the flow field. A laser is used due to its high illumination power and short pulse duration, which is necessary in order to capture clear images of the seeding particles. Once illuminated, the seeding particles emit light of a wavelength longer than that of the laser light, which is transmitted through the dichroic mirror and captured by the CCD-camera. After a short period of time Δt, the particles have moved some distance inside the microfluidic device. At this time $(t + \Delta t)$, the laser is fired again to send a second pulse and another image of the fluorescent seeding particles is captured by the CCD camera. We now have two images of the particle field captured at two different times, namely t and $t + \Delta t$. By means of statistical methods, it is now possible to estimate the velocity field based on the displacement of the particles occurring between the two consecutive images. The images are divided into smaller interrogation regions. Local particle movement can be estimated by using cross-correlation of the pixel brightness of corresponding interrogation regions of the two images of one pair. This yields one displacement vector for each region, which can be converted into a velocity vector, knowing Δt [168]. The actual PIV processing is usually performed using FFT giving several peaks for the cross-correlation where

the peak height is a measure of the probability for that particular displacement value. The principle of micro PIV is shown in Figure 3.6.1.

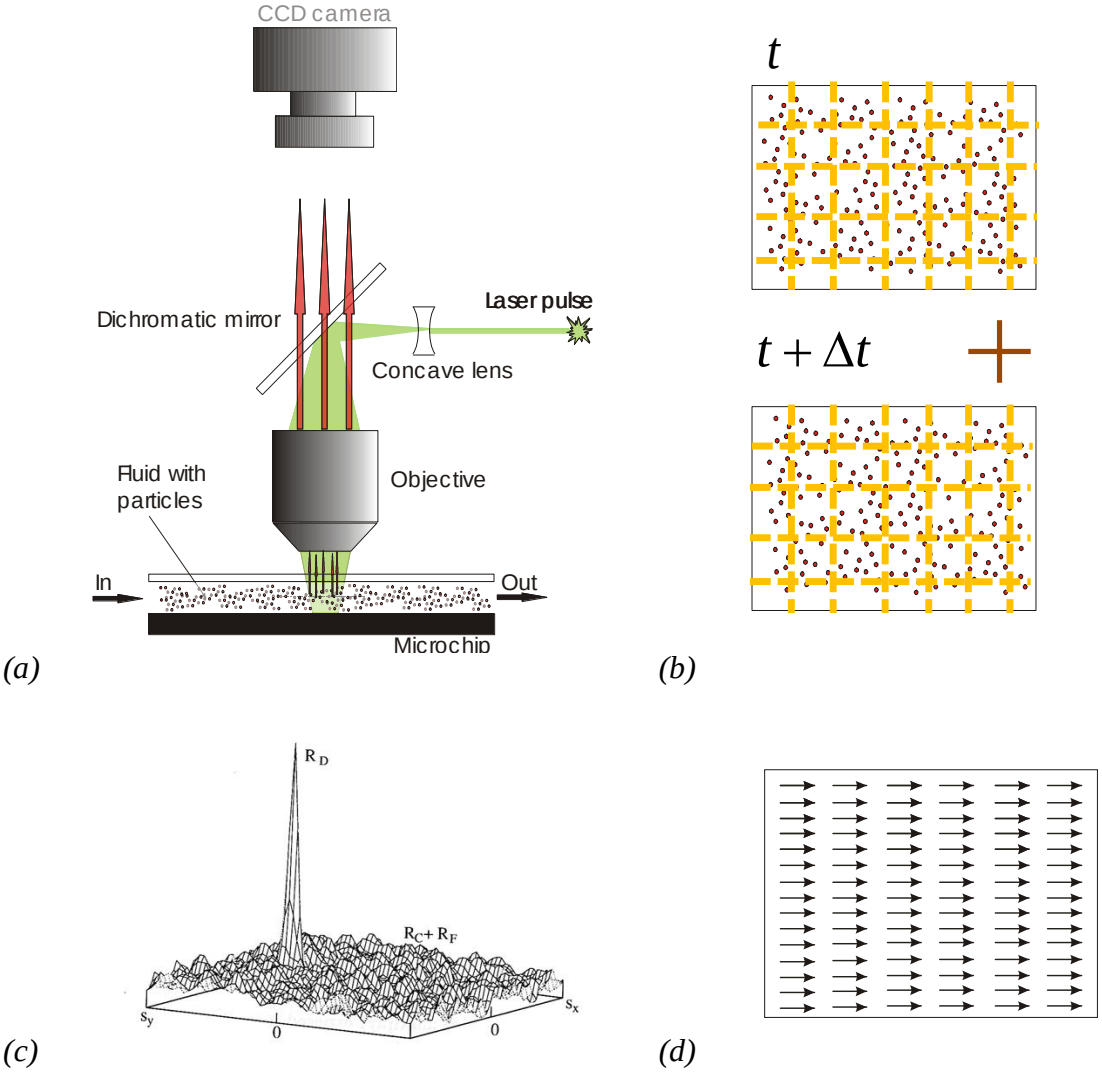

Figure 3.6.1 Micro Particle Image Velocimetry (micro PIV) measurement technique for calculating the velocity field inside a microchannel [168]**; (a) two laser pulses are exposured with a time difference through a filter (b) in a cross-correlation method, the captured images are compared in two different frames with Δt**

between them (c) Cross-correlation function R of image transmissivity

(d) vector field inside micro chip at exposured area is achieved.

Advanced calculation techniques extract the maximum amount of information from the raw images and are as important as high quality hardware. Three methods which manipulate the interrogation windows during processing are very successful. A cell shift during the calculation means that a first pass extracts a likely displacement vector for one interrogation window. In a second pass this rough estimation is used to look in the second frame not at the exact same cell position but at a position already shifted into the estimated direction. The advantage is that more identical particles can be found in both frames' interrogation window. The second technique is based on the first and can also be combined with others; here, a first pass starts with a larger interrogation window and following passes use this result and continue with smaller cell sizes. The third and most advanced technique uses a window deformation which leads to interrogation cells which are not square but their edges follow the local flow and therefore capture even more identical particles while still being able to correctly capture strong local variations.

To conclude, the main differences between PIV and micro PIV are the method of illumination and imaging. Furthermore, Brownian motion and the Saffman effect (particle migration in a shear flow), which can often be neglected in PIV experiments, might become important in micro PIV experiments. A review on micro PIV can for instance be found in the book by K. S. Breuer [167].

CHAPTER 4

Moving Temporary Wall in Microfluidic Devices

4.1 Introduction

As discussed in Chapter 1, the typical low-Reynolds number flow regime in microfluidic systems offers the opportunity for fundamentally different flow control strategies compared to macroscopic flow systems. In this chapter, a new microfluidic transport concept is shown where a temporary hydrogel wall is formed in a microfluidic channel. Specifically, controllable formation of a temporary wall in a microfluidic channel that can separate two co-streaming fluids is investigated. This concept allows having the two fluids in direct contact or keeping them apart from each other by changing the flow channel architecture through the addition of a separating wall during device operation. Diffusion of ions from one fluid stream into a co-streaming thermally responsive polymer solution is used to lower the local gelation temperature of the polymer, leading to formation of a gel wall in the center of the flow channel. This wall allows well controlled transport of particles from one stream into the other, as will be shown.

This mechanism relies on reversible gel formation of a thermally responsive polymer (Pluronic) in response to the concentration of certain ions as described in Chapter 2. We discussed and showed the effect of salts (sodium phosphate for instance) on reducing the gel formation temperature of Pluronic solutions by rheometry measurements in Section2.3. In a microchannel at a fixed temperature, Pluronic and sodium phosphate solutions are flowing side by side where diffusion of the salt into the Pluronic solution produces a so-called mixed region with a concentration gradient across the channel. As a result of this diffusion of salt into the Pluronic solution, there is a zone in this mixed region with a gel formation temperature equal or below of the fixed temperature of the whole device; in this zone the Pluronic solution forms a gel (see Figure 4.2.1).

Several flow control concepts were discussed in Section 1.3 and various hydrogel-based flow control methods were described in Section 2.1. Here we present a simple concept for formation of a temporary separating wall between two co-streaming fluids in a microfluidic device based on the thermally responsive hydrogel used in [9]. The gel wall at the interface can be removed at any time by lowering the device temperature by a few degrees. As opposed to the work by Beebe and co-workers [72], this mechanism does not depend on the swelling of a hydrogel, but rather on phase transition; in addition, our proposed concept does not require photolithographic patterning of a polymer inside a microchannel.

4.2 Experimental Results

A Y-shaped microfluidic channel system (depth: 10 µm, width: 500 µm) is fabricated by soft lithography as described in Section 3.2. Solutions of both, Pluronic (15 wt %) and sodium phosphate (0.5 – 1.0 mol/L) were prepared using distilled water and filtered afterwards with 2 µm HPF Millex Syringe Filters. Carboxylated 0.51 µm large fluorescent polystyrene microspheres (Fluoresbrite by Polysciences, Inc.) at a concentration of 0.02 wt% were used in the Pluronic solution for flow visualization (Sections 4.2.1, 4.2.3 and 4.2.5).

For Micro PIV measurements in section 4.2.2, Fluospheres® Carboxylated modified microspheres 0.2 µm large with orange fluorescent (540/560) (from Invitrogen Corporation) at a concentration of 0.02 wt% were used. The fluorescent dye Rhodamine B from (Sigma-Aldrich Co.) was mixed into one of the streams and used to evaluate diffusion. The fluids were driven at controlled pressure using an 8-channel pressure source MFCS-8C 1000 by FLUIGENT. Experimental setup and visualization method has been described in Section 3.5.

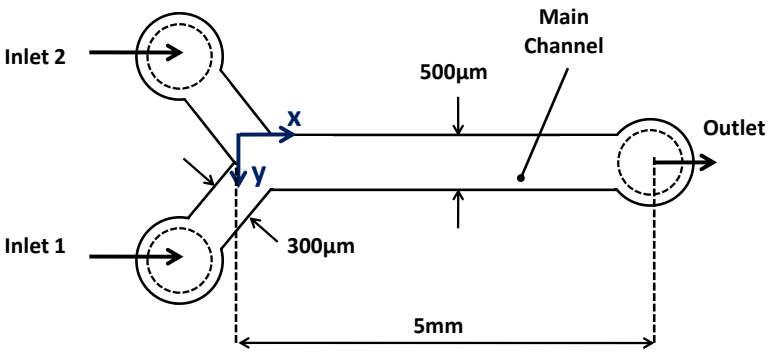

(a)

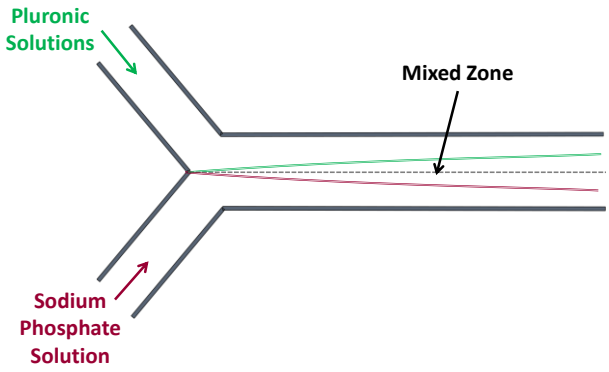

(b)

Figure 4.2.1 (a) Outline of the Y-shaped microfluidic device used for experimentation; the device consist of a structured PDMS piece that is bonded to a glass substrate; fluids are coming from inlet 1 and 2 and exiting the channel from the outlet, (b) Pluronic and Na_3PO_4 solutions are flowing side by side in the device where diffusion along the channel produces a mixed zone where the concentration of saline in the Pluronic stream increases along the channel.

4.2.1 Wall Formation inside the Channel

In a first set of experiments sodium phosphate solution with the concentration of 1 mol/L in distilled water and Pluronic solution with the concentration of 15 wt% seeded with 0.51 µm large fluorescent yellow particles at concentration of 0.02 wt%

are injected with syringe pumps to flow inside the channel. The temperature of the whole device is kept at ambient temperature measured as 24°C during the experiment. Because of the much higher viscosity of the Pluronic solution compared to the saline solution at this temperature, Pluronic was injected with the flow rate of $Q_p = 3\mu l/h$ and saline (sodium phosphate solution) with almost ten times greater flow rate, $Q_s = 30\,\mu l/h$, to keep the interface near middle of the channel. The gel region shown in Figure 4.2.2 is the area in which the particles look sharp. In the experiment shown in Figure 4.2.2, both fluids are injected by conventional syringe pumps that use stepper motors to push the plunger of each stream syringe. This results in the wavy shape pattern of the gel wall boundary near the Pluronic solution (Figure 4.2.2) whereas the high flow velocity of the saline stream spares it from disturbance caused by pulsatile flow produced by stepper motors.

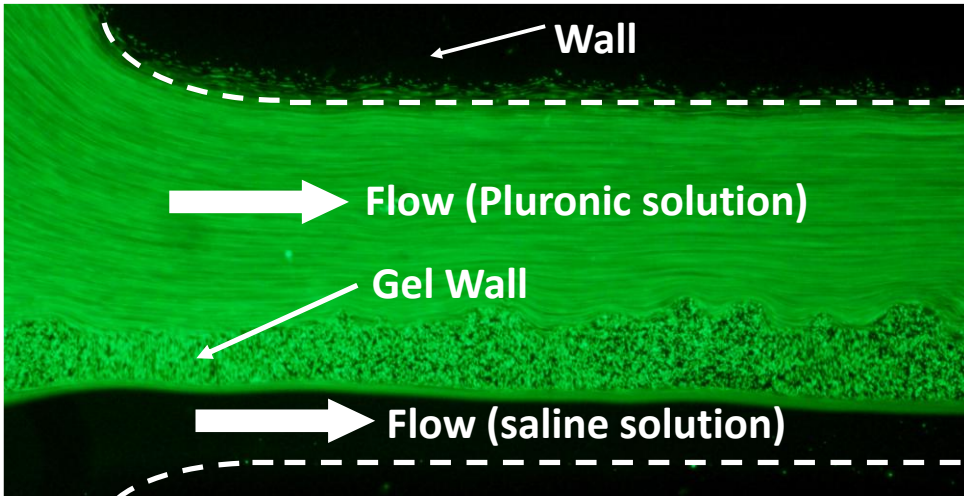

Figure 4.2.2 Wall formation inside a 500µm wide and 10µm high microfluidic channel

4.2.2 Flow Field in the Microchannel

Micro PIV is used to measure the velocity across the channel. Since the velocity of the saline solution is much higher than the velocity of the Pluronic solution, the flow profiles for both streams were determined in two different experiments under the same flow conditions in order to achieve higher accuracy. For measuring the flow velocity of the Pluronic solution, a UV light was used as illumination source to capture 0.51 µm large fluorescent polystyrene microspheres. The velocity vector field of the Pluronic stream is shown in Figure 4.2.3.a and Figure 4.2.3.b with different resolutions at the cross section. Because of the higher velocity of the saline solution, laser pulses were used for illumination, and the solution was seeded with 0.2 µm large carboxylated microspheres. However, care needed to be taken when adding particles to the saline solution, as these particles tend to agglomerate in the saline solutions. Therefore, PIV measurements for those solutions are difficult to achieve as there is a high risk of clogging the device with particles. Both separate microPIV measurements have been combined into the graph in Figure 4.2.4, which shows the velocity profile of the fluids for one channel cross-section.

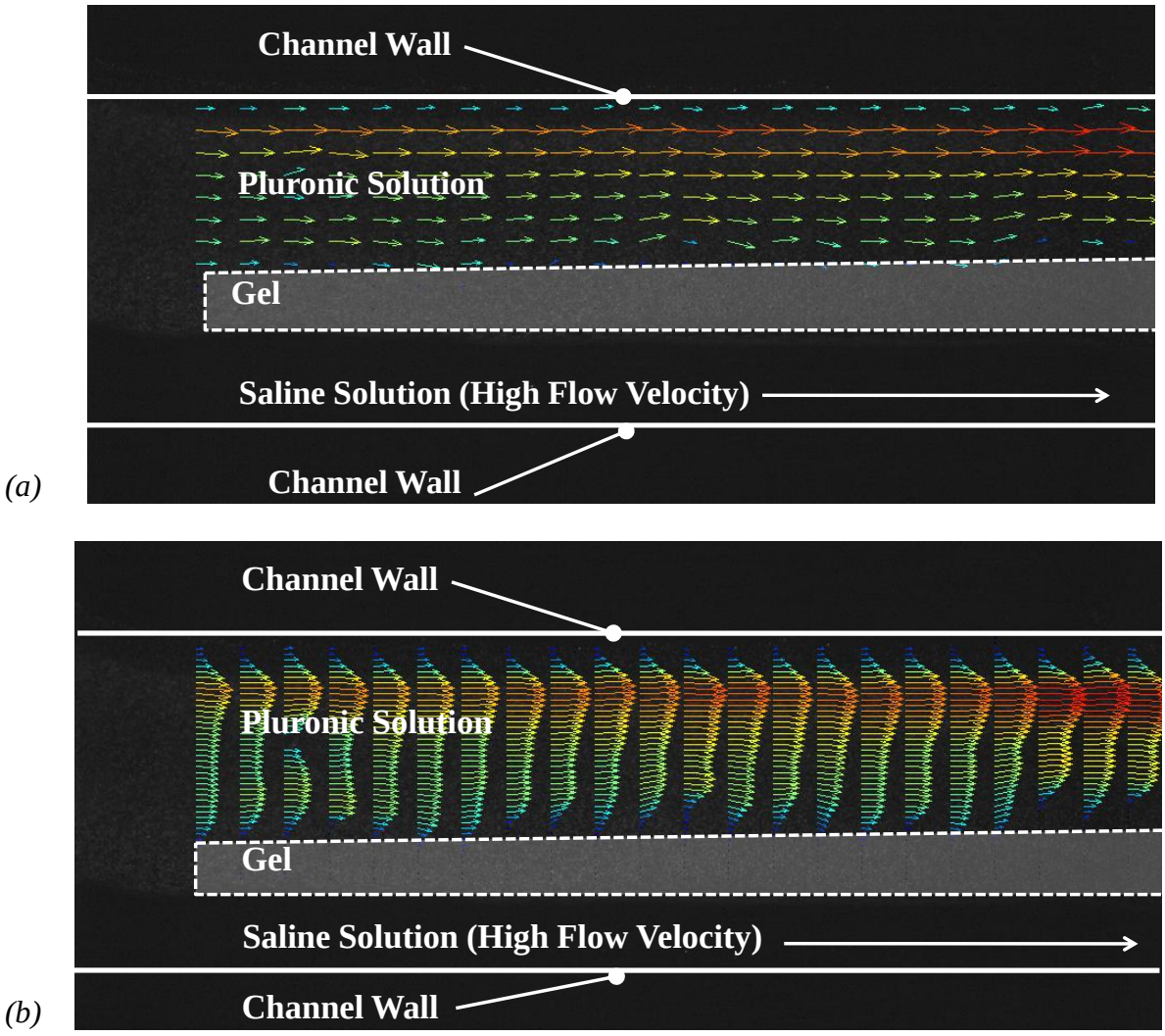

Figure 4.2.3 Flow field of the Pluronic solution in the channel at a flow rate of $Q_p = 3\mu l/h$ in the presence of a 1 mol/L saline solution at a flow rate of $Q_s = 30\mu l/h$, and at a temperature T = 24°C. In (b) a finer resolution for the vector field measurement is chosen so that the velocity profile of the Pluronic solution is better illustrated.

The velocity profile of the Pluronic solution shown in Figure 4.2.3 and Figure 4.2.4 is asymmetric with a lower velocity near the gel wall. This lower velocity indicates a higher viscosity of the Pluronic solution near the gel wall and according to

Fig. 2.3.4 this higher viscosity can be related to sodium phosphate diffusing into the Pluronic solution.

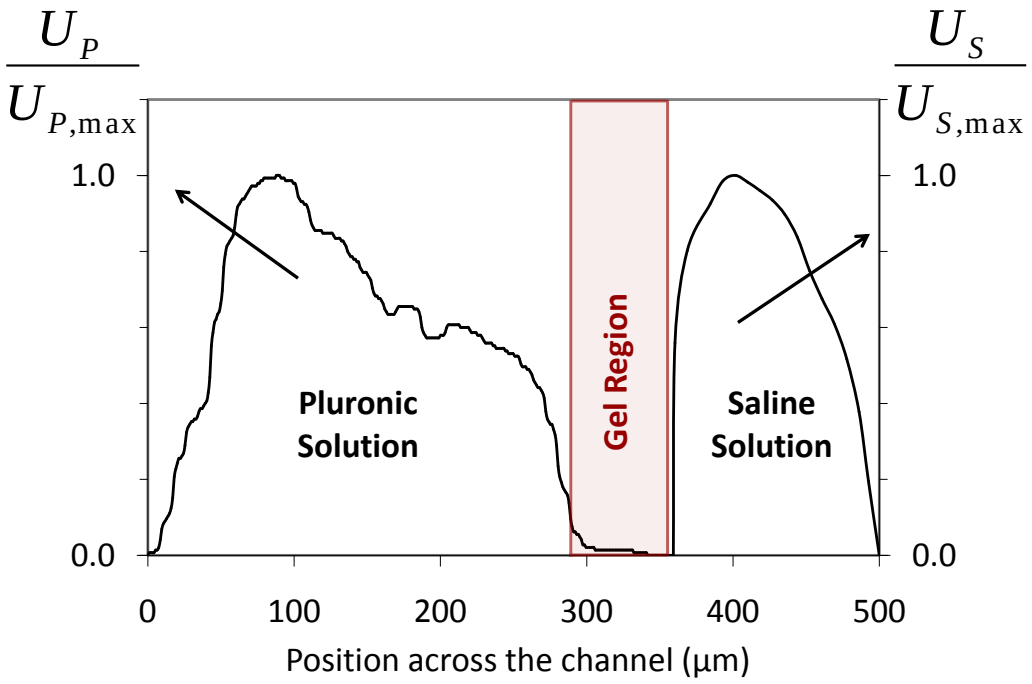

Figure 4.2.4 Flow velocity profiles from PIV at x = 1.5 mm, normalized separately for the Pluronic solution and the sodium phosphate solution with the flow rates of $Q_p = 3\mu l/h$ and $Q_s = 30\mu l/h$ respectively.

The PIV measurements also show a very small movement of the gel wall. However this movement is not clear and also uniform with the flow control setup used for this experiment; i.e. syringe pump. To achieve a better accuracy for the phenomena investigation, a FLUGENT 8-channel pressure source MFCS-8C 1000 was used to provide pressures up to 1 bar with a 14 bit resolution to introduce the two fluids into the microfluidic device. The pressures can be set independently through a

PC in closed loop control. Even though the response time of this device seems still not perfectly fast enough to avoid flows disturbance, it is sufficient to investigate the mechanics of the wall formation that will be explained in the following sections.

4.2.3 Variation of Wall Thickness

When two flow streams go side by side, they have had more time for diffusion downstream along the channel and so a wider boundary of the mixed zone is being expected. Figure 4.2.5 shows the wall thickness along the flow channel for different experimental conditions. In all cases, the wall thickness increases almost linearly over the first 1.5 mm along the channel while the wall thickness W was in the range 50 µm – 200 µm depending on the experimental conditions. The wall thickness is smaller for higher pressures driving the two fluids for the same sodium phosphate concentration in the saline stream. Higher pressures lead to faster flow and therefore to a faster convective transport of ions with the Pluronic stream after diffusing across the wall. As a consequence, gel formation in the Pluronic stream occurs further downstream compared to a slower flow. This leads to the formation of a thinner gel wall. Similarly, a higher sodium phosphate concentration leads to a thicker gel wall due to a higher flux of ions into the Pluronic stream.

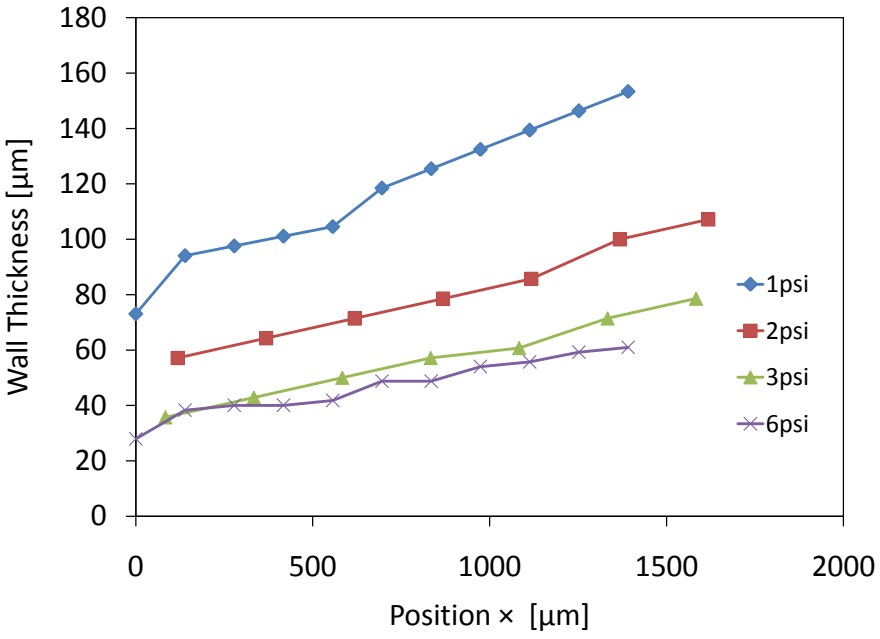

(a)

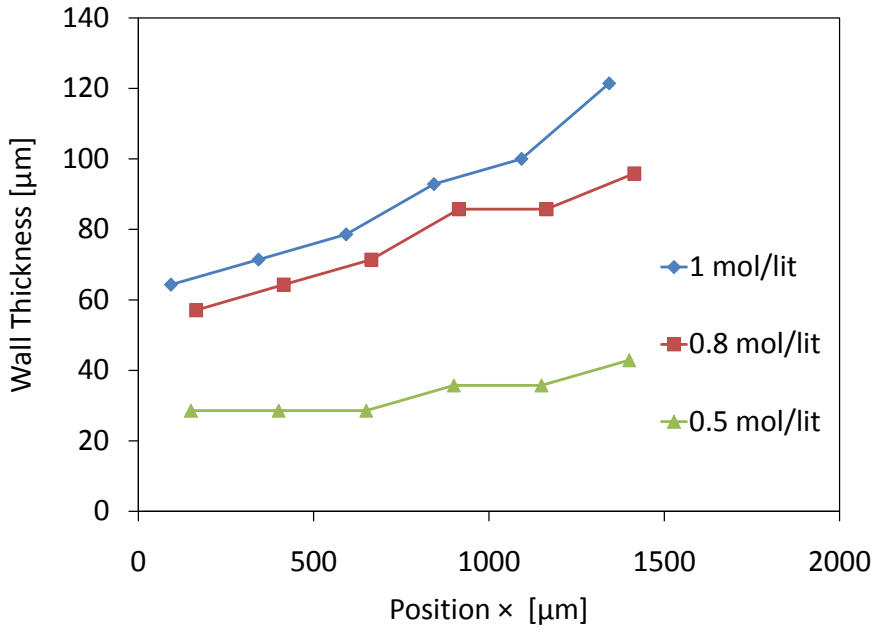

(b)

Figure 4.2.5 Thickness of the gel wall formed by a 15 wt% Pluronic F127 solution and sodium phosphate solution (a) at a concentration of 0.65 mol/L for different pressures (b) at a pressure $p = 5\ psi$ driving the flow for different concentrations. The temperature of the device in both experiments is 24°C.

The increase of the wall thickness along the channel in both experiments of Figure 4.2.5 seems linear. At higher pressures, convection is stronger and less diffusion across the channel occurs at the same time scale compared to the flow driven by lower pressures (see Section 4.3). The rate of changes in the wall thickness is expected to be accordingly less at higher pressure. Also at higher saline concentration, the diffusion is increased linearly with concentration so that the increase of the wall thickness along the channel increases linearly. This is shown in Figure 4.2.6.a and Figure 4.2.6.b, which are based on the data from Figure 4.2.5.

Figure 4.2.6.a suggests that the changing of wall thickness versus pressure can be estimated as $a_1 p^{-1}$ as a good approximation. Considering pressure as a representative parameter representative for convection, this observation will be important for the analytical discussion of the phenomena that in Section 4.3.

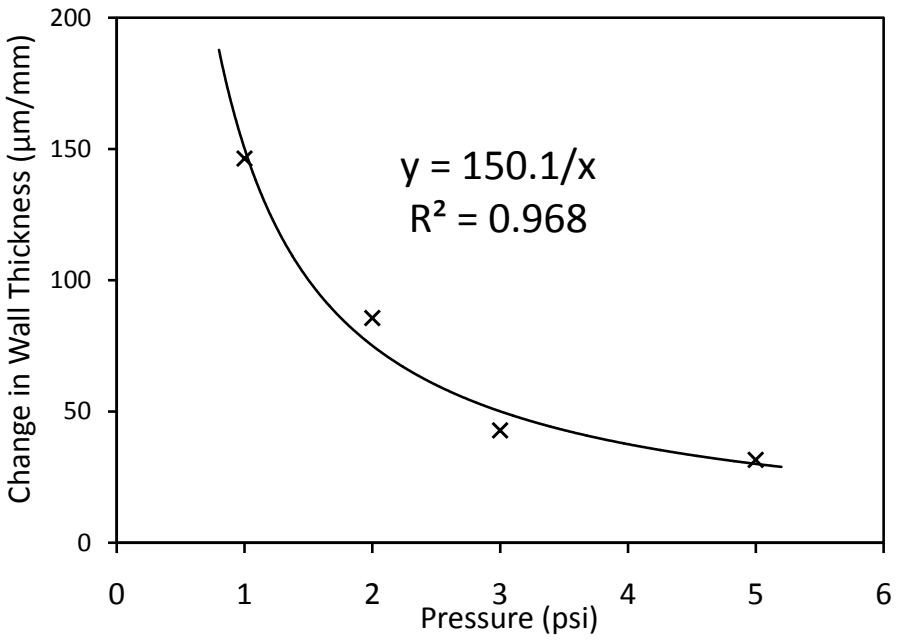

(a)

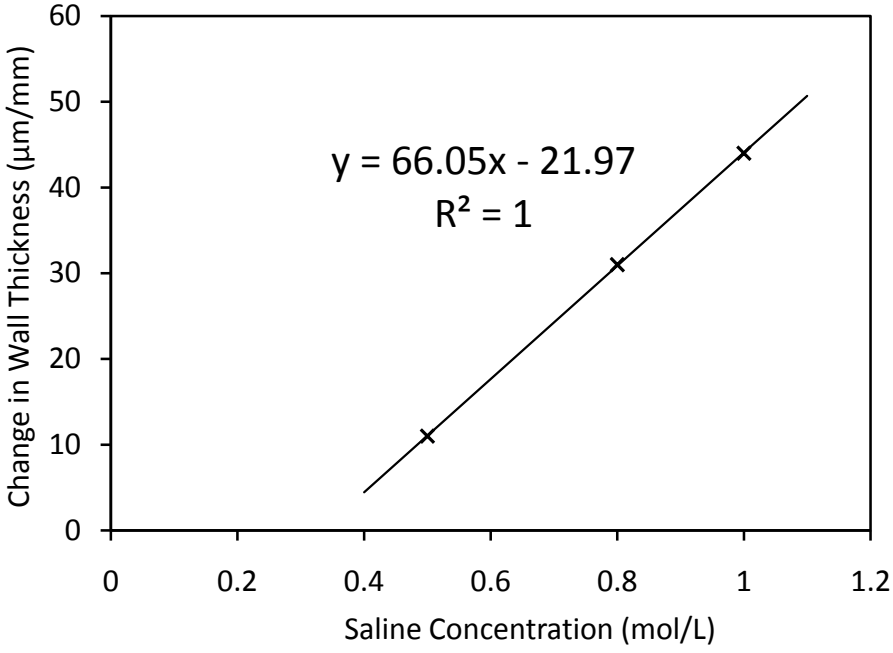

(b)

Figure 4.2.6 Change of the gel wall thickness per length along the channel as a function of (a) the pressure p driving the fluids and (b) the sodium phosphate concentration. The solid lines show curve fits to (a) $a_1 p^{-1}$ (b) $a_2 c_s + a_3$

Also, under the experimental conditions of $p = 5$ psi and at ambient temperature T = 24°C (Figure 4.2.6.b), the experimental data suggests there exists a critical concentration of sodium phosphate in its bulk stream $c_c = \frac{21.97}{66.05} \cong 0.33$ mol/L below which no increase in wall thickness occurs, and it can be assumed that no gel wall can be formed under these conditions below this critical concentration c_c = 0.33 mol/L. For instance, Figure 4.2.7.b shows no gel formation at saline concentration of 0.2 mol/L at T = 24°C.

(a)

(b)

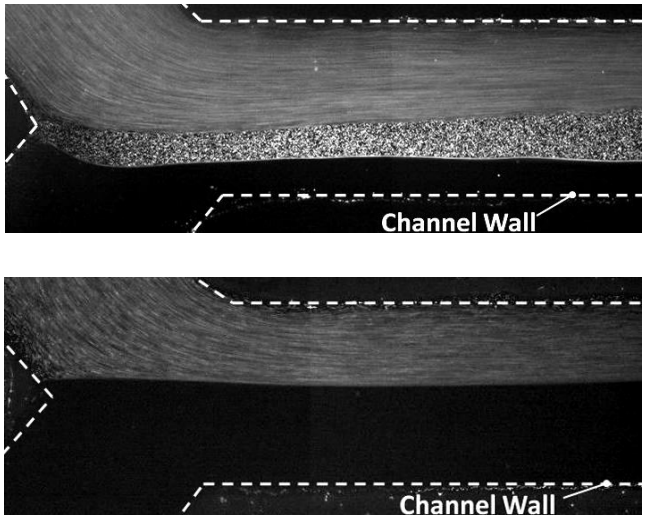

Figure 4.2.7 Epifluorescence images of the Pluronic solution (top bright stream) beside saline (bottom dark stream) flowing side by side at an ambient temperature T = 24°C; the Pluronic stream is seeded with fluorescent particles for flow visualization; (a) 15 wt% Pluronic solution and Na_3PO_4 solution with c_s= 1 mol/L at 5 psi (wall present), (b) 15 wt% Pluronic solution and Na_3PO_4 solution with c_s = 0.2 mol/L at 5 psi (no gel wall).

4.2.4 Diffusion across the Microchannel

In our Y-shaped microfluidic device, Pluronic solution 15wt% and sodium phosphate solution are moving side by side. As mentioned above, diffusion happens between two streams under the low Péclet number conditions of the experiments, which then might lead to gel formation at the interface. This is because of sodium phosphate molecules diffuse into the Pluronic solution stream; their smaller molecular size compared to Pluronic F127 molecules (almost 75 times greater in molecular weight) makes the diffusion practically unidirectional from the saline stream into the Pluronic stream. Accordingly, measuring the concentration of sodium phosphate across the channel represents the diffusion between streams. Also it can be used to predict the gel wall thickness and position across the channel and potentially to correlate these results with the rheometry results in Section 2.3.

Lacking any means to measure the concentration of sodium phosphate at a high spatial resolution in all locations of the microfluidic systems in a non-invasive way, a low concentration of the fluorescent dye Rhodamine B, was used as a sample compound to evaluate cross channel diffusion. The dye was introduced into the saline stream. The fluorescence intensity in the channel is observed, which correlates with the dye concentration. The size of a Rhodamine molecule is comparable to that of sodium phosphate with molecular weights of 479 Da and 164 Da, respectively, and their diffusion constants in aqueous solution at 24°C are comparable with $5 \cdot 10^{-6}$ cm^2/s [169] and $6 \cdot 10^{-6}$ cm^2/s [42], respectively.

Figure 4.2.8 shows an experiment without wall formation for which, the saline solution is fluorescently labeled. The intensity of the emission light can be used as an

indication of fluorescent dye concentration in the solution. Figure 4.2.8 shows that the intensity of the dye is decreasing toward Pluronic solution.

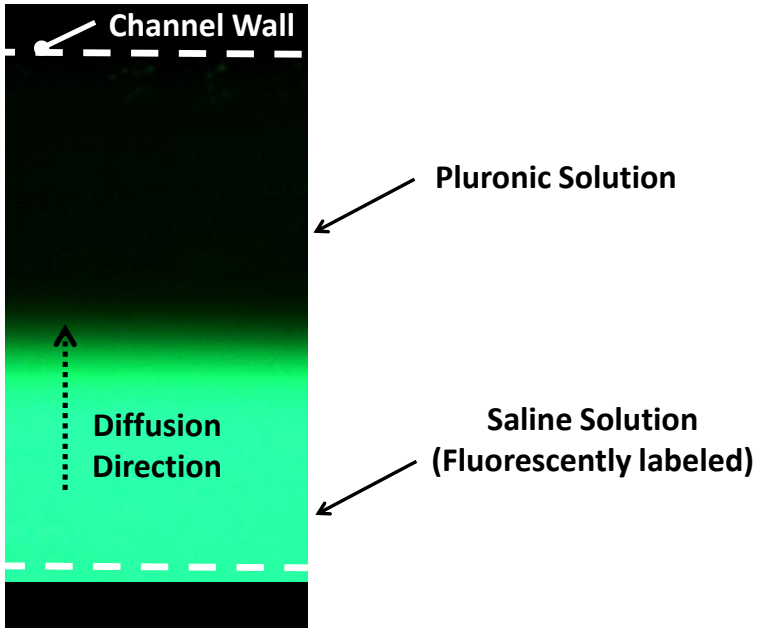

Figure 4.2.8 Section of the main channel of the device. Rhodamine B as a fluorescent dye is introduced into saline solution with the concentration of 0.3g/L. Brightness signal intensity of fluorescent under UV light can be calibrated with its bulk concentration to show the amount of dye diffusing into Pluronic stream across the channel.

The intensity of light across the channel is shown in Figure 4.2.9. The graph has been corrected for background intensity.

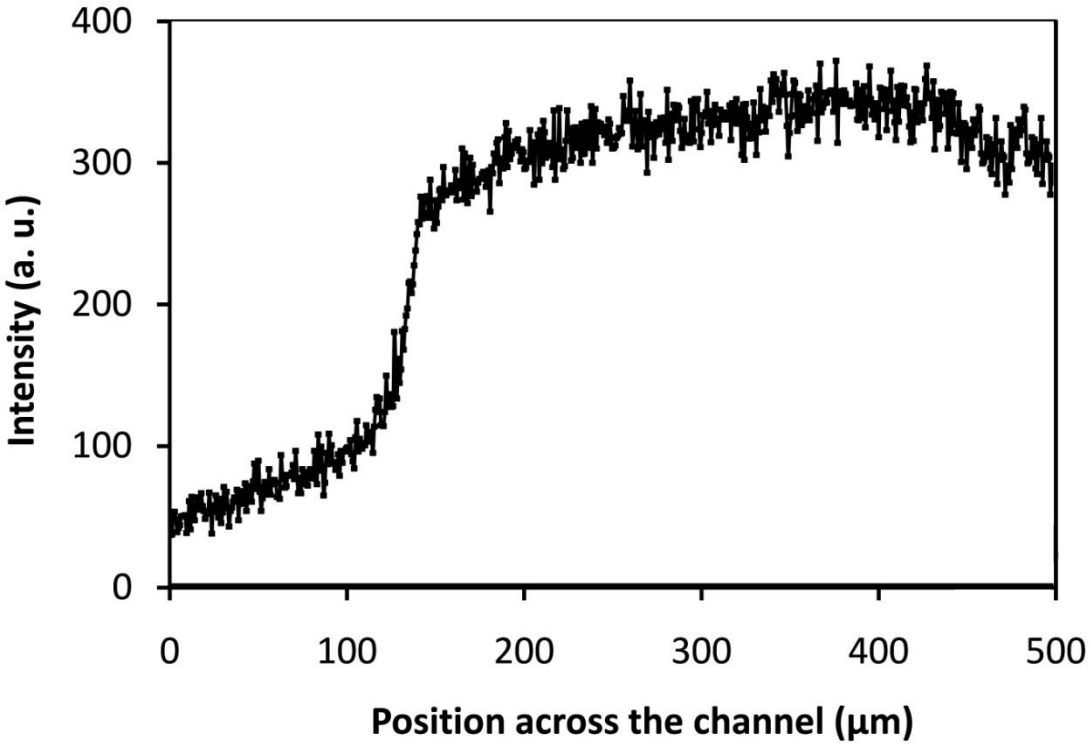

Figure 4.2.9 Intensity of fluorescent dye across the channel at x = 3 mm downstream from the channel junction. Sodium Phosphate solution with the concentration of 0.2 mol/L is moving along Pluronic solution 15wt%; no gel formation is observed at the interface.

Figure 4.2.10 shows the fluorescence intensity of Rhodamine (B) diffusing from the saline solution across the gel wall into the 15 wt% Pluronic F127 solution. The sodium phosphate concentration is $C_S = 1$ mol/L, and this profile has been measure 3 mm downstream from the channel junction where the bulk Rhodamine concentration in the saline solution is 0.3 g/L and the temperature of the whole device is kept at room temperature, T=24ºC. With these conditions for the experiment a gel wall is formed at the interface as shown in Figure 4.2.7.a.

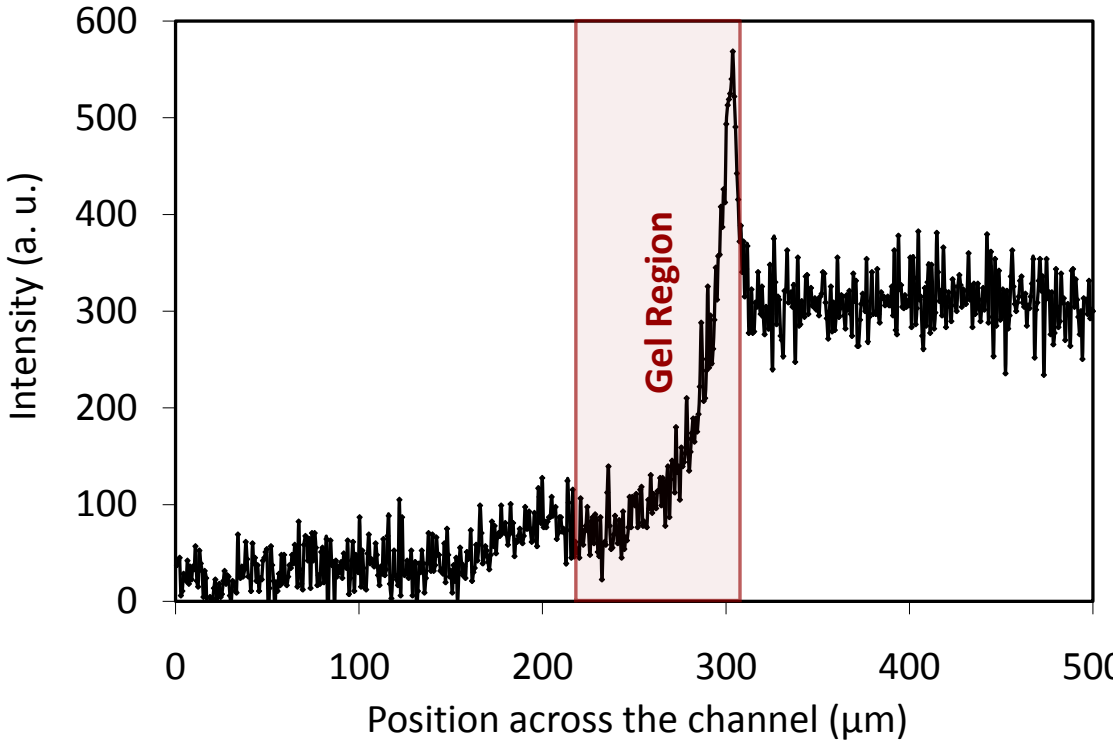

Figure 4.2.10 Fluorescence intensity of Rhodamine B diffusing from the saline solution across the gel wall into the 15 wt% Pluronic F127 solution, C_S = 1 mol/L, at x = 3 mm far from the entrance.

Two peaks in the diffusion graph across the channel distinguish the gel boundaries and those are related to different brightness of the dye in (from left to right, i.e. Pluronic solution stream to Saline stream) Pluronic solution-Gel-Saline solution. The dye is about 3.2 times brighter in the Pluronic solution than in the saline solution, and it is 2 times brighter in the Pluronic solution compared to the gel, as verified through experiments shown in Figure 4.2.11. These experiments reveal different brightness of the same concentration of dye in the Pluronic solution, sodium phosphate solution and a Pluronic gel under UV light in the same microchannel

device with the same flow conditions. These ratios correlate very well with the ratio of intensity changes at the gel edges in Figure 4.2.10.

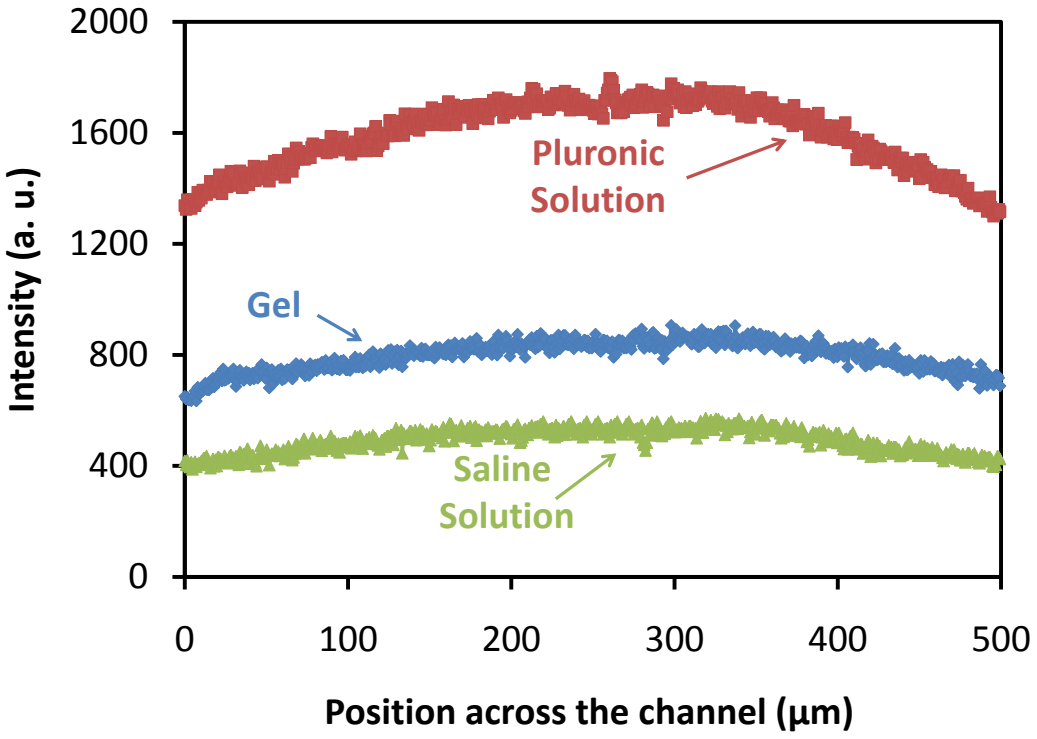

Figure 4.2.11 Fluorescence intensity of Rhodamine B in different regions; Pluronic solution, Sodium Phosphate solution (Saline) and Gel. Experiments show higher brightness intensity of dye inside Pluronic solution than Saline and Gel region.

Also, regarding Figure 4.2.10, correlating the fluorescence brightness with the concentration of Rhodamine B and with the concentration of sodium phosphate in the system yields a sodium phosphate concentration of around 0.1 mmol/L at the edge of the gel wall and the Pluronic stream. This value corresponds very well to the sodium phosphate concentration necessary for gel formation at T = 24°C in the phase diagram shown in Section 2.3, Figure 2.6.

4.2.5 Mechanics of Wall Formation

We discussed and measured gel wall characteristics and features in the previous sections. Here we show the mechanism of this solid gel wall formation and its effect on the flow conditions after it is fully established. According to the assumptions in Section 4.2.4 diffusion of Pluronic into the saline stream will be neglected in the following discussion because of the much higher molecular weight of the Pluronic molecules (above 12 kDa) compared to sodium phosphate. Figure 4.2.122 shows a sketch of the sodium phosphate concentration across the channel according to the measurements described in Section 4.2.4. The salt concentration decreases from a maximum in the saline stream toward the Pluronic solution until it reaches its minimum. Keeping the whole device at room temperature, T = 24 ºC, regions where the saline concentration is above the necessary minimum value for gel formation and the below critical concentration will turn into gel. According to the phase diagram shown in Figure 2.3.5, this happens when the sodium phosphate concentration is between 0.112 mol/L and 0.253 mol/L.

The gel wall starts to form at the junction of the two feeding channels and then it continues along the whole length of the channel at the interface between the two fluids; the thickness of the wall and the conditions in which it can be kept stable were discussed in Section 4.2.4.

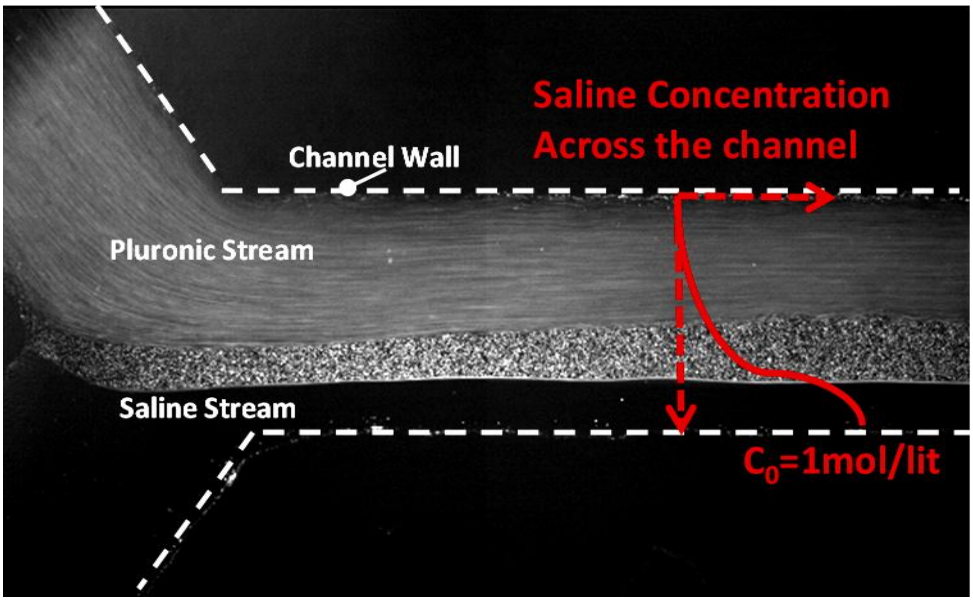

Figure 4.2.12 Saline concentration across the channel; a 15wt% Pluronic Solution seeded with fluorescent particles moving along the sodium phosphate solution with the concentration of 1 mol/L at T=24ºC.

Steady diffusion of sodium phosphate towards the Pluronic stream will increase the sodium phosphate concentration of the gel wall near the saline stream above the critical concentration $C_{S,crit}$, so that the gel has to turn liquid at this location. Simultaneously, continuous diffusion of sodium phosphate across the wall and into the Pluronic solution will increase the concentration of sodium phosphate in the Pluronic stream near the wall to above the concentration threshold for gel formation according to Figure 2.3.5. This means that the gel wall is constantly being dissolved on the side that is in contact with the saline stream, and gel is constantly generated on the side of the wall that is in contact with the Pluronic stream. As a consequence, the wall can only have a fixed position in the channel, if the gel that constitutes the wall moves across the channel.

Several images of the microfluidic systems were combined to form the streak images shown in Figure 4.2.12.a, where the streaks indicate the wall movement. This slow motion of the wall is also shown by the vector field from PIV in Figure 4.2.123.b. The PIV measurement of the velocity of the wall reveals steady motion at nearly constant velocity $v_y = 5\mu m/s$ along the channel from the Pluronic stream toward the saline stream. It also shows increasing velocity in direction of the fluid streams along the channel; this is most likely induced by the viscous forces of the fluid streams acting on the wall, which increases slightly in width along the channel. The cross channel velocity v_y is insensitive to the velocity of the fluids. This indicates a constant gel removal rate by the saturated saline solution near the gel wall along the entire channel, which is maintained by the sufficiently high flow velocity of the saline solution.

The position of the wall is constant for steady state flow conditions, which indicates that the motion of the gel across the channel is not caused by a pressure difference between the two fluid streams. The cross channel motion towards the saline stream has been observed for different pressures driving the two streams where either the pressure driving the Pluronic stream or the pressure driving the saline solution was higher.

(a)

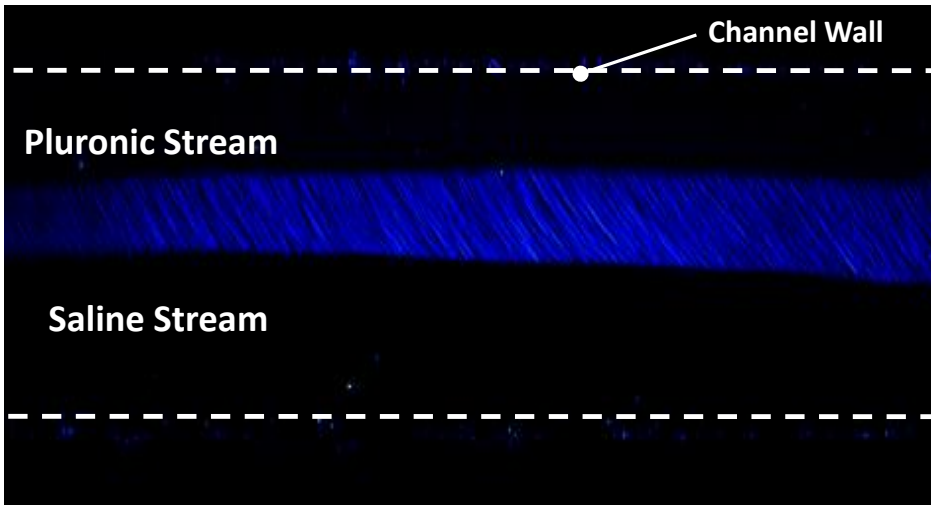

(b)

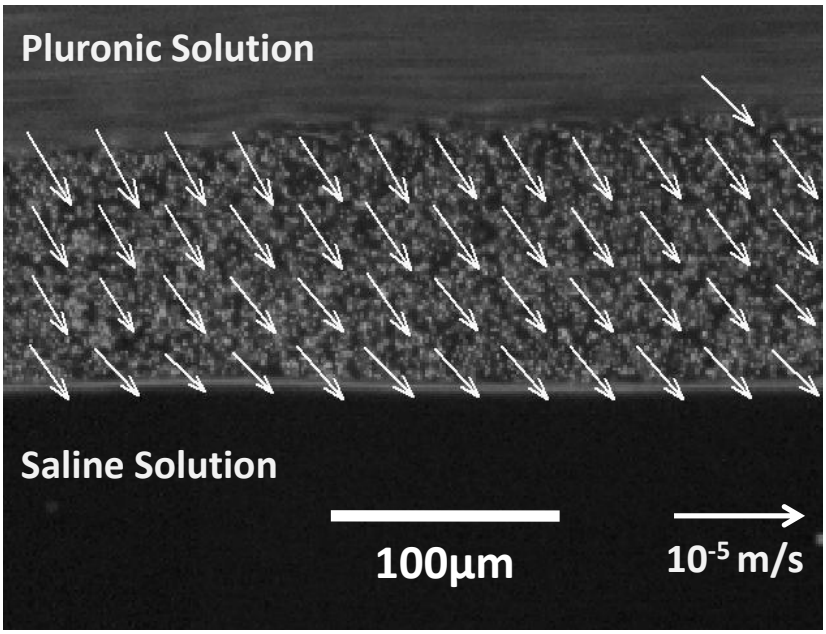

Figure 4.2.13 Movement of the wall; (a) Average of 50 streak images shows the direction of motion of the gel wall along the channel at a constant pressure p = 5 psi; (b) the velocity field from PIV of the moving wall shows a velocity toward the saline solution. The much higher velocities of the two streams compared to wall movement are not shown in this picture.

4.3 Analytical Discussion

This situation where two miscible streams are brought beside each other to flow side by side in a microfluidic device (Figure 4.2.1) has been studied both numerically and experimentally in the literature [14, 48, 52, 53, 170-179]. Transverse diffusion from one stream to the other is the only way of mixing and as a consequence the diffusion distance or mixing width downstream in the channel can be related to the time elapsed since the two streams have come into contact at the entrance. Similar to our assumption in previous sections, the following analytical discussion would be only based on transverse diffusion of salt (sodium phosphate) into the adjacent stream of Pluronic solution. Thus, the boundary of the mixing layer at the position x along the channel for a 2d model when the average velocity of the two streams inside the microchannel is $\bar{V}$, can be expressed as $(2Dx/\bar{V})^{1/2}$ where D is the diffusion constant of salt into the Pluronic solution. For a 3d model, Salmon *et al.* showed that the difference compared to a 2d model is relatively small, and the 2d model can be safely used in terms of height-averaged concentrations and velocities for the case of high aspect ratio channels [176]. However, these diffusion models are not applicable for the present case of a gel wall in the channel center.

Experiments show that at steady state the wall thickness only increases by a small amount along the investigated channel length of 1.5 mm, while the wall thickness W was in the range 50 µm – 200 µm depending on the experimental conditions. With a fixed sodium phosphate concentration on either side of the wall and a relatively constant wall thickness, the flux of sodium phosphate across the wall is constant along the channel, and the edge of the wall in contact with the Pluronic

solution can be considered a constant source of sodium phosphate. Diffusion of ions into a Pluronic solution with an ion concentration just below the gel formation concentration will lead to gel formation and advancement of the gel in direction of the Pluronic stream. This propagation of the gel wall through mass diffusion can be investigated through the equivalent heat diffusion problem, where the temperature T is equivalent to the concentration C_S and the heat flux q corresponds to the molecular flux Φ. The temperature distribution $T(x) - T_0 \sim q\sqrt{x/U}$ along a plate $T(x) \sim q$ that provides a constant heat flux q into the fluid depends on the location *x*, the free stream velocity *U* and a reference temperature T_0 [180]. This corresponds to an increasing sodium phosphate concentration at the wall surface along the channel. However, if this concentration becomes higher than $C_{S,crit}$, there will be a location in the channel close to the wall with $C = C_{S,crit}$, and the region between the original wall surface and this location should have solidified to gel.

In the equivalent thermal problem, this location scales as the thermal boundary layer for the case of forced convection in laminar flow over a flat plate with a known wall temperature. The assumption of a thermal (or concentration) boundary layer much smaller than the velocity boundary layer (which here spans the entire channel) is justified by the concentration profile in the Pluronic stream from Figure 4.2.10. The thermal boundary layer $\delta_T \sim \sqrt{x/U}$ of a wall with constant temperature depends through the local Reynolds number Re_x on location *x* and the free stream (or average) velocity *U* of the Pluronic solution [1]. This thermal boundary layer thickness relates to the mass diffusion problem considered in form of a mass diffusion length. For the expected small changes of the concentration at the

location of the original wall surface along the channel we assume it is justified to superimpose the results for concentration increase and the diffusion length for constant concentration at the boundary. This is also justified by the relatively large wall thickness compared to the thickness changes along the channel. For the equivalent thermal problem we therefore find a thermal boundary layer thickness $\delta_T \sim q\sqrt{x/U}\sqrt{x/U} = qx/U$ that is proportional to the heat flux at the wall q and to the location along the channel *x*, while it is inversely proportional to the free stream velocity *U*.

If we interpret the increase of this thermal boundary layer along the channel as an increase in the wall thickness $\delta_c \sim \Phi x/U$ for the mass diffusion problem, then this result correlates very well with our experimental observations. The wall thickness increases linearly along the channel as shown in Figure 2a, and the increase in thickness $\alpha_w \sim d\delta_c/dx \sim \Phi/U$ is proportional to 1/*U* as confirmed by the data in Figure 4.2.6 (a), assuming that in the viscous limit of our experiments the pressure driving the fluid p is proportional to the corresponding flow rate Q or the flow velocity *U*. In addition, if we assume that the molecular flux Φ is proportional to the sodium phosphate concentration in the saline stream C_{S0}, then the change in wall thickness α_w has to be proportional to C_{S0}, as shown in Figure 4.2.6 (b).

4.4 Conclusion

Knowledge of the effect of sodium phosphate on the gel formation of Pluronic solutions and an understanding of mass diffusion in microfluidic environments are sufficient for a physical understanding of the dynamics of the observed wall formation in microfluidic channels. While this mechanism allows forming a temporary wall separating two fluid streams, this wall also serves as a vehicle to slowly transport entities from one stream into the other stream. This transport principle could be applied to cells that slowly move from one stream through the wall along a concentration gradient into a medium of elevated concentration of certain ions, so that the cells would have sufficient time to adapt. Since the cross-channel transport velocity of the wall v_y is constant, and the wall thickness can be varied through the flow velocity of the fluid streams, the temporal concentration gradient dC_S/dt that objects experience as they move across the wall can be selected through the flow velocity of the two streams.

CHAPTER 5

A Multi-layer Microfluidic Platform Using Thermally Actuated Polymer Solutions

5.1 Introduction

PDMS and soft lithography that were discussed in Chapter 3 have led to the development of many complex integrated microfluidic systems [142, 146, 151, 157-160, 181]. The MSL technology that was described in Section 3, allows integrating thousands of channels into a dense network for controlling aqueous solutions with a nanoliter scale accuracy, which has recently found several practical applications including protein crystallization [182-185], gene expression [186-188]and cell sorting [189-191]. However, flow control in these devices currently requires a compressed air supply and complex manifold for actuation of the pneumatic valves of the microfluidic system [135]. So while PDMS can be used to make extremely complex microfluidic devices with a large number of integrated valves, it makes it very hard to control the fluid flow in the system without a large external system for pressure-driven valves. Therefore, approach cannot be used to make portable analytical devices.

The use of thermally actuated polymer solutions for controlled shunting of flow between multiple channels using local heaters was demonstrated by Stoeber *et al.* [9]. The heat induces reversible gel formation of the polymer-containing fluid (Pluronic solution) thus creating a localized valving mechanism. Even though the polymer (Pluronic) is biocompatible, the need to premix a polymer into the main solution remains a significant problem for this approach.

Combining the advantages of these two proven technologies, in this chapter we demonstrates a new 2-stage valving concept for PDMS-based microfluidic systems that uses the advantages of thermally responsive polymer solutions while keeping the Pluronic solution separate from the fluid of interest. This method can electrically control flow through a system of PDMS channels with only one control pressure source, compared to the pressure manifold needed in existing systems. Thus microfluidics systems could be created that require only electrical power and two pressure sources, one for the control fluid and one for the main fluid, and that are much more portable than current technology allows.

This new technology will enable a new platform for highly integrated microfluidic systems with various applications in the growing field of biotechnology. Compared to currently available systems, this technology will allow generating inexpensive portable bioanalysis tools. The concept of active valving using Pluronic solutions will be discussed in Section 5.2.1, the PDMS valve will be reviewed in Section 5.2.2, and the new valving concept, a combination of both technologies will be described in Section 5.2.3.

5.2 Flow Control Mechanisms

5.2.1 Principle of an Active Thermal Hydrogel Valve

Hydrogel-based flow control was reviewed in Section 2.2, here the concept of active valving using Pluronic solutions will be discussed. In a very simple valving approach, a flow conduit is blocked by transforming the thermally responsive fluid into a hydrogel within the microchannel, which then blocks the channel. Heaters can be integrated into the channel network so that selective activation of a particular heater locally generates heat, which increases the fluid temperature beyond the gel formation temperature of the thermally responsive fluid. This then leads to localized gel formation as illustrated in Figure 5.2.1. As the fluid is present everywhere in the microfluidic network, localized heating and subsequent gel formation can be achieved in an arbitrary location and at any time in the microfluidic system [9]. As gel formation of Pluronic solutions is completely reversible, the hydrogel returns to its liquid phase upon cooling, and the gel block disappears, opening the channel again to flow.

Stoeber *et al.* demonstrated valve performance using this method and Pluronic solution as the working fluid [9]. A 15 wt% Pluronic F127 solution was driven through the device at a constant flow rate using a syringe pump. At an ambient temperature of 20°C a temperature increase of 7°C was required to reach the gel temperature of 27°C according to Figure 2.3.1. 100 ms long 400 mW pulses were generated with an electric heater of resistance $R = 1.5\ k\Omega$. These pulses provided

sufficient heat to raise the fluid temperature in the vicinity of the heater to form a local gel that subsequently blocked the flow channel.

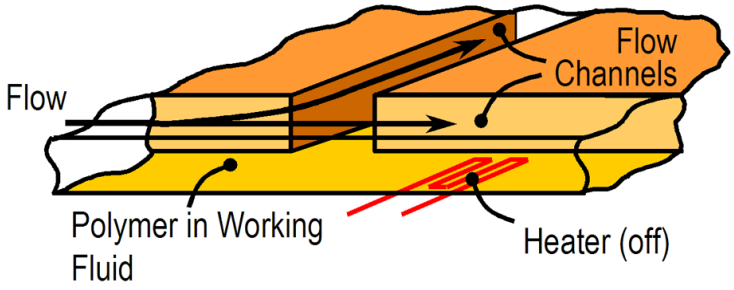

(a)

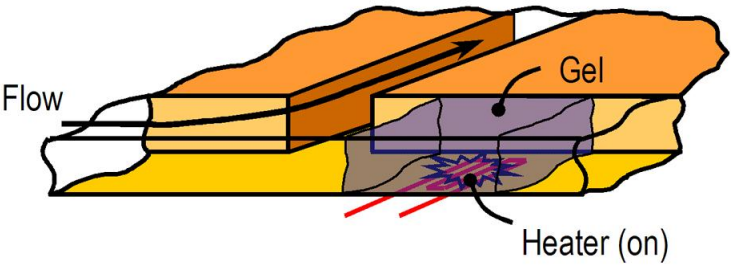

(b)

Figure 5.2.1 A schematic illustration of the principle of an active valve using a thermally responsive fluid in a microfluidic network. (a) Fluid from one channel is diverted into two channels at a channel bifurcation; (b) activating an integrated heater leads to localized gel formation in the corresponding microchannel, which subsequently blocks this channel to flow [9]**.**

Figure 5.2.2 shows the velocity field of the flow right before (a) and immediately after (b) activating the electric heater. For all experiments, valve closing occurred during less than 33 ms according to the data form PIV (see Section 3.6).

Valve opening was expected to occur slower as it relies on passive heat dissipating into the silicon substrate. However, the time to open the valve was also much shorter than 33 ms, the time between image frames. Valve closing and opening was demonstrated for 0.25 - 4 Hz cycles of 100 ms to 1 s long 400 mW pulses [9].

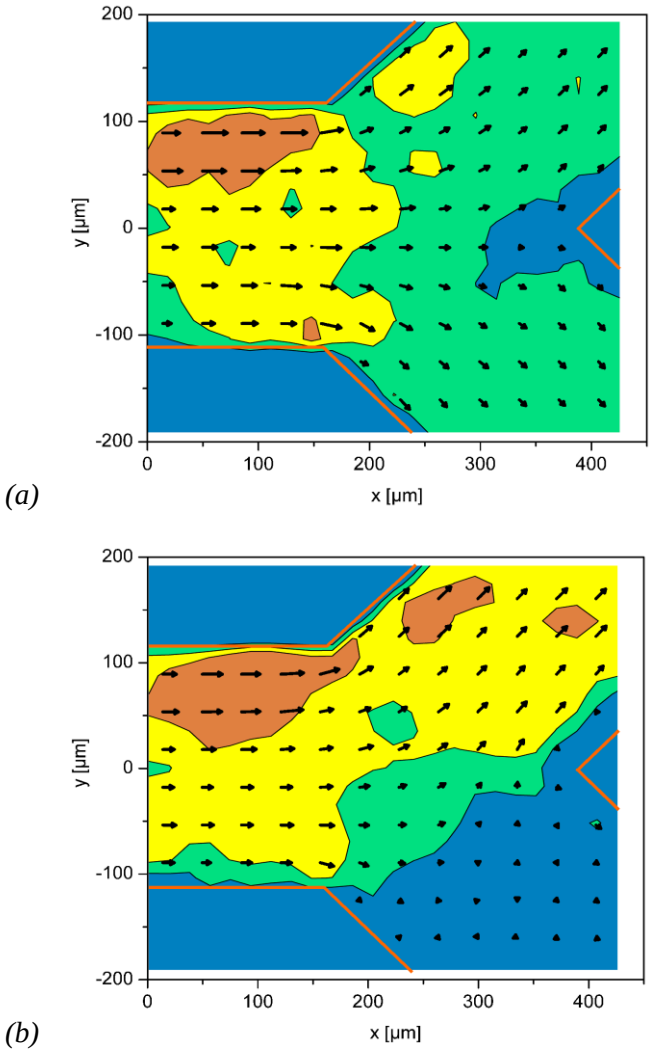

Figure 5.2.2 The flow field at the channel bifurcation shown in Figure 5.2.1. The velocities were evaluated from images of the seed particles PIV; (a) before valve actuation, (b) 33 ms later; blue: below 40 µm/s, green: 40-80 µm/s, yellow: 80-120 µm/s, orange: 120-160 µm/s [9].

5.2.2 Principle of a Low-Actuation Pressure Microfluidic PDMS Valve

This microflow control method uses multilayer soft lithography as described in Section 3.3 for fabricating pumps and valves in PDMS [135]. As mentioned, in this method a two layer microfluidic chip is fabricated in PDMS and bonded to a glass substrate. Two molds are used to form two different channels; the working channel where the working fluid flows and the control channel where air (or water) is pressurized. In some locations of the flow network, working and control channels are meeting perpendicularly and are only separated by a thin membrane. Pressurizing a control channel deflects this thin membrane into the main channel, stopping the fluid. Figure 5.2.3 shows the schematic layout of this soft multilayer valve operation. To prevent pressure drop along the control channel, it can be designed with a dead-end.

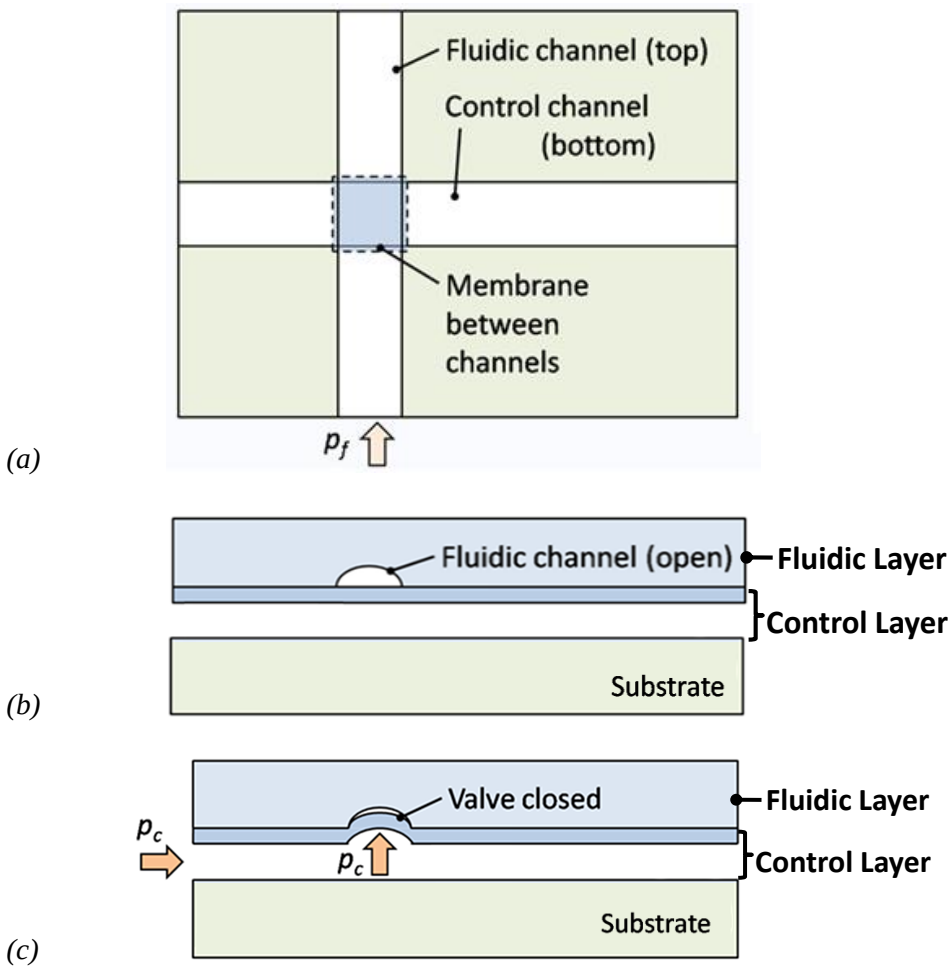

Figure 5.2.3 Multilayer PDMS valve schematic layout, (a) top-view: one fluidic channel above one control channel, the channels are separated at their intersection by a membrane. (b) side-view: the control channel is not pressurized and the valve is open (c) side-view: pressurizing the control channel deflects the membrane upward and it closes the working channel at the intersection.

As mentioned in Section 3.3, control channel molds are usually rounded by baking the photoresist to reflow and this will allow the membrane to fully close the channel at lower pressure and prevent any leakage. Figure 5.2.4 shows the top view and a cross sectional view of the device at the intersection of one control channel and

one fluidic channel before (a) and after (b) the control channel is pressurized. The pressure required inside the control channel to fully deflect the membrane depends on the thickness of the membrane [160].

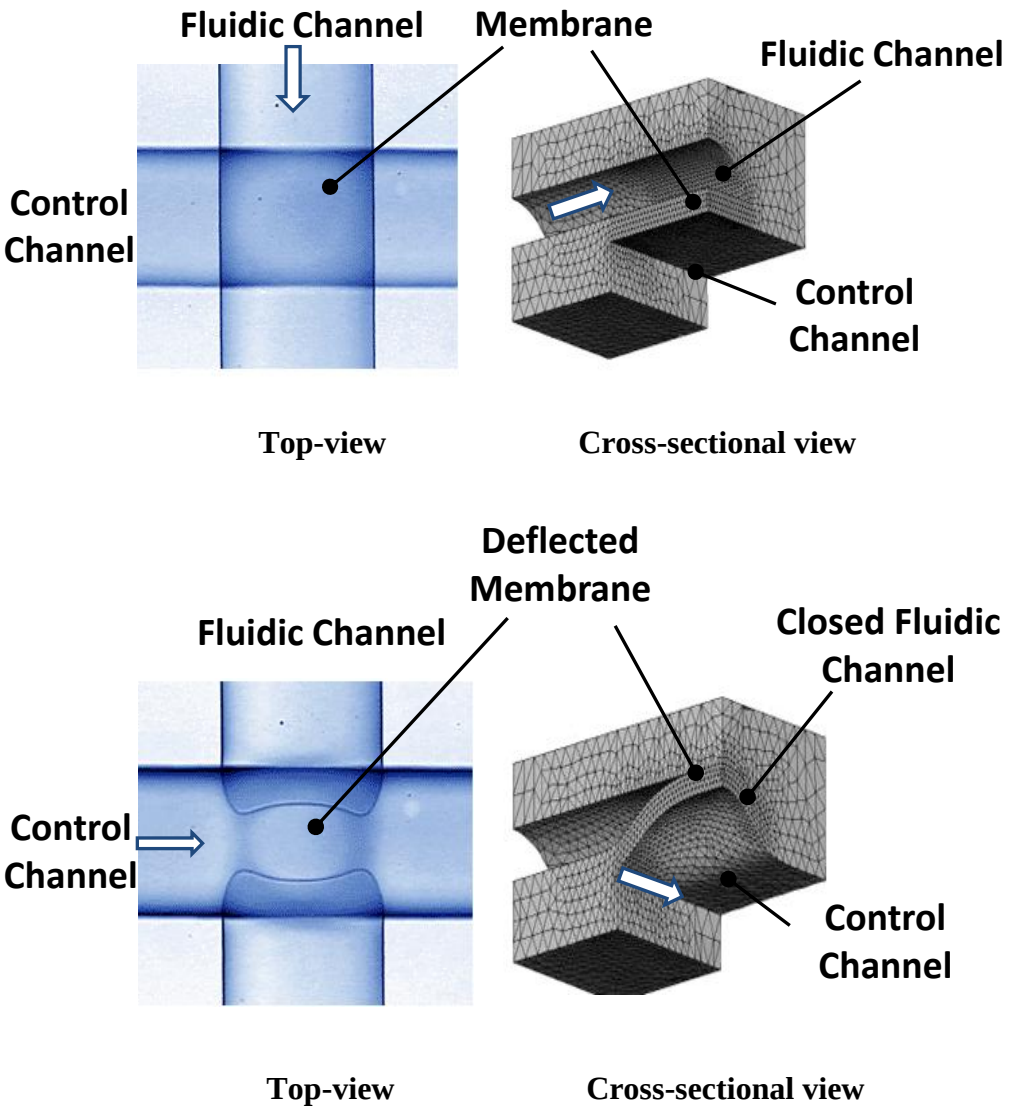

Figure 5.2.4 Top-view and cross-sectional view of the multilayer PDMS microfluidic valve, (a) before pressurizing the control channel, and (b) after pressurizing the control channel , the membrane is deflected effecting a tight seal of the fluidic channel [160]**.**

5.2.3 Principle of a Thermally Actuated Microfluidic Relay Valve

The microfluidic relay valve is actuated by a thermally responsive polymer (Pluronic) solution (5.2.1) that is driven through a control channel by a constant pressure source (section 5.2.2). Fabrication of this device has been described in Section 3.3. A multilayer PDMS chip including fluidic and control layers is bonded to a glass substrate with 320 nm high heaters. The PDMS device is optically aligned to these heaters before permanent bonding in order to ensure that the heater elements are well-positioned with respect to the control channels. For providing a tight seal in order to prevent leakage inside the control channels near the heaters, they are pressed together for 3 hours with a 10 lb load after bonding with oxygen plasma. The heater elements are coated and sealed with a thin Parylene layer by the method described in Section 3.4. This also prevents diffusion of water out of the hydrogel and possible evaporation into the PDMS.

The valving concept of this microfluidic relay valve is illustrated in Figure 5.2.5 for one fluidic (working) channel and one control channel. Figure 5.2.5 (a) shows a schematic top view of the device. Pluronic solution is driven through the control channel by a constant pressure source of P_c and a working fluidic is driven inside the fluidic channel with a pressure source of P_f and a heater is located in the control channel upstream from the intersection with the main channel. The pressure of the control fluid (Pluronic solution) is high enough that the thin membrane (~10 μm) between control and fluidic channel at the intersection is fully deflected and the valve is normally closed as shown in Figure 5.2.5 (b).

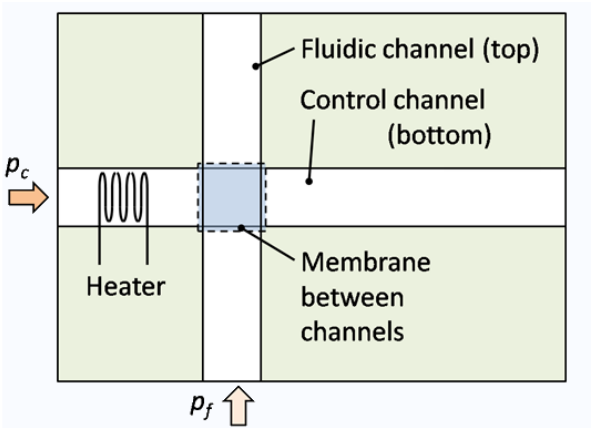

(a)

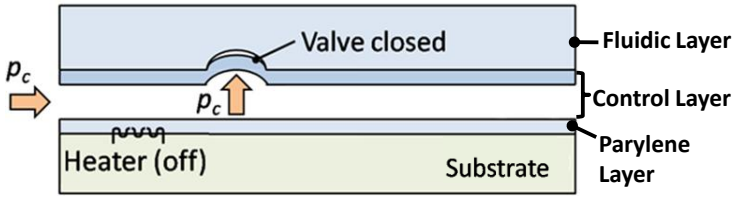

(b)

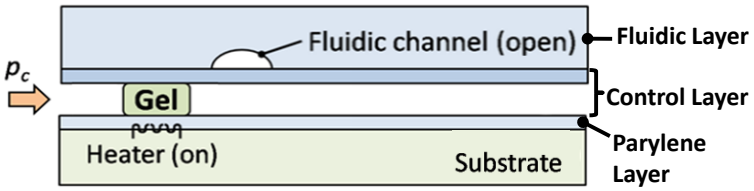

(c)

Figure 5.2.5 Concept of the microfluidic relay valve; a) schematic top-view of the device layout with one fluidic channel above one control channel including heater; b) Side-view: When the heater is turned off, the thermally responsive fluid is driven through the control channel by a constant pressure source P_c, high enough to deflect the membrane; c) Side-view: When the heater is turned on, gel blocks the control channel and allows the membrane returning back and opening the fluid channel to flow at P_f.

When the heater is turned on with a 15 mW pulse, it provides sufficient heat in a very short time to raise the fluid temperature in the vicinity of the heater to form a local gel that subsequently blocks the control channel. Thus, the pressure is not transferred to the membrane and the membrane deflects back and opens the fluidic channel as shown in Figure 5.2.5.c. This process is completely reversible, i.e. when the heater is turned off, heat dissipates and the gel disappears so that the membrane can deflect again to close the fluidic channel.

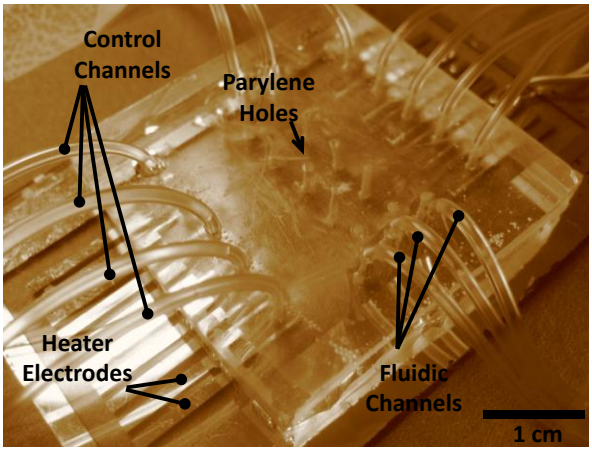

Figure 5.2.6 A thermally actuated microfluidic relay valve

5.3 Experimental Results

The fabrication and principle of this thermally triggered microfluidic relay valve were discussed in Section 3.3 and Section 5.2.3, respectively. Here the performance of the valve will be shown for a multilayer microfluidic chip that includes 100 µm wide and 10 µm high control and fluid channels. The thickness of the membrane for closing the valve is about 10 µm, and the inside of the control channels is coated with a 1 µm Parylene layer. A 15 wt% Pluronic solution is driven through the control channel and water is flowing inside the fluidic channel. In Section 5.3.1 the functioning of the device with the conventional way of pressurizing the Pluronic solution will be shown and in Section 5.3.2 the capability of the heaters to locally form a gel inside control channels will be discussed. The performance of the whole device will be demonstrated in Section 5.3.3.

5.3.1 Membrane Deflection through Pressure

To characterize the amount of pressure P_c that is required to fully deflect the membrane, the Pluronic solution inside the control channel is driven at different pressures and distilled water is flowing in the fluidic channel with an inlet pressure $P_f = 3$ psi. The schematic top-view of the control and working channels is shown in Figure 5.3.1.

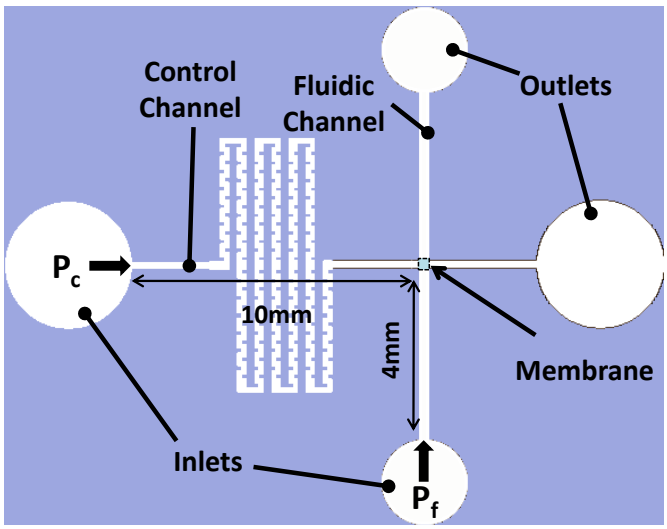

Figure 5.3.1 Schematic of the control and working channels; the membrane at the intersection has the dimension of 100 µm × 100 µm and it is 10 µm thick.

Figure 5.3.2 shows the membrane deflection at different pressure of the control channel until the working fluid is fully stopped and the membrane fully pinches off the fluidic channel and closes it. Figure 5.3.3 shows the normalized area of the channel closed at different pressures. The amount of valve closing is calculated from the fluorescence signal of the fluorescently labeled fluid in the main channel that is displaced by the deflected membrane. The signal is normalized with respect to the fluorescence signal from the flow channel outside the area of the membrane and with respect to background fluorescence from the control channel. These measurements show that $P_c = 20$ psi is sufficient to reach the full deflection and to close the working channel. This will be verified through PIV data that in Section 5.3.3.

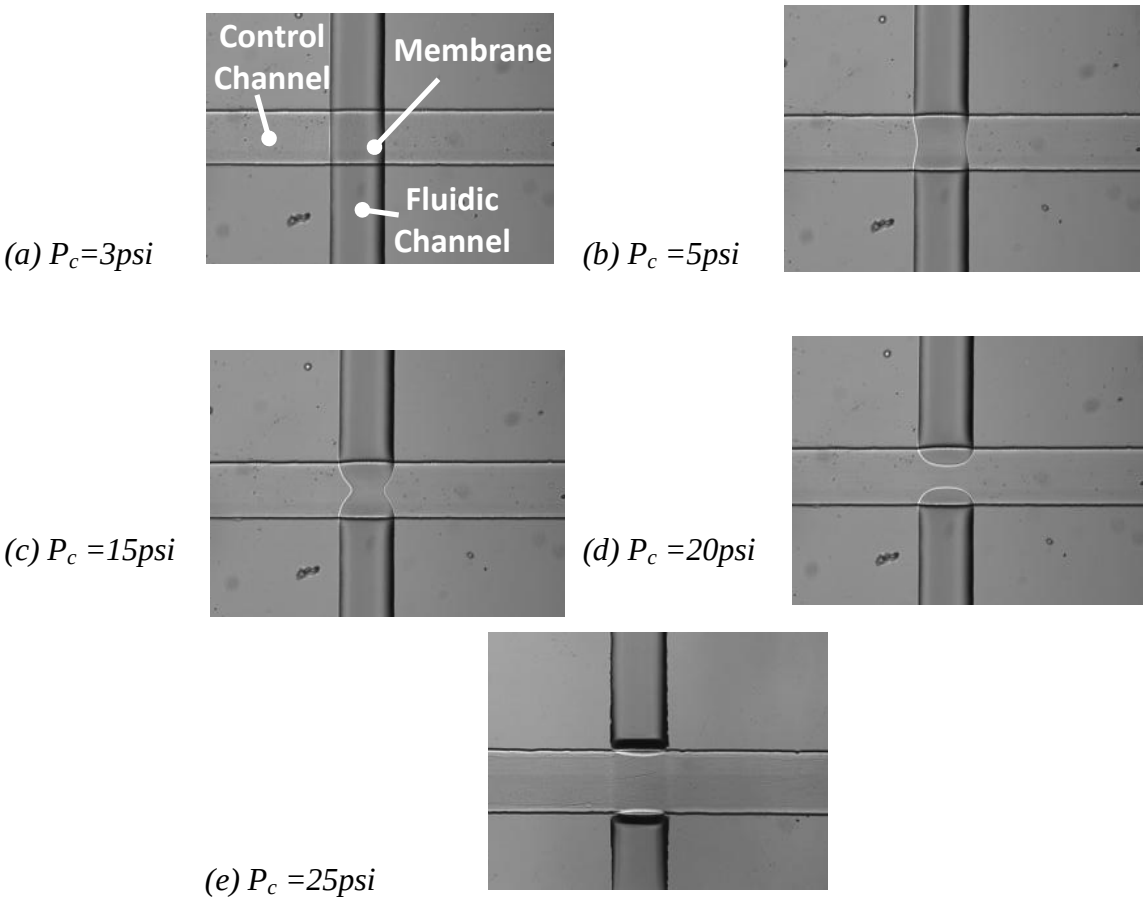

Figure 5.3.2 Membrane deflection at different pressure of the control channel shown in Figure 5.3.1; while there is no deflection at the pressure P_c = 3 psi (equal to P_f), the membrane is fully deflected at the pressure P_c = 20 psi and closes the fluidic layer. Higher pressures of the control channel as shown in (e) results to control channel expansion.

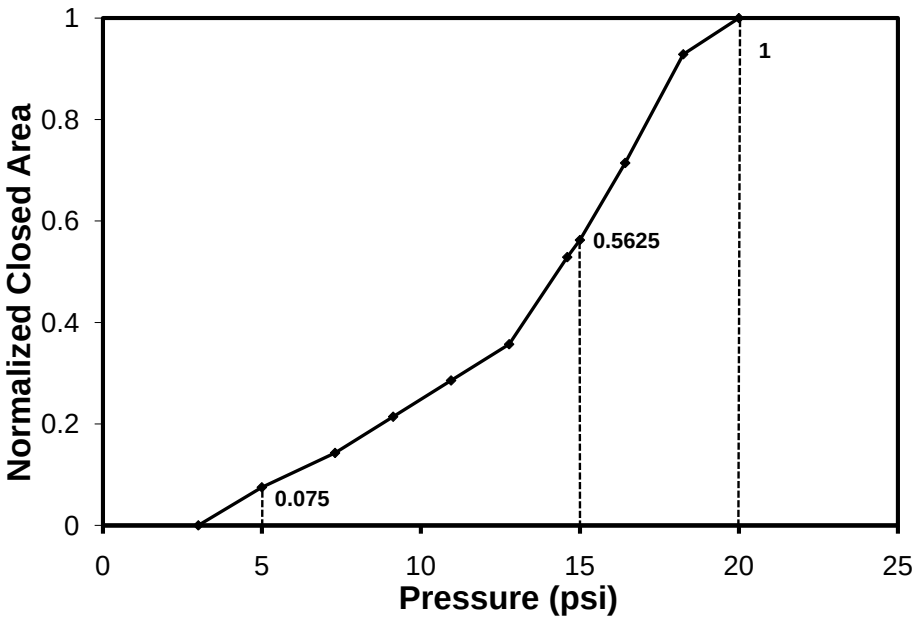

Figure 5.3.3 Closing the working channel (P_f = 3 psi) through pressurizing the control channel; at P_c = 20 psi the working channel is effectively closed.

5.3.2 Flow Control with Heaters

The second characterization of the device serves to measure the maximum pressure of the Pluronic solution inside the control channel that can be stopped by gel formation induced by the heaters. If the flow is driven too fast by the inlet pressure, the Pluronic solution at ambient temperature does not have enough time to receive the heat from the heater and form a gel. Thus a compromise needs to be found for this pressure that cannot be increased too much, but that on the other hand should be high enough to deflect the membrane (see Figure 5.3.3).

The time scale at which the gel moves in the vicinity of the heater can be increased with increasing the length of the channel near the heater element. In order

to be suitable for high density integration of the device, this can be done with a serpentine shape shown in Figure 5.3.1 that produces a length of nearly 20 mm for the channel in a 1.2 mm long and 1.5 mm wide chip area. But there is also a limitation for the length of the control channel as the pressure downstream diminishes because of the channel resistivity. Also, the Parylene gas diffusing length through the control channel with the process described in section 3.4 is fairly low and it confines the maximum length of the control channel.

The amount of heat that can be transferred into the Pluronic solution at the specified time scale can be enhanced with increasing the power of the given pulse. Nevertheless, here, the least possible amount of power (15 mW) was used for the sake of the scalability and efficiency of the device. The control channels of the device are 10 µm high and 100 µm wide and their lengths are shown in Figure 5.3.1. At the conditions above, flow of 15 wt% Pluronic solution can be stopped until $P_c = 20$ psi, the maximum pressure of the control channel. The control channel near the heater element where the 15 wt% Pluronic solution seeded with fluorescent particles is flowing from the bottom to the top is shown in Figure 5.3.4. As shown in Section 2.3, a 15 wt% Pluronic solidifies and becomes a gel at T = 28ºC and comparing it to the ambient temperature of the environment T = 24ºC it is a good choice. Higher concentrations of the Pluronic solution, which undergo gel formation above T = 24ºC can be used for this device and they give a faster flow stoppage for the same given pulse.

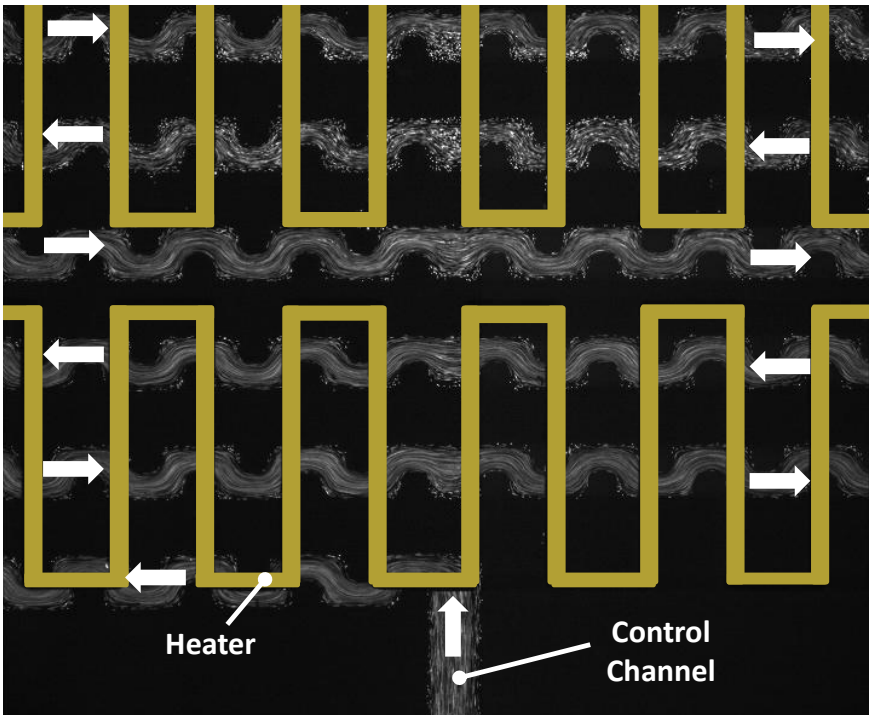

Figure 5.3.4 Pluronic solution 15wt% seeded with fluorescent particles is flowing inside the control channel near the heater element when the heater is off. When the heater is turned on the Pluronic solution receives enough heat in this area to form a gel and block the channel depending on the pressure driving the fluid.

The time to stop flow control by these 70 Ω heaters and for the control channel with the above dimensions at P_c = 20 psi can be determined using PIV. This has been shown in Figure 5.3.5.a. It shows the stoppage of the 15 wt% Pluronic solution inside the control channel upon an applying voltage shown in Figure 5.3.5.b. A section of the channel near the membrane is chosen to determine the response time of the valve. PIV was used to determine the average velocity of this section of the channel and by calculating the time it takes for the velocity to decrease from its initial value to zero. For the conditions mentioned above, this response time is about 5 sec,

which is reasonably good for the intended application of the device. However, the response time depends highly on the control channel cross-sectional dimensions near the heater.

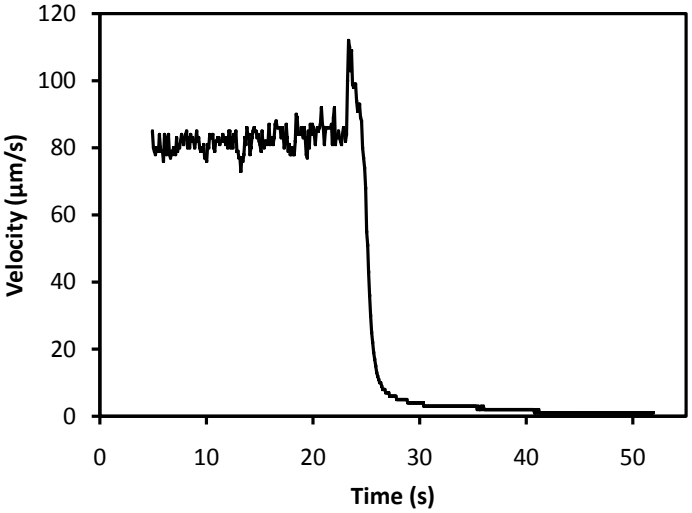

(a)

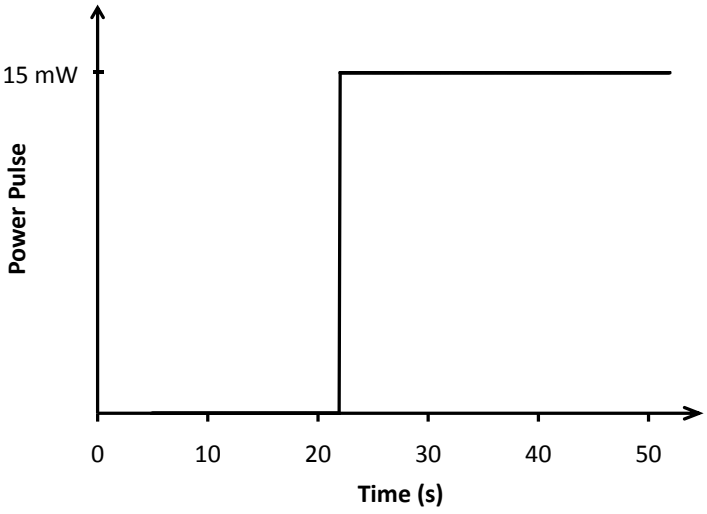

(b)

Figure 5.3.5 Performance of the heater shown in Figure 5.3.4 at P_c = 20 psi; (a) average velocity for a section of the control channel is calculated using PIV before and after heater activation; (b) the 15 mW power versus time, the device can be kept closed for several minutes without a major change to the re-liquefying time.

It will be shown in the next section that for the designed control channel lengths with a 10 µm thick membrane, the membrane can be fully deflected at P_c = 20 psi to close the fluidic channel driven by a 3 psi pressure. As mentioned this gel formation is very reproducible and when the heater is turned off, the gel liquefies and starts to flow again.

5.3.3 Demonstration of the Thermally Actuated Microfluidic Relay Valve

As mentioned above the pressure that drives the Pluronic solution inside the control channel needs to be high enough to fully deflect the membrane and at the same time not too high so that the flow can be stopped with the heaters upon a given pulse. It was shown in the section 5.3.1 that for the current device with the dimension mentioned the 10 µm thick membrane can be fully deflected at P_c = 20 psi or higher pressures to close and seal the fluidic channel in which fluid is driven with the pressure of P_f = 3 psi. In Section 5.3.2, the maximum pressure of the control channel at which the fluid can be stopped by the heater and with a 15 mW power pulse was measured as Pc = 20 psi. So it can be concluded that the pressure P_c = 20 psi is the ideal pressure source for the control channels when the pressure of the fluidic channel is P_f = 3 psi or lower. The performance of the device is shown in the Figure 5.3.6 where the average velocity of a section of a channel near the membrane is measured for both control and working fluid by PIV. The average velocity of each channel is normalized, i.e. the average velocity of the section is divided by its maximum value over the time period of the valve operation. Figure 5.3.6 shows that when the heater is

turned on at t = 10 sec, it takes a few seconds for the flow to stop inside the control channel at which point the working channel is opened to flow. At t = 35 sec the heater is turned off and the heat dissipates and the control channel near the heater is cooled down. Therefore, the Pluronic solution liquefies again so that the pressure P_c is available at the membrane. This closes the valve and the working fluid is stopped. The closing time of the valve, Δt_2 is almost 3.6 times greater that $\Delta t_{1,}$ the opening time of the valve, which is mainly due to the time of heat dissipation required for the device to cool down. Using low power for actuating the heater will guarantee that the valve can be kept open for several minutes without a major change in the closing response time, Δt_2.

For measuring the average velocity by PIV, a 15 wt% Pluronic solution in the control channel and distilled water as the working fluid inside the fluidic channel are seeded with fluorescent particles as shown in Figure 5.3.7. The stopped particles are clearly visible when the valve is closed (a); Figure 5.3.7.b shows the moment where the valve starts to open up, and Figure 5.3.7.c shows the fully opened valve, where the fluid reaches its maximum initial velocity.

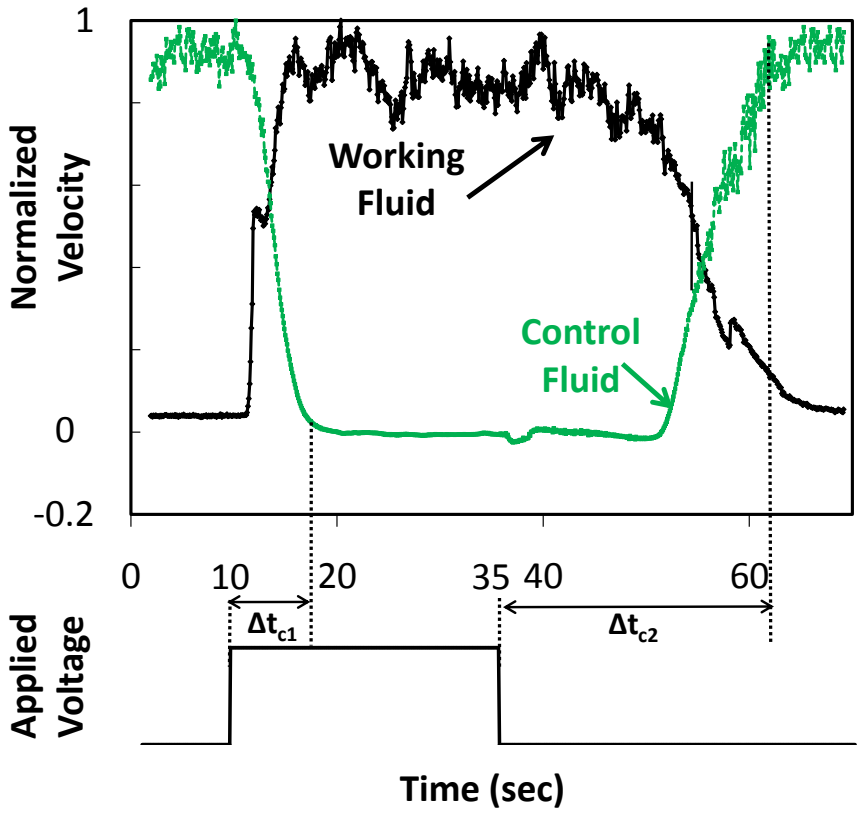

Figure 5.3.6 Valve operation; Normalized velocity profile of each fluid is shown versus time upon an applied voltage pulse between t =10 s and t = 35 s; the heat pulse results in local gel formation inside control channel near the heaters. The process is reversible and the control fluid is cooled below its gel temperature and is opened to flow with $\Delta t_{c2} \cong 3.6\ \Delta t_{c1}$.

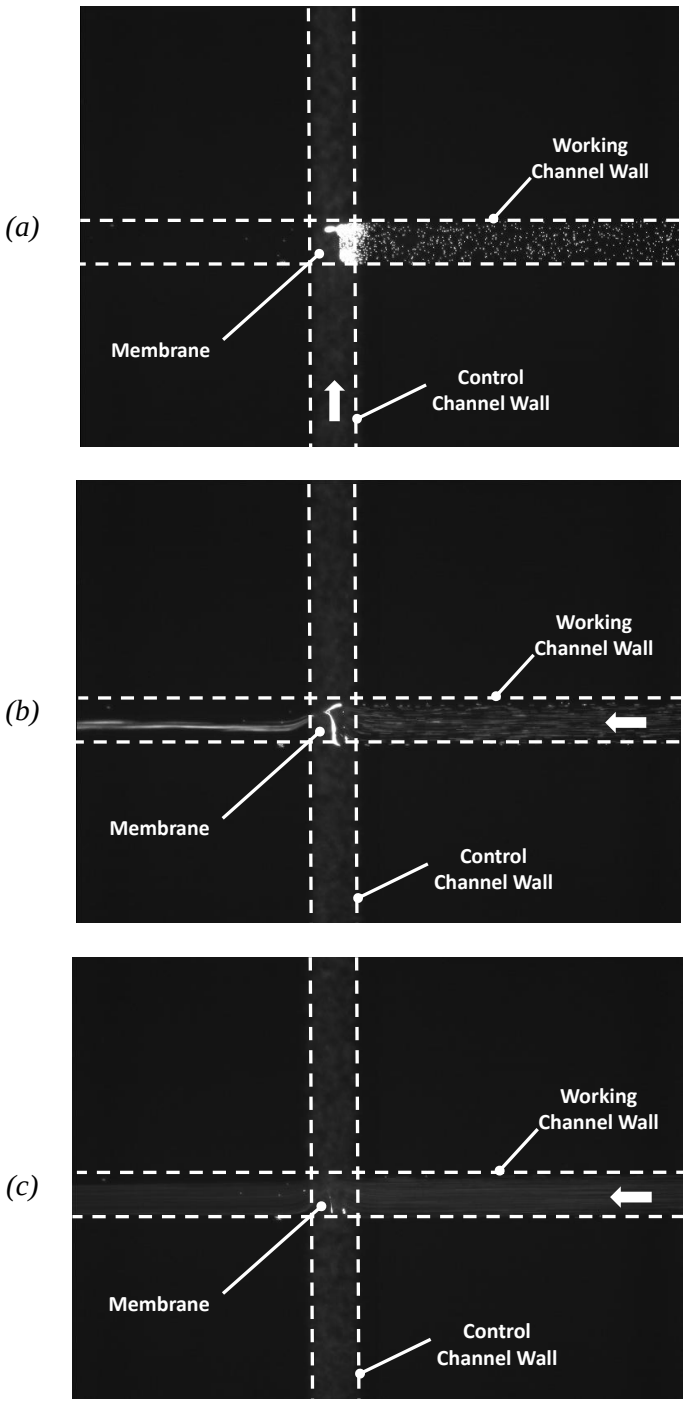

Figure 5.3.7 Control and fluidic channels seeded with Fluorescent particles with a concentration of 0.02 wt % when the heater is switched on the control channel is blocked and the fluidic channel

starts to flow (the control channel is out of focus). The valve is closed at (a); it starts to open at (b) and it is near fully-opened at (c).

The velocity field in a section of each control and working fluid shown in Figure 5.3.7 is included in Figure 5.3.8 before (a) and after (b) heater activation and opening the valve.

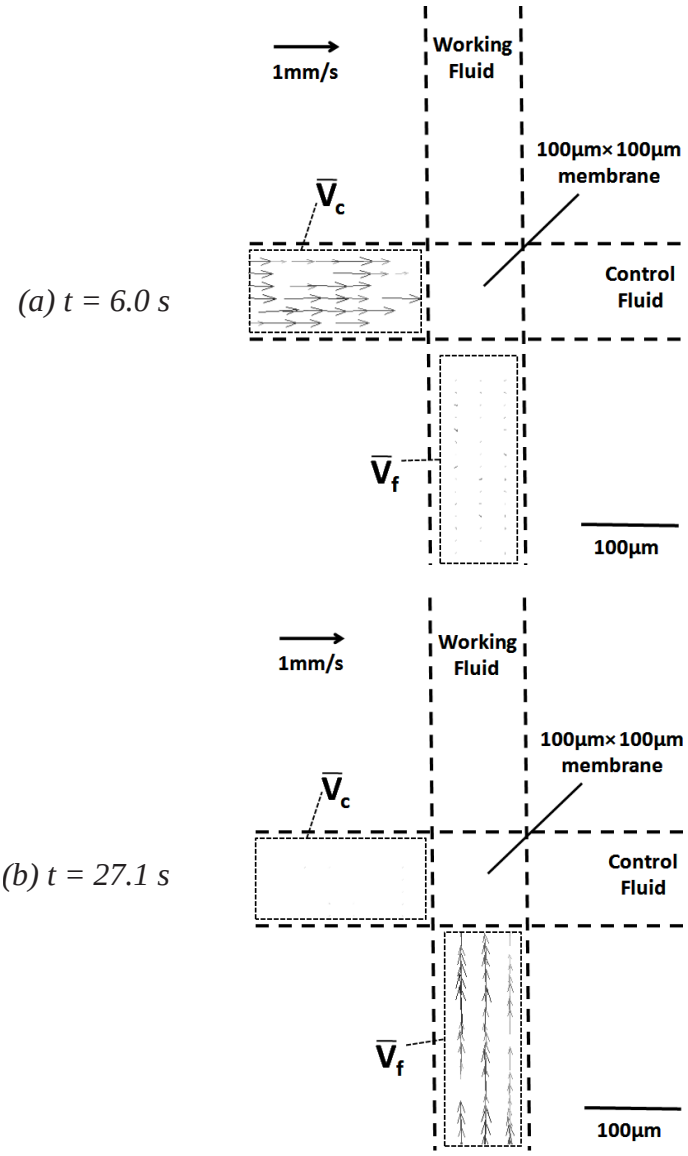

Figure 5.3.8 Velocity vector fields for control and working fluids before and after heater activation; (a) at t = 6 s the heater is off and the working fluid channel is closed while control fluid is driven with

the average velocity V_c; (b) at t = 27.1 s the heater is on and the valve for the working fluid is opened to flow with the average velocity of V_f while the control fluid is stopped.

5.4 Conclusion

Two flow control mechanisms in microfluidic devices were explained and the concept of the microfluidic relay valve taking the advantage of these two technologies was presented. The performance of this valve was demonstrated and its response time was measured for a basic on-off experiment using micro PIV. The valve was actuated with 15 mW power with a response time around $\Delta t \cong 5\ s$ while 15 wt% Pluronic solutions were driven in the control channels using a constant pressure source P_c = 20 psi.

CHAPTER 6

Conclusion

6.1 Summary

Two different flow control mechanisms based on thermally responsive polymer solutions have been discussed, all of which are based on the presence of the thermally responsive polymer Pluronic in the microfluidic system. These concepts allow easy integration into lab-on-a-chip devices.

First, a cross-channel transport concept has been developed in which a gel wall is formed in the center of a microfluidic channel at the diffusive interface between a Pluronic solution and a sodium phosphate solution. The wall is generated on one of its sides and it is dissolved on its second side, leading to a steady motion across the channel. During wall generation, particles or living cells can be included in the wall, which then move at the same velocity as the wall and are transported from one fluid stream into the second fluid stream. It is possible to maintain a concentration gradient of diffusive compounds across the wall and the transition time of objects moving across the wall can be adjusted through the flow rates of the fluid streams and the concentration of the compound that leads to a lower gel formation temperature of the Pluronic solution (here: sodium phosphate). Here, this was demonstrated for 15 wt% Pluronic solution and 3 different concentrations of sodium

phosphate (0.5, 0.8 and 1 mol/L) at several identical driving pressures for both between from 1 psi and 25 psi and the temperature of the device was kept at ambient temperature (T= 24°C).

Furthermore, the concept of a thermally actuated microfluidic relay valve was presented. Microfluidic systems with channels in two layers have been fabricated from PDMS and demonstrated with a glass substrate containing heaters; control channels were located in one layer that communicates with the main channels through flexible PDMS membranes. A constant pressure source (here around 20 psi) drives a thermally responsive polymer solution through all control channels in parallel and this pressure is high enough to close the valve and stop the working fluid (driven by a 3 psi pressure source) in the fluidic channels. Heaters (with the resistivity of 70 Ω) are integrated into the control channels upstream from the membranes. Upon heating one heater (with a power of 15 mW), the solution solidifies in that location and forms a gel that closes the control channel and that prevents transferring the pressure downstream to the membrane so that the valve opens and the working fluid starts flowing. The process is repeatable and the response time is sufficiently fast (here was around 5 sec for opening and around 15 sec for closing the valve).

6.2 Future Work

For the cross-channel transport concept, the future work could be the demonstrating practical utility of the device and transporting particles (such as cells) from one stream to another. Also a characterization of the wall thicknesses for different temperatures of the device can be done to verify the understanding of the

concept. Numerical simulations of the phenomena could be performed to verify experimental results and the analytical discussion. Finally, using the other materials for the gel wall formation can be investigated.

Also the thermally actuated microfluidic valve concept presented here needs a relatively high pressure inside the control channels to deflect the membranes downstream. The pressure decreases along the channel and the characteristic of the valve depends on the distance of the membrane from the control channel inlets. Therefore future work could focus on using another heater in the control channels downstream near the outlet of the control channel so that the channel can be kept closed by forming a gel near this heater during pressurizing of the membrane. Also, improving the performance of the valve using an optimized design and reducing the size of the device could be future steps. Finally, the demonstration of the manipulation of biological materials on-chip using this technology and in particular sorting and characterization of biological cells can be investigated.

Bibliography

[1] S. Shoji and M. Esashi, "Microflow devices and systems," *J Micromech Microengineering,* vol. 4, pp. 157-171, 1994.

[2] C. Yu, S. Mutlu, P. Selvaganapathy, C. H. Mastrangelo, F. Svec and J. M. J. Fréchet, "Flow Control Valves for Analytical Microfluidic Chips without Mechanical Parts Based on Thermally Responsive Monolithic Polymers," *Nat. Biotechnol.*, vol. 19, pp. 717-721, 2001.

[3] E. Carlen and C. Mastrangelo, "Electrothermally activated paraffin microactuators," *Microelectromechanical Systems, Journal of,* vol. 11, pp. 165-174, 2002.

[4] E. Carlen and C. Mastrangelo, "Surface micromachined paraffin-actuated microvalve," *Microelectromechanical Systems, Journal of,* vol. 11, pp. 408-420, 2002.

[5] R. Liu, Q. Yu, J. Bauer, J. Moore and D. Beebe, "Hydrogel microvalves fabricated using in-situ polymerization," in *Technical Digest of the Solid-State Sensor and Actuator Workshop, Hilton Head Island, SC, USA,* 2000, pp. 222-226.

[6] J. Melin, G. Gimenez, N. Roxhed, van der Wijngaart, W. and G. Stemme, "A passive 2-dimensional liquid sample micromixer," *Proceedings of mTAS,* vol. 3, pp. 5–9,

[7] P. Belgrader, M. Okuzumi, F. Pourahmadi, D. A. Borkholder and M. A. Northrup, "A microfluidic cartridge to prepare spores for PCR analysis," *Biosensors and Bioelectronics,* vol. 14, pp. 849-852, 2000.

[8] Y. Shirasaki, H. Makazu, K. Tashiro, S. Ikeda, T. Sekigushi, S. Shoji, S. Tsukita and T. Funatsu, "A Novel Biomolecule Sorter Using Thermosensitive Hydrogel in Micro Flow System," *Micro Total Analysis Stems,* vol. 2, pp. 925-927, 2002.

[9] B. Stoeber, Z. Yang, D. Liepmann and S. Muller, "Flow control in microdevices using thermally responsive triblock copolymers," *Microelectromechanical Systems, Journal of,* vol. 14, pp. 207-213, 2005.

[10] C. Willert and M. Gharib, "Digital particle image velocimetry," *Exp. Fluids,* vol. 10, pp. 181-193, 1991.

[11] J. Westerweel, "Fundamentals of digital particle image velocimetry," *Measurement Science and Technology,* vol. 8, pp. 1379-1392, 1997.

[12] S. K. W. Dertinger, D. T. Chiu, N. Li Jeon and G. M. Whitesides, "Generation of Gradients Having Complex Shapes Using Microfluidic Networks," *ANALYTICAL CHEMISTRY-WASHINGTON DC-,* vol. 73, pp. 1240-1246, 2001.

[13] N. L. Jeon, S. K. W. Dertinger, D. T. Chiu, I. S. Choi, A. D. Stroock and G. M. Whitesides, "Generation of solution and surface gradients using microfluidic systems," *Langmuir,* vol. 16, pp. 8311-8316, 2000.

[14] A. Hatch, A. E. Kamholz, K. R. Hawkins, M. S. Munson, E. A. Schilling, B. H. Weigl and P. Yager, "A rapid diffusion immunoassay in a T-sensor," *Nat. Biotechnol.,* vol. 19, pp. 461-465, 2001.

[15] I. Glasgow, H. Beebe, D. J. S. J. C. Lyman, J. Chan and N. Wheeler, "Handling individual mammalian embryos using microfluidics," *IEEE Transactions on Biomedical Engineering,* vol. 48, pp. 570-578, 2001.

[16] J. Yang, Y. Huang, X. B. Wang, F. F. Becker and P. R. C. Gascoyne, "Cell separation on microfabricated electrodes using dielectrophoretic/gravitational field-flow fractionation," *Anal. Chem.,* vol. 71, pp. 911–918, 1999.

[17] D. T. Chiu, N. L. Jeon, S. Huang, R. S. Kane, C. J. Wargo, I. S. Choi, D. E. Ingber and G. M. Whitesides, "Patterned deposition of cells and proteins onto surfaces by using three-dimensional microfluidic systems," *Proceedings of the National Academy of Sciences,* vol. 97, pp. 2408-2413, 2000.

[18] A. Folch, B. H. Jo, O. Hurtado, D. J. Beebe and M. Toner, "Microfabricated elastomeric stencils for micropatterning cell cultures," *J. Biomed. Mater. Res.,* vol. 52, pp. 346-353, 2000.

[19] D. Bosch, B. Heimhofer, G. Muck, H. Seidel, U. Thumser and W. Welser, "A silicon microvalve with combined electromagnetic/electrostatic actuation," *Sensors and Actuators A,* vol. 37, pp. 38, 1993.

[20] I. Chakraborty, W. Tang, D. Bame and T. Tang, "MEMS micro-valve for space applications," *Sensors & Actuators: A.Physical,* vol. 83, pp. 188-193, 2000.

[21] C. Rich and K. Wise, "A high-flow thermopneumatic microvalve with improved efficiency and integrated state sensing," *Microelectromechanical Systems, Journal of,* vol. 12, pp. 201-208, 2003.

[22] A. A. Deshmukh, D. Liepmann and A. P. Pisano, "Characterization of a micro-mixing, pumping, and valving system," in *Proceedings of the 11th International Conference on Solid State Sensors and Actuators (Transducers' 01), Munich, Germany, June,* 2001, pp. 10-14.

[23] M. Koch, A. Brunnschweiler and A. Evans, *Microfluidic Technology and Applications.* Research Studies Press,

[24] M. J. Madou, *Fundamentals of Microfabrication: The Science of Miniaturization.* CRC Press, 2002,

[25] W. S. N. Trimmer, "Microrobots and micromechanical systems," *Sensors and Actuators,* vol. 19, pp. 267-287, 1989.

[26] E. Peters, F. Svec and J. Frechet, "Thermally responsive rigid polymer monoliths," *Adv Mater,* vol. 9, pp. 630–633, 1997.

[27] N. T. Nguyen and S. T. Wereley, *Fundamentals and Applications of Microfluidics.* Artech House, 2002,

[28] S. Haeberle and R. Zengerle, "Microfluidic platforms for lab-on-a-chip applications," *Lab on a Chip,* vol. 7, pp. 1094-1110, 2007.

[29] S. Ghosal, "Fluid mechanics of electroosmotic flow and its effect on band broadening in capillary electrophoresis," *Electrophoresis,* vol. 25, pp. 214-228, 2004.

[30] L. M. Fu, R. Yang, G. Lee and H. Liu, "Electrokinetic Injection Techniques in Microfluidic Chips," *ANALYTICAL CHEMISTRY-WASHINGTON DC-,* vol. 74, pp. 5084-5091, 2002.

[31] A. L. Garcia, L. K. Ista, D. N. Petsev, M. J. O'Brien, P. Bisong, A. A. Mammoli, S. R. J. Brueck and G. P. López, "Electrokinetic molecular separation in nanoscale fluidic channels," *Lab on a Chip,* vol. 5, pp. 1271-1276, 2005.

[32] R. F. Probstein, *Physicochemical Hydrodynamics: An Introduction.* John Wiley & Sons, 1994,

[33] F. Mugele and J. Baret, " Electrowetting: from basics to applications," *J Phys Condens Matter,* vol. 17, 2005.

[34] M. G. Pollack, R. B. Fair and A. D. Shenderov, "Electrowetting-based actuation of liquid droplets for microfluidic applications," *Appl. Phys. Lett.,* vol. 77, pp. 1725, 2000.

[35] J. Lee and C. J. Kim, "Surface-tension-driven microactuation based on continuouselectrowetting," *Journal of Microelectromechanical Systems,* vol. 9, pp. 171-180, 2000.

[36] D. Chatterjee, B. Hetayothin, A. R. Wheeler, D. J. King and R. L. Garrell, "Droplet-based microfluidics with nonaqueous solvents and solutions," *Lab on a Chip,* vol. 6, pp. 199-206, 2006.

[37] J. Voldman, "ELECTRICAL FORCES FOR MICROSCALE CELL MANIPULATION,"

[38] M. Barbic, J. J. Mock, A. P. Gray and S. Schultz, "Electromagnetic micromotor for microfluidics applications," *Appl. Phys. Lett.,* vol. 79, pp. 1399, 2001.

[39] A. Wixforth, C. Strobl, C. Gauer, A. Toegl, J. Scriba and Z. v. Guttenberg, "Acoustic manipulation of small droplets," *Analytical and Bioanalytical Chemistry,* vol. 379, pp. 982-991, 2004.

[40] A. Wixforth, "Acoustically driven planar microfluidics," *Superlattices and Microstructures,* vol. 33, pp. 389-396, 2003.

[41] D. Beyssen, L. Le Brizoual, O. Elmazria and P. Alnot, "Microfluidic device based on surface acoustic wave," *Sensors & Actuators: B.Chemical,* vol. 118, pp. 380-385, 2006.

[42] T. S. Wiedmann, H. Herrington, C. Deye and D. Kallick, "Distribution and Diffusion of Sodium Taurocholate and Egg Phosphatidylcholine Aggregates in Rat Intestinal Mucin," *Pharm. Res.,* vol. 18, pp. 1489-1496, 2001.

[43] T. M. Squires and S. R. Quake, "Microfluidics: Fluid physics at the nanoliter scale," *Reviews of Modern Physics,* vol. 77, pp. 977-1026, 2005.

[44] H. Bruus, *Theoretical Microfluidics Oxford Master Series in Condensed Matter Physics.* Oxford University Press, 2008,

[45] G. Karniadakis, A. Beskok and N. Aluru, "Microflows and nanoflows: fundamentals and simulation,(Eds SS Antman, JE Marsden, and L. Sirovich), 2005,"

[46] P. Tabeling, *Introduction to Microfluidics.* Oxford University Press, 2005,

[47] J. M. Ottino and S. Wiggins, "Introduction: mixing in microfluidics," *Philosophical Transactions of the Royal Society A: Mathematical, Physical and Engineering Sciences,* vol. 362, pp. 923-935, 2004.

[48] R. F. Ismagilov, A. D. Stroock, P. J. A. Kenis, G. Whitesides and H. A. Stone, "Experimental and theoretical scaling laws for transverse diffusive broadening in two-phase laminar flows in microchannels," *Appl. Phys. Lett.,* vol. 76, pp. 2376, 2000.

[49] N. T. Nguyen and Z. Wu, "Micromixers—a review," *J.Micromech.Microeng,* vol. 15, 2005.

[50] V. Hessel, H. Löwe and F. Schönfeld, "Micromixers—a review on passive and active mixing principles," *Chemical Engineering Science,* vol. 60, pp. 2479-2501, 2005.

[51] E. Cussler, *Diffusion: Mass Transfer in Fluid Systems.* Cambridge University Press, 1997,

[52] A. E. Kamholz and P. Yager, "Molecular diffusive scaling laws in pressure-driven microfluidic channels: deviation from one-dimensional Einstein approximations," *Sensors & Actuators: B.Chemical,* vol. 82, pp. 117-121, 2002.

[53] A. E. Kamholz and P. Yager, "Theoretical Analysis of Molecular Diffusion in Pressure-Driven Laminar Flow in Microfluidic Channels," *Biophys. J.,* vol. 80, pp. 155-160, 2001.

[54] R. Bird, W. Stewart, E. Lightfoot and R. E. Meredith, "Transport Phenomena," *J. Electrochem. Soc.,* vol. 108, pp. 78C, 1961.

[55] B. Stoeber, C. M. J. Hu, D. Liepmann and S. J. Muller, "Passive flow control in microdevices using thermally responsive polymer solutions," *Phys. Fluids,* vol. 18, pp. 053103, 2006.

[56] W. Kwang and H. Chong, "A review of microvalves," *J Micromech Microengineering,* vol. 16, pp. 13-39, 2006.

[57] C. B. Liu, C. Y. Gong, Y. F. Pan, Y. D. Zhang, J. W. Wang, M. J. Huang, Y. S. Wang, K. Wang, M. L. Gou and M. J. Tu, "Synthesis and characterization of a thermosensitive hydrogel based on biodegradable amphiphilic PCL-Pluronic (L35)-PCL block copolymers," *Colloids Surf. Physicochem. Eng. Aspects*, vol. 302, pp. 430-438, 2007.

[58] E. S. Gil and S. M. Hudson, "Stimuli-reponsive polymers and their bioconjugates," *Progress in Polymer Science,* vol. 29, pp. 1173-1222, 2004.

[59] R. YOSHIDA, K. SAKAI, T. OKANO and Y. SAKURAI, "Pulsatile drug delivery systems using hydrogels," *Adv. Drug Deliv. Rev.*, vol. 11, pp. 85-108, 1993.

[60] A. S. Hoffman, "Applications of thermally reversible polymers and hydrogels in therapeutics and diagnostics," *J. Control. Release,* vol. 6, pp. 297-305, 1987.

[61] L. E. Bromberg and E. S. Ron, "Temperature-responsive gels and thermogelling polymer matrices for protein and peptide delivery," *Adv. Drug Deliv. Rev.*, vol. 31, pp. 197-221, 1998.

[62] M. Malmsten and B. Lindman, "Self-assembly in aqueous block copolymer solutions," *Macromolecules,* vol. 25, pp. 5440-5445, 1992.

[63] K. Zhang and A. Khan, "Phase Behavior of Poly (ethylene oxide)-Poly (propylene oxide)-Poly (ethylene oxide) Triblock Copolymers in Water," *Macromolecules,* vol. 28, pp. 3807-3812, 1995.

[64] B. H. Lee, Y. M. Lee, Y. S. Sohn and S. C. Song, "A Thermosensitive Poly (organophosphazene) Gel," *Macromolecules,* vol. 35, pp. 3876-3879, 2002.

[65] K. Yoshida, M. Kikuchi, J. H. Park and S. Yokota, "Fabrication of micro electro-rheological valves (ER valves) by micromachining and experiments," *Sensors & Actuators: A.Physical,* vol. 95, pp. 227-233, 2002.

[66] J. PARK, K. YOSHIDA and S. YOKOTA, "A Micro Fluid Control System Using Homogeneous ER Fluid." *Transactions of the Japan Society of Mechanical Engineers.C,* vol. 66, pp. 2700-2706, 2000.

[67] R. Pal, M. Yang, B. N. Johnson, D. T. Burke and M. A. Burns, "Phase change microvalve for integrated devices," *Anal. Chem.*, vol. 76, pp. 3740-3748, 2004.

[68] R. H. Liu, J. Bonanno, J. Yang, R. Lenigk and P. Grodzinski, "Single-use, thermally actuated paraffin valves for microfluidic applications," *Sensors & Actuators: B.Chemical,* vol. 98, pp. 328-336, 2004.

[69] R. H. Liu, J. Yang, R. Lenigk, J. Bonanno and P. Grodzinski, "Self-Contained, Fully Integrated Biochip for Sample Preparation, Polymerase Chain Reaction Amplification, and DNA Microarray Detection," *Science,* vol. 261, pp. 895-897, 1993.

[70] L. Gui and J. Liu, "Ice valve for a mini/micro flow channel," *J Micromech Microengineering,* vol. 14, pp. 242-246, 2004.

[71] M. Madou, "Fundamentals of Microfabrication, 1997,"

[72] D. J. Beebe, J. S. Moore, J. M. Bauer, Q. Yu, R. H. Liu, C. Devadoss and B. H. Jo, "Functional hydrogel structures for autonomous flow control inside microfluidic channels," *Nature,* vol. 404, pp. 588-590, 2000.

[73] T. Tanaka, "Collapse of Gels and the Critical Endpoint," *Phys. Rev. Lett.,* vol. 40, pp. 820-823, 1978.

[74] F. Iemma, U. G. Spizzirri, F. Puoci, R. Muzzalupo, S. Trombino, R. Cassano, S. Leta and N. Picci, "pH-Sensitive hydrogels based on bovine serum albumin for oral drug delivery," *Int. J. Pharm.,* vol. 312, pp. 151-157, 2006.

[75] B. Johnson, D. Niedermaier, W. Crone, J. Moorthy and D. Beebe, "Mechanical Properties of a pH Sensitive Hydrogel," *Society for Experimental Mechanics, Annual Conference Proceedings,* 2002.

[76] M. Lei, A. Salim, R. Siegel and B. Ziaie, "A hydrogel-actuated microvalve for smart flow control," *Engineering in Medicine and Biology Society, 2004.EMBC 2004.Conference Proceedings.26th Annual International Conference of the,* vol. 1, 2004.

[77] A. Richter, G. Paschew, S. Klatt, J. Lienig, K. F. Arndt and H. J. P. Adler, "Review on Hydrogel-based pH Sensors and Microsensors," *Sensors,* vol. 8, pp. 561-581, 2008.

[78] J. Y. Park, H. J. Oh, D. J. Kim, J. Y. Baek and S. H. Lee, "A polymeric microfluidic valve employing a pH-responsive hydrogel microsphere as an actuating source," *J Micromech Microengineering,* vol. 16, pp. 656, 2006.

[79] R. Liu, Q. Yu and D. Beebe, "Fabrication and characterization of hydrogel-based microvalves," *Microelectromechanical Systems, Journal of,* vol. 11, pp. 45-53, 2002.

[80] A. Baldi, Y. Gu, P. Loftness, R. Siegel and B. Ziaie, "A hydrogel-actuated environmentally sensitive microvalve for active flow control," *Microelectromechanical Systems, Journal of,* vol. 12, pp. 613-621, 2003.

[81] W. Kuhn, B. Hargitay, A. Katchalsky and H. Eisenberg, "Reversible dilation and contraction by changing the state of ionization of high-polymer acid networks," *Nature,* vol. 165, pp. 514-516, 1950.

[82] W. Kuhn, O. Kuenzle and A. Katchalsky, "Verhalten polyvalenter Fadenmolekelionen in Loesung," *Helv. Chim. Acta,* vol. 31, pp. 1994-2037, 1948.

[83] K. F. Arndt, D. Kuckling and A. Richter, "Application of sensitive hydrogels in flow control," *Polym. Adv. Technol.,* vol. 11, pp. 496-505, 2000.

[84] R. Bashir, J. Hilt, O. Elibol, A. Gupta and N. Peppas, "Micromechanical cantilever as an ultrasensitive pH microsensor," *Appl. Phys. Lett.,* vol. 81, pp. 3091, 2002.

[85] B. Stoeber, D. Liepmann and S. Muller, "Microflow control using thermally responsive triblock copolymers," in *Proceedings of the Seventh International Symposium on Micro Total Analysis Systems, Squaw Valley, CA,* 2003, pp. 183–186.

[86] A. K. Richter, D. Howitz and S. T. G. Arndt, "Electronically controllable microvalves based on smart hydrogels: magnitudes and potential applications," *Microelectromechanical Systems, Journal of,* vol. 12, pp. 748-753, 2003.

[87] A. Richter, S. Howitz, D. Kuckling, K. Kretschmer and K. F. Arndt, "Automatically and Electronically Controllable Hydrogel Based Valves and Microvalves-Design and Operating Performance," *MACROMOLECULAR SYMPOSIA,* vol. 210, pp. 447-456, 2004.

[88] J. W. GARDNER, "VARADAN Vijay k, AUADELKARIN Osama O. Microsensors, MEMS, and smart devices [M]. England," 2002.

[89] M. Suzuki, "Amphoteric polyvinyl alcohol hydrogel and electrohydrodynamic control method for artificial muscles," *DeRossi (Ed.), New York,* vol. 221, 1991.

[90] R. Kishi, H. Ichijo and O. Hirasa, "Thermo-Responsive Devices Using Poly (vinyl methyl ether) Hydrogels," *J Intell Mater Syst Struct,* vol. 4, pp. 533, 1993.

[91] K. Kajiwara and S. B. Ross-Murphy, "Synthetic gels on the move," *Nature,* vol. 355, pp. 208-209, 1992.

[92] Y. Osada, H. Okuzaki and H. Hori, "A polymer gel with electrically driven motility," *Nature*, vol. 355, pp. 242-244, 1992.

[93] Y. Ueoka, J. Gong and Y. Osada, "Chemomechanical Polymer Gel with Fish-like Motion," *J Intell Mater Syst Struct*, vol. 8, pp. 465, 1997.

[94] K. Park and H. Park, "Smart hydrogels," *Concise Polymeric Materials Encyclopedia*, pp. 1476–1478, 1999.

[95] L. Dong and A. Hoffman, "Reversible polymeric gels and related systems," *ACS Symp. Ser.*, 1987.

[96] K. Park, W. S. W. Shalaby and H. Park, *Biodegradable Hydrogels for Drug Delivery*. CRC Press, 1993,

[97] B. Jeong, S. W. Kim and Y. H. Bae, "Thermosensitive sol–gel reversible hydrogels," *Adv. Drug Deliv. Rev.*, vol. 54, pp. 37-51, 2002.

[98] L. C. DONG and A. HOFFMAN, "Thermally reversible hydrogels. III: Immobilization of enzymes for feedback reaction control," *J. Controlled Release*, vol. 4, pp. 223-227, 1986.

[99] T. Kissel, Y. Li and F. Unger, "ABA-triblock copolymers from biodegradable polyester A-blocks and hydrophilic poly (ethylene oxide) B-blocks as a candidate for in situ forming hydrogel delivery systems for proteins," *Adv. Drug Deliv. Rev.*, vol. 54, pp. 99-134, 2002.

[100] B. Jeong, Y. H. Bae, D. S. Lee and S. W. Kim, "Biodegradable block copolymers as injectable drug-delivery systems," *NATURE-LONDON-*, pp. 860-861, 1997.

[101] E. Ruel-Gariépy and J. C. Leroux, "In situ-forming hydrogels—review of temperature-sensitive systems," *European Journal of Pharmaceutics and Biopharmaceutics*, vol. 58, pp. 409-426, 2004.

[102] S. W. O. N. CHOI, S. I. Y. CHOI, B. JEONG, S. W. A. N. KIM and D. O. O. S. LEE, "Thermoreversible Gelation of Poly (ethylene oxide) Biodegradable Polyester Block Copolymers. II," *Journal of Polymer Science: Part A: Polymer Chemistry*, vol. 37, pp. 2207-2218, 1999.

[103] M. Ebara, M. Yamato, M. Hirose, T. Aoyagi, A. Kikuchi, K. Sakai and T. Okano, "Copolymerization of 2-Carboxyisopropylacrylamide with N-Isopropylacrylamide

Accelerates Cell Detachment from Grafted Surfaces by Reducing Temperature," *BIOMACROMOLECULES-WASHINGTON-,* vol. 4, pp. 344-349, 2003.

[104] K. Nakajima, S. Honda, Y. Nakamura, F. López-Redondo, S. Kohsaka, M. Yamato, A. Kikuchi and T. Okano, "Intact microglia are cultured and non-invasively harvested without pathological activation using a novel cultured cell recovery method," *Biomaterials,* vol. 22, pp. 1213-1223, 2001.

[105] M. Yamato, C. Konno, A. Kushida, M. Hirose, M. Utsumi, A. Kikuchi and T. Okano, "Release of adsorbed fibronectin from temperature-responsive culture surfaces requires cellular activity," *Biomaterials,* vol. 21, pp. 981-986, 2000.

[106] M. A. Nandkumar, M. Yamato, A. Kushida, C. Konno, M. Hirose, A. Kikuchi and T. Okano, "Two-dimensional cell sheet manipulation of heterotypically co-cultured lung cells utilizing temperature-responsive culture dishes results in long-term maintenance of differentiated epithelial cell functions," *Biomaterials,* vol. 23, pp. 1121-1130, 2002.

[107] K. Uchida, K. Sakai, E. Ito, O. Hyeong Kwon, A. Kikuchi, M. Yamato and T. Okano, "Temperature-dependent modulation of blood platelet movement and morphology on poly (N-isopropylacrylamide)-grafted surfaces," *Biomaterials,* vol. 21, pp. 923-929, 2000.

[108] A. Chilkoti, M. R. Dreher, D. E. Meyer and D. Raucher, "Targeted drug delivery by thermally responsive polymers," *Adv. Drug Deliv. Rev.,* vol. 54, pp. 613-630, 2002.

[109] J. Weidner, "Drug delivery and drug targeting: Drug targeting using thermally responsive polymers and local hyperthermia," *Drug Discov. Today,* vol. 6, pp. 1239-1241, 2001.

[110] B. Jeong, K. M. Lee, A. Gutowska and Y. H. An, "Thermogelling Biodegradable Copolymer Aqueous Solutions for Injectable Protein Delivery and Tissue Engineering," *BIOMACROMOLECULES-WASHINGTON-,* vol. 3, pp. 865-868, 2002.

[111] H. SCHILD, "Poly(N-isopropylacrylamide): experiment, theory and application," *Progress in Polymer Science,* vol. 17, pp. 163-249, 1992.

[112] K. Kuroda, "Thermally responsive polymers and their applications," 2003.

[113] Y. Qiu and K. Park, "Environment-sensitive hydrogels for drug delivery," *Adv. Drug Deliv. Rev.,* vol. 53, pp. 321-339, 2001.

[114] W. Brown, K. Schillen and S. Hvidt, "Triblock copolymers in aqueous solution studied by static and dynamic light scattering and oscillatory shear measurements: influence of relative block sizes," *J. Phys. Chem.,* vol. 96, pp. 6038-6044, 1992.

[115] B. Jeong, Y. Choi, Y. Bae, G. Zentner and S. Kim, "New biodegradable polymers for injectable drug delivery systems," *J. Controlled Release,* vol. 62, pp. 109-114, 1999.

[116] B. Jeong, Y. H. Bae and S. W. Kim, "Drug release from biodegradable injectable thermosensitive hydrogel of PEG–PLGA–PEG triblock copolymers," *J. Controlled Release,* vol. 63, pp. 155-163, 2000.

[117] P. Alexandridis and T. Alan Hatton, "Poly (ethylene oxide)□ poly (propylene oxide)□ poly (ethylene oxide) block copolymer surfactants in aqueous solutions and at interfaces: thermodynamics, structure, dynamics, and modeling," *Colloids Surf. Physicochem. Eng. Aspects,* vol. 96, pp. 1-46, 1995.

[118] M. Guzálin, F. Garcia and J. Molpeceres, "Gelatine Gels and Polyoxyethylene-Polyoxypropylene Gels: Comparative Study of Their Properties," *Drug Dev. Ind. Pharm.,* vol. 20, pp. 2041-2048, 1994.

[119] B. K. Lau, Q. Wang, W. Sun and L. Li, "Micellization to gelation of a triblock copolymer in water: Thermoreversibility and scaling," *JOURNAL OF POLYMER SCIENCE PART B POLYMER PHYSICS,* vol. 42, pp. 2014-2025, 2004.

[120] J. Escobar-Chávez, M. López-Cervantes, A. Naik, Y. Kalia, D. Quintanar-Guerrero and A. Ganem-Quintanar, "Applications of thermo-reversible pluronic F-127 gels in pharmaceutical formulations." *Journal of Pharmacy and Pharmaceutical Sciences,* vol. 9, pp. 339-358, 2006.

[121] M. Bohorquez, C. Koch, T. Trygstad and N. Pandit, "A Study of the Temperature-Dependent Micellization of Pluronic F127," *J. Colloid Interface Sci.,* vol. 216, pp. 34-40, 1999.

[122] C. Wu, T. Liu, B. Chu, D. K. Schneider and V. Graziano, "Characterization of the PEO-PPO-PEO Triblock Copolymer and Its Application as a Separation Medium in Capillary Electrophoresis," *Macromolecules,* vol. 30, pp. 4574-4583, 1997.

[123] S. Senkow, S. K. Mehta, G. Douhéret, A. H. Roux and G. Roux-Desgranges, "Aqueous solutions of some amphiphilic poly (ethylene oxide)–poly (propylene oxide)–poly (ethylene oxide) triblock copolymers. A thermodynamic study over a wide

concentration range at temperatures between 288.15 and 328.15 K," *Physical Chemistry Chemical Physics,* vol. 4, pp. 4472-4480, 2002.

[124] Y. Su, J. Wang and H. Liu, "Formation of a Hydrophobic Microenvironment in Aqueous PEO-PPO-PEO Block Copolymer Solutions Investigated by Fourier Transform Infrared Spectroscopy," *J Phys Chem B,* vol. 106, pp. 11823-11828, 2002.

[125] A. Caragheorgheopol, H. Caldararu, I. Dragutan, H. Joela and W. Brown, "Micellization and Micellar Structure of a Poly (ethylene oxide)/Poly (propylene oxide)/Poly (ethylene oxide) Triblock Copolymer in Water Solution, As Studied by the Spin Probe Technique," *Langmuir,* vol. 13, pp. 6912-6921, 1997.

[126] E. Ricci, M. V. L. B. Bentley, M. Farah, R. E. S. Bretas and J. Marchetti, "Rheological characterization of Poloxamer 407 lidocaine hydrochloride gels," *European Journal of Pharmaceutical Sciences,* vol. 17, pp. 161-167, 2002.

[127] J. P. Habas, E. Pavie, A. Lapp and J. Peyrelasse, "Understanding the complex rheological behavior of PEO–PPO–PEO copolymers in aqueous solution," *J. Rheol.,* vol. 48, pp. 1, 2003.

[128] M. Maheshwari, A. Paradkar, S. Yamamura and S. Kadam, "Preparation and characterization of Pluronic-colloidal silicon dioxide composite particles as liquid crystal precursor," *AAPS PharmSciTech,* vol. 7, pp. 70-76, 2006.

[129] N. Pandit, T. Trygstad, S. Croy, M. Bohorquez and C. Koch, "Effect of Salts on the Micellization, Clouding, and Solubilization Behavior of Pluronic F127 Solutions," *J. Colloid Interface Sci.,* vol. 222, pp. 213-220, 2000.

[130] Y. Rhee, Y. Shin, C. Park, S. Chi and E. Park, "Effect of Flavors on the Viscosity and Gelling Point of Aqueous Poloxamer Solution," *Arch. Pharm. Res.,* vol. 29, pp. 1171, 2006.

[131] B. C. Anderson, S. M. Cox, A. V. Ambardekar and S. K. Mallapragada, "The effect of salts on the micellization temperature of aqueous poly (ethylene oxide)-b-poly (propylene oxide)-b-poly (ethylene oxide) solutions and the dissolution rate and water diffusion coefficient in their corresponding gels," *J. Pharm. Sci.,* vol. 91, pp. 180-188, 2002.

[132] M. Almgren, W. Brown and S. Hvidt, "Self-aggregation and phase behavior of poly (ethylene oxide)-poly (propylene oxide)-poly (ethylene oxide) block copolymers in aqueous solution," *Colloid & Polymer Science,* vol. 273, pp. 2-15, 1995.

[133] E. Joergensen, S. Hvidt, W. Brown and K. Schillen, "Effects of Salts on the Micellization and Gelation of a Triblock Copolymer Studied by Rheology and Light Scattering," *Macromolecules,* vol. 30, pp. 2355-2364, 1997.

[134] V. Bazargan and B. Stoeber, "Formation of temporary separating walls in microfluidic devices," in 2008,

[135] M. A. Unger, H. P. Chou, T. Thorsen, A. Scherer and S. R. Quake, "Monolithic Microfabricated Valves and Pumps by Multilayer Soft Lithography," *Science,* vol. 288, pp. 113, 2000.

[136] A. V. Kabanov, E. V. Batrakova and V. Y. Alakhov, "Pluronic® block copolymers as novel polymer therapeutics for drug and gene delivery," *J. Controlled Release,* vol. 82, pp. 189-212, 2002.

[137] X. Xiong, K. Tam and L. Gan, "Synthesis and Aggregation Behavior of Pluronic F127/Poly (lactic acid) Block Copolymers in Aqueous Solutions," *Macromolecules,* vol. 36, pp. 9979-9985, 2003.

[138] S. F. Khattak, S. R. Bhatia and S. C. Roberts, "Pluronic F127 as a Cell Encapsulation Material: Utilization of Membrane-Stabilizing Agents," *Tissue Eng.,* vol. 11, pp. 974-983, 2005.

[139] L. R. Harriott, "Limits of lithography," *Proc IEEE,* vol. 89, pp. 366-374, 2001.

[140] Y. Xia and G. M. Whitesides, "SOFT LITHOGRAPHY," *Annual Reviews in Materials Science,* vol. 28, pp. 153-184, 1998.

[141] Y. Xia, "0. M. Whitesides. Soft lithography," *Angew.Chem.Mt.Ed,* vol. 37, pp. 550-575, 1998.

[142] J. C. McDonald, D. C. Duffy, J. R. Anderson, D. T. Chiu, H. Wu, O. J. Schueller and G. M. Whitesides, "Fabrication of microfluidic systems in poly(dimethylsiloxane)," *Electrophoresis,* vol. 21, pp. 27-40, Jan. 2000.

[143] J. A. Rogers and R. G. Nuzzo, "Recent progress in soft lithography," *Materials Today,* vol. 8, pp. 50-56, 2005.

[144] J. P. Urbanski, W. Thies, C. Rhodes, S. Amarasinghe and T. Thorsen, "Digital microfluidics using soft lithography," *Lab on a Chip*, vol. 6, pp. 96-104, 2006.

[145] R. Ito and S. Okazaki, "Pushing the limits of lithography," *Nature*, vol. 406, pp. 1027-1031, 2000.

[146] S. R. Quake and A. Scherer, "From Micro-to Nanofabrication with Soft Materials," *Science*, vol. 290, pp. 1536-1540, 2000.

[147] D. Psaltis, S. R. Quake and C. Yang, "Developing optofluidic technology through the fusion of microfluidics and optics," *NATURE-LONDON-*, vol. 442, pp. 381, 2006.

[148] A. D. Stroock and G. M. Whitesides, "Components for integrated poly (dimethylsiloxane) microfluidic systems," *Electrophoresis*, vol. 23, pp. 3461-3473, 2002.

[149] USHIO Inc., "
,"

[150] J. E. Mark, *Polymer Data Handbook.* New York: Oxford University Press, 1999,

[151] J. C. McDonald and G. M. Whitesides, "Poly (dimethylsiloxane) as a Material for Fabricating Microfluidic Devices," *Acc. Chem. Res.*, vol. 35, pp. 491-500, 2002.

[152] D. C. Duffy, J. C. McDonald, O. J. A. Schueller and G. M. Whitesides, "Rapid Prototyping of Microfluidic Systems in Poly (dimethylsiloxane)," *ANALYTICAL CHEMISTRY-WASHINGTON DC-*, vol. 70, pp. 4974-4984, 1998.

[153] M. K. Chaudhury and G. M. Whitesides, "Direct measurement of interfacial interactions between semispherical lenses and flat sheets of poly (dimethylsiloxane) and their chemical derivatives," *Langmuir*, vol. 7, pp. 1013-1025, 1991.

[154] S. K. Sia and G. M. Whitesides, "Microfluidic devices fabricated in Poly (dimethylsiloxane) for biological studies," *Electrophoresis*, vol. 24, pp. 3563-3576, 2003.

[155] T. Thorsen, S. J. Maerkl and S. R. Quake, "Microfluidic Large-Scale Integration," *Science*, vol. 298, pp. 580, 2002.

[156] L. Kersey, V. Ebacher, V. Bazargan, R. Wang and B. Stoeber, "The effect of adhesion promoter on the bond strength of PDMS," *Lab on a Chip*, August 2008.

[157] G. Vozzi, C. Flaim, A. Ahluwalia and S. Bhatia, "Fabrication of PLGA scaffolds using soft lithography and microsyringe deposition," *Biomaterials,* vol. 24, pp. 2533-2540, 2003.

[158] J. S. Marcus, W. F. Anderson and S. R. Quake, "Parallel picoliter RT-PCR assays using microfluidics," *Anal. Chem.,* vol. 78, pp. 956-958, 2006.

[159] J. F. Zhong, Y. Chen, J. S. Marcus, A. Scherer, S. R. Quake, C. R. Taylor and L. P. Weiner, "A microfluidic processor for gene expression profiling of single human embryonic stem cells," *Lab on a Chip,* vol. 8, pp. 68-74, 2008.

[160] V. Studer, G. Hang, A. Pandolfi, M. Ortiz, W. F. Anderson and S. R. Quake, "Scaling properties of a low-actuation pressure microfluidic valve," *J. Appl. Phys.,* vol. 95, pp. 393, 2003.

[161] Y. S. Shin, K. Cho, S. H. Lim, S. Chung, S. J. Park, C. Chung, D. C. Han and J. K. Chang, "PDMS-based micro PCR chip with Parylene coating," *J Micromech Microengineering,* vol. 13, pp. 768-774, 2003.

[162] H. S. Noh, Y. Huang and P. J. Hesketh, "Parylene micromolding, a rapid and low-cost fabrication method for parylene microchannel," *Sensors & Actuators: B.Chemical,* vol. 102, pp. 78-85, 2004.

[163] Specialty Coating Systems Inc.,

[164] G. Yang, S. Ganguli, J. Karcz, W. GILL and T. LU, "High deposition rate parylene films," *J Crystal Growth,* vol. 183, pp. 385, 1998.

[165] J. Santiago, S. Wereley, C. Meinhart, D. Beebe and R. Adrian, "A particle image velocimetry system for microfluidics," *Exp. Fluids,* vol. 25, pp. 316-319, 1998.

[166] C. Meinhart, S. Wereley and J. Santiago, "PIV measurements of a microchannel flow," *Exp. Fluids,* vol. 27, pp. 414-419, 1999.

[167] K. S. Breuer, *Microscale Diagnostic Techniques.* Springer, 2005,

[168] R. D. Keane and R. J. Adrian, "Theory of cross-correlation analysis of PIV images," *Applied Scientific Research,* vol. 49, pp. 191-215, 1992.

[169] S. A. Rani, B. Pitts and P. S. Stewart, "Rapid Diffusion of Fluorescent Tracers into Staphylococcus epidermidis Biofilms Visualized by Time Lapse Microscopy," *Antimicrobial Agents Chemother.,* vol. 49, pp. 728-732, 2005.

[170] A. E. Kamholz, E. A. Schilling and P. Yager, "Optical Measurement of Transverse Molecular Diffusion in a Microchannel," *Biophys. J.,* vol. 80, pp. 1967-1972, 2001.

[171] A. E. Kamholz, B. H. Weigl, B. A. Finlayson and P. Yager, "Quantitative Analysis of Molecular Interaction in a Microfluidic Channel: The T-Sensor," *ANALYTICAL CHEMISTRY-WASHINGTON DC-,* vol. 71, pp. 5340-5347, 1999.

[172] Z. Wu, N. T. Nguyen and X. Huang, "Nonlinear diffusive mixing in microchannels: theory and experiments," *J Micromech Microengineering,* vol. 14, pp. 604-611, 2004.

[173] Z. Wu and N. T. Nguyen, "Convective–diffusive transport in parallel lamination micromixers," *Microfluidics and Nanofluidics,* vol. 1, pp. 208-217, 2005.

[174] Z. Wu and N. T. Nguyen, "Hydrodynamic focusing in microchannels under consideration of diffusive dispersion: theories and experiments," *Sensors & Actuators: B.Chemical,* vol. 107, pp. 965-974, 2005.

[175] J. B. Salmon, C. Dubrocq, P. Tabeling, S. Charier, D. Alcor, L. Jullien and F. Ferrage, "An approach to extract rate constants from reaction-diffusion dynamics in a microchannel," *Anal. Chem.,* vol. 77, pp. 3417–3424, 2005.

[176] J. B. Salmon and A. Ajdari, "Transverse transport of solutes between co-flowing pressure-driven streams for microfluidic studies of diffusion/reaction processes," *J. Appl. Phys.,* vol. 101, pp. 074902, 2007.

[177] J. JIMÉNEZ, "The growth of a mixing layer in a laminar channel," *J. Fluid Mech.,* vol. 535, pp. 245-254, 2005.

[178] J. M. Chen, T. L. Horng and W. Y. Tan, "Analysis and measurements of mixing in pressure-driven microchannel flow," *Microfluidics and Nanofluidics,* vol. 2, pp. 455-469, 2006.

[179] W. M. Rohsenow and H. Y. Choi, *Heat, Mass, and Momentum Transfer.* Prentice-Hall Englewood Cliffs, NJ, 1961,

[180] A. Bejan, *Heat Transfer.* John Wiley & Sons, 1993,

[181] M. Lounaci, P. Rigolet, C. Abraham, M. Le Berre and Y. Chen, "Microfluidic device for protein crystallization under controlled humidity," *Microelectronic Engineering,* vol. 84, pp. 1758-1761, 2007.

[182] C. L. Hansen, S. Classen, J. M. Berger and S. R. Quake, "A Microfluidic Device for Kinetic Optimization of Protein Crystallization and In Situ Structure Determination," *J. Am. Chem. Soc.,* vol. 128, pp. 3142-3143, 2006.

[183] C. Hansen and S. R. Quake, "Microfluidics in structural biology: smaller, faster… better," *Curr. Opin. Struct. Biol.,* vol. 13, pp. 538-544, 2003.

[184] D. Erickson and D. Li, "Integrated microfluidic devices," *Anal. Chim. Acta,* vol. 507, pp. 11-26, 2004.

[185] H. P. Chou, M. A. Unger, A. Scherer and S. R. Quake, "Integrated elastomer fluidic lab-on-A-chip-surface patterning and DNA diagnostics," in *Proceedings of the Solid State Actuator and Sensor Workshop, Hilton Head, South Carolina,*

[186] J. W. Hong, V. Studer, G. Hang, W. F. Anderson and S. R. Quake, "A nanoliter-scale nucleic acid processor with parallel architecture," *Nat. Biotechnol.,* vol. 22, pp. 435-439, 2004.

[187] H. P. Chou, M. A. Unger and S. R. Quake, "A Microfabricated Rotary Pump," *Biomed. Microdevices,* vol. 3, pp. 323-330, 2001.

[188] A. Y. Fu, H. P. Chou, C. Spence, F. H. Arnold and S. R. Quake, "An Integrated Microfabricated Cell Sorter," *ANALYTICAL CHEMISTRY-WASHINGTON DC-,* vol. 74, pp. 2451-2457, 2002.

[189] V. Studer, R. Jameson, E. Pellereau, A. Pépin and Y. Chen, "A microfluidic mammalian cell sorter based on fluorescence detection," *Microelectronic Engineering,* vol. 73, pp. 852-857, 2004.

[190] D. R. Reyes, D. Iossifidis, P. A. Auroux and A. Manz, "Micro Total Analysis Systems. 1. Introduction, Theory, and Technology," *ANALYTICAL CHEMISTRY-WASHINGTON DC-,* vol. 74, pp. 2623-2636, 2002.

[191] P. A. Auroux, D. Iossifidis, D. R. Reyes and A. Manz, "Micro Total Analysis Systems. 2. Analytical Standard Operations and Applications," *ANALYTICAL CHEMISTRY-WASHINGTON DC-,* vol. 74, pp. 2637-2652, 2002.

[192] P. Linderholm and P. Asberg, "3D / Multi-Layered PDMS Microfluidic Systems," 30 May, 2000.

[193] A. Emslie, F. Bonner and L. Pecr, "Flow of a viscous liquid on a rotating disk," *J. Appl. Phys.,* vol. 29, pp. 858, 1958.

[194] A. Acrivos, M. Shah and E. Petersen, "Momentum and heat transfer in laminar boundary-layer flows of non-Newtonian fluids past external surfaces," *AICHE J.,* vol. 6, pp. 312-317, 1960.

[195] D. Meyerhofer, "Characteristics of resist films produced by spinning," *J. Appl. Phys.,* vol. 49, pp. 3993, 1978.

[196] M. W. George, "Monolayers on Disordered Substrates: Self-Assembly of Alkyltrichlorosilanes on Surface-Modified Polyethylene and Poly (dimethylsiloxane)," *Macromolecules,* vol. 26, pp. 5870-5875, 1993.

Appendices

A. Spin Coating

Spin coating is an inexpensive and fast method for producing thin films of polymers from solutions, and other liquid materials, with a well defined thickness. Spin coating was used to define the thickness of the photoresist in the photolithography process and also for controlling the thickness of a thin PDMS layer. A schematic view of a spin coater is shown in Figure A.1. The polymer in liquid form is dispensed onto the substrate, which was placed onto a vacuum chuck, see Figure A.1; the substrate is then spun at a certain speed for a certain amount of time to produce the desired polymer film thickness.

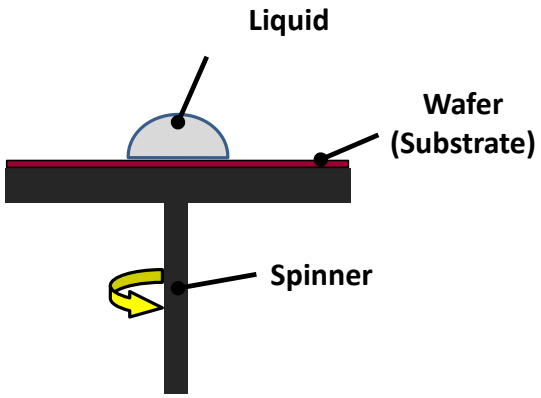

Figure A.1 A schematic view of a spin coater

The theory behind spin coating is rather complex, and several models has been developed that take into account process parameters such as solvent evaporation rates, the air flow around the spin coater and surface energies [192-195]. Here the

most basic model described by Emslie *et al.* (1958) [193] is presented. They used cylindrical polar coordinates (r, θ, z) to describe the behavior of a Newtonian liquid on a rotating disk. The centrifugal force on a segment volume of area A and height ∂z can be described as

$$F_{centrifugal} = m\omega^2 r = A \cdot \partial z \cdot \rho\omega^2 r$$

where ρ is the density of the liquid and ω is the angular velocity. For a Newtonian fluid the shear stress is proportional to [195]the relative difference in velocity between two layers of liquid, $\sigma_{shear} = -\mu \frac{\partial v}{\partial z}$. Therefore the shear force can be found as $F_{shear} = -A \cdot \mu \frac{\partial v}{\partial z}$.

The centrifugal force of the layer was balanced by the shear force and so it can be concluded that

$$-\mu \frac{\partial v}{\partial z} = \rho\omega^2 r \, \partial z \text{ or } -\frac{\partial}{\partial z}(\mu \frac{\partial v}{\partial z}) = \frac{\partial}{\partial z}(\rho\omega^2 r \, \partial z)$$

can be simplified to $-\mu \frac{\partial^2 v}{\partial z^2} = \rho\omega^2 r$. This equation can be solved with considering non-slip velocity at the interface between the disk and the fluid ($v|_{z=0} = 0$) and zero shear at the surface of the liquid ($\frac{\partial v}{\partial z}\Big|_{z=h} = 0$) as the boundary conditions. The velocity profile then can be integrated as

$$v = \frac{1}{\mu} \cdot (-\frac{\rho\omega^2 r z^2}{2} + \rho\omega^2 r h z).$$

Thus the total radial flow per unit length of circumference can be obtained by the flow over the height of the film as

$$q = \int_0^h v dz = \frac{\rho\omega^2 r h^3}{3\mu}.$$

To find an expression that describes the rate of change for the height at any given radius, the increase in volume (ΔV) of any arbitrary circle segmentoid is calculated as

$$\Delta V = (\pi\,(r+\Delta r)^2 - \pi\, r^2)\cdot\frac{\theta}{2\pi}\cdot\Delta h = (\Delta r\,(2r+\Delta r))\frac{\theta}{2}\cdot\Delta h,$$

where r is the distance to the inner boundary, θ is the angle of the volume segment, Δh its height and Δr its length. The continuity condition states that the accumulation of mass at any surface must equal the difference in inflow and outflow,

$$\Delta V = (\emptyset_{in} - \emptyset_{out})\cdot\Delta t = -(-q(r)\cdot\theta r + q(r+\Delta r)\cdot\theta(r+\Delta r))\cdot\Delta t$$

and so

$$\frac{\Delta h}{\Delta t} = -\frac{1}{(2r+\Delta r)}\frac{(rq\,(r+\Delta r)+\Delta r q\,(r+\Delta r)-rq\,(r))}{(\Delta r/2)} \xrightarrow{\Delta r\to 0} -\frac{1}{r}\,\frac{\partial(rq)}{\partial r}$$

or

$\frac{\partial h}{\partial t} = -\frac{1}{r}\,\frac{\partial(rq)}{\partial r}$ where $= \int_0^h v dz = \frac{\rho\omega^2 r h^3}{3\mu}$, so the thickness of the layer h versus time t can be found as

$$\frac{\partial h}{\partial t} = -\frac{\rho\omega^2}{3\mu}\cdot\frac{1}{r}\cdot\frac{\partial(r^2h^3)}{\partial r}.$$

If the surface is completely flat from the beginning, there exists a special solution that depends only on time since

$$\frac{\partial h}{\partial r} = 0 \longrightarrow \frac{\partial h}{\partial t} = -k\cdot\frac{1}{r}\cdot\frac{\partial(r^2h^3)}{\partial r} = -2kh^3 \text{ where } k = \frac{\rho\omega^2}{3\mu}$$

In this case

$$\frac{\partial h}{\partial t} = -2\frac{\rho\omega^2}{3\mu}\cdot h^3,$$

which can be explicitly solved for the thickness

$$\mathrm{h} = \frac{h_0}{\sqrt{1+4\frac{\rho\omega^2}{3\mu}\cdot {h_0}^2 t}},$$

where h_0 is the initial thickness of the uniform film.

B. Protocol for the Fabrication of SPR220-7.0 Mold

The following procedure has been used for producing 10 μm thick patterns through photolithography process on a 4-inch silicon wafer using SPR220-7.0, a positive photoresist (from Shipley Company, L.L.C., Marlborough, MA). SPR220-7.0 is the thickest photoresist in SPR series and it is sensitive to wavelengths in the range 365 nm to 436 nm and gives a good uniformity for single coating around 10 μm.

Preparation Steps

- A silicon wafer is cleaned by rinsing with acetone, methanol, and then with DI water and it is dried with gentle N_2 blowing.
- A 4-inch wafer is baked for dehydration for 5 minutes at 110°C.

Spin Coating

- The wafer is place on the spinner using the appropriate chuck.
- HMDS (hexamethyldisilazan) is poured with a pipette over the wafer so that 50 % of the wafer is covered. HMDS helps the bonding of the SPR photoresist to the silicon (or glass) wafers. HMDS is very toxic and the whole process should be done under fume hood.
- HMDS is spun at 3500 rpm for 35 seconds.
- SPR220-7.0 photoresist is poured over the wafer using pipettes. Since it is a viscous resist it takes some time to draw it up into the pipette. Almost 50

% of the wafer is covered with one continuous single droplet of the poured fluid.

- SPR220-7.0 is spun for 5 sec at 500 rpm and 40 sec at 1500 rpm.
- The wafer is let sit on the spinner for 1 minute.

Photoresist Soft bake

- The wafer is put on the hot plate for 2 min at 90°C and 3 min at 115°C
- The wafer is slowly cooled to room temperature for 10 min

UV-Light Exposure

- The wafer is loaded into a mask aligner for light exposure (Canon PLA-501F double-side 100mm mask aligner, Cleanroom, Nanofabrication Facility, UBC) that has a Hg-lamp without a filter and with a intensity of about 10 mW/cm^2.
- The printed mask on a transparent sheet is attached to a thick glass plate and is loaded as the photomask into the mask aligner.
- UV-light is exposed to the layer for 90 sec.
- The wafer is let sit on the mask aligner for 1 min.
- The wafer is cooled down at the room temperature 21°C for 30 min for dehydration.

Photoresist Develop

- Two MF-24A developer (or MF 319, both from Shipley) and DI-water baths are prepared.
- The wafer is placed into the MF-24A for 5 min and visually checked.

- If the developments looks completed, the wafer is placed into the water bath for 1 min and is rinsed with DI water and dried with a N_2 gun.
- The pattern is checked under the microscope and especially the corners are examined for complete development. The developing process can be repeated if additional development needed in the corners.
- The thickness of the pattern then is measured using a needle profiler (or Wyko NT1100 optical).

Reflow Process*

- The wafer is placed on the hot plate for 2 min at 90°C.
- Using a ramp of 5°C/min the wafer is baked until 140°C.
- The wafer is then baked for 30 min at 140°C.
- The wafer is cooled down from 140°C to 90°C in a ramp of 5°C/min and then afterwards is let sit for 30 min to cool down to the ambient temperature.
- The shape and the thickness of the pattern then are measured using Wyko NT1100 optical.

* For multilayer soft lithography fabrication technique used in Chapter 3 and Chapter 5.

C. Oxygen Plasma Bonding Protocol

Oxygen plasma bonding was used here to bond PDMS to the glass substrate. Oxygen plasma reacts with the surface of PDMS and helps the bonding of PDMS to the glass through modifying its surface [196]. Single atom Plasma is created by exposing oxygen gas (O_2) to non-ionizing radiation that provides high enough energy for the gas to knock out an electron from one of its shells. This process is done under vacuum in order to create plasma. In RF generated plasma, a radio frequency voltage is applied between two electrodes, causing the free electrons to oscillate. These oscillations lead to collisions between the high energy electrons and the gas molecules or atoms, thereby giving rise to sustained plasma [192]. The oxygen plasma treats the surfaces following the process below, using TRION MINILOCK, a reactive ion etcher with a vacuum load-lock (Cleanroom, Nanofabrication Facility, UBC).

Bonding of PDMS Devices to the Glass Substrate Using Oxygen Plasma Method

- A glass substrate is cleaned with acetone, isopropanol, and methanol and dried with a N_2 gun.
- The PDMS device is put inside the equipment chamber upside down so the channels side faces up. The glass substrate is also placed inside the chamber with the side that is going to be bonded to PDMS facing up.
- Descum process is used with the power of 30 W for 10 seconds at 20°C with the oxygen (O_2) pressure of 100 mTorr.

- The treated surfaces of the PDMS device and the glass are pressed together to bond together.

D. Spinning of PDMS Protocol

RTV 615 PDMS from GE Silicones was used to fabricate the micro channels. It also was used for devices described in Chapter 3 and Chapter 5 to create a thin layer of PDMS over the mold through spinning. The following procedure was used to achieve a 20 µm PDMS layer over a mold with 10 µm high patterns. The spinning curve of RTV 615 PDMS is shown in Figure D.1.

- PDMS RTV 615 A and 615 B are weighted for a mass ratio of 20 to 1 and poured in a clean container.
- The samples are mixed using a mixer model ARE-250 (from THINKY Corporation, Tokyo, Japan) for 4 min and 20 sec for de-aeration.
- The mixture is poured over the substrate and it covers about 50 % of the mold starting from the center.
- The wafer is spun for at 500 rpm for 10 sec and 3500 rpm for 40 sec.
- The PDMS is put into the oven for 1.5 hours at 80°C

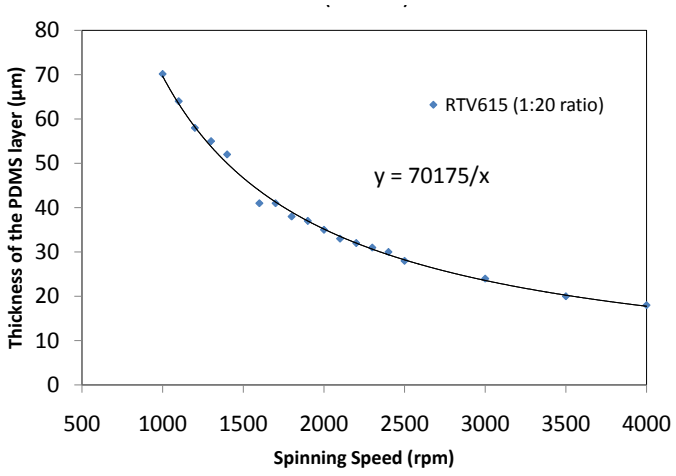

Figure D.1 PDMS Spinning Curve

E. Fabrication of the Heaters by Lift-Off Process

Heaters on the glass substrate are fabricated using a lift-off process. A negative photomask of the final shape of the heater was transferred onto a glass substrate using SPR220-7.0 photoresist and then Cr with the thickness of 20 nm and gold with the thickness of 300 nm is evaporated on the substrate. The photoresist is then removed with acetone and the heaters remain on the glass substrate. The exact procedure is as detailed below.

Preparation Steps

- A glass substrate (75 mm by 25 mm from Fisher Scientific Inc.) is cleaned by rinsing it with acetone and methanol and DI water and it is dried with gentle N_2 blowing.
- The glass substrate is baked for dehydration for 5 minutes at 110°C.

Spin Coating

- The glass substrate is place on a spinner using the appropriate chuck.
- HMDS (hexamethyldisilazan) is poured with a pipette over the wafer so that 50 % of the wafer is covered. A monolayer of HMDS improves bonding of SPR photoresist to silicon (or glass) substrates.
- HMDS is spun at 3500 rpm for 35 seconds.
- SPR220-7.0 photoresist is poured over the substrate using a pipette. Almost 50 % of the glass substrate is covered with one continuous single droplet of fluid.
- SPR220-7.0 is spun for 5 sec at 500 rpm and for 40 sec at 4000 rpm.

- The glass substrate is let sit on the spinner for 1 minute.

Photoresist Soft bake

- The glass substrate is placed on the hot plate for 2 min at 115°C.
- The glass substrate is slowly cooled to room temperature for 10 min.

UV-Light Exposure

- The glass substrate is loaded into a mask aligner for light exposure (Canon PLA-501F double-side 100 mm mask aligner, Cleanroom, Nanofabrication Facility, UBC) that has a Hg-lamp without a filter and with an intensity of about 10 mW/cm^2.
- The printed negative photomask on a transparent sheet is attached to a thick glass plate and is loaded as the photomask into the mask aligner.
- UV-light is exposed to the layer for 60 sec.
- The glass substrate is let sit on the mask aligner for 1 min.
- The glass substrate is cooled down to the room temperature of 21°C for 20 min.

Photoresist Develop

- The glass substrate is placed in chlorobenzene bath for 40 sec.
- The chlorobenzene is removed from the substrate using gentle blowing with a N_2 gun.
- The glass substrate is placed into the developer MF-24A (or MF 319, both from Shipley) for 3 min and visually observed to follow the development process.

- The glass substrate is rinsed with DI water and dried with N_2 gun.
- The pattern is checked under a microscope, including a check if the corners are completely developed.

Evaporation

- The glass substrate is loaded into the Evaporator 2000 (DeeWong, Cleanroom, Nanofabrication Facility, UBC).
- Cr and gold are deposited onto the glass substrate with the thicknesses mentioned above. The layer thickness is controlled using a crystal thickness monitor.
- The glass substrate is allowed to sit for 10 min for cooling down at atmospheric pressure before it is taken out of the evaporation chamber.

Photoresist Removal

- The glass substrate is put in an acetone bath for 15 min.
- The glass substrate is rinsed with DI water and dried using gentle blowing with a N_2 gun.